Approaches for extending insulin catheter longevity

Julia A. King

A dissertation

submitted in partial fulfillment of the

requirements for the degree of

Doctor of Philosophy

University of Washington

2022

Reading Committee:

Buddy D. Ratner, Chair

Elizabeth A. Nance

David G. Castner

Program Authorized to Offer Degree:

Department of Chemical Engineering

University of Washington

Abstract

Approaches for extending insulin catheter longevity

Julia A. King

Chair of the Supervisory Committee:
Prof. Buddy D. Ratner, Professor
Departments of Bioengineering and Chemical Engineering

Implantable medical devices serve a wide range of therapeutic purposes; however, they are an alien material in the body and are subject to the effects of the body's immune reaction—the foreign body response (FBR). For insulin catheters, a foreign body capsule occludes the catheter tip within 2-3 days, thereby eliminating any therapeutic effects. Here, a few approaches are proposed to reduce the extent of the FBR to lengthen the medical device lifetime and lessen the disease management burden. The first approach is to minimize initial protein adsorption on the device—a traditional method of improving biocompatibility. In this work, a nonfouling zwitterionic polymer, poly(sulfobetaine methacrylate) (pSBMA), was grafted to the surface as a polymer brush coating using an alternative polymerization initiator—a plasma-deposited bromoester. The plasma-deposited initiator robustly covers the entirety of the surface

independently of device material or shape. To further-optimize these polymer brush coatings, the effects of polymer brush length and density were investigated utilizing self-assembled monolayers. Quartz crystal microbalance with dissipation was used to measure protein adsorption after *in situ* polymerization and sum frequency generation spectroscopy measured water structure at the interface. In a second approach to reduce the FBR, macrophages will be guided to an alternative, 'pro-healing', phenotype—M2. A *de novo* version of interleukin-4 (IL-4) was computationally designed with high stability, binding affinity, and an additional cysteine residue. In this work, an S_N2 reaction was used to substitute the cysteine on a brominated surface, immobilizing the therapeutic. The reaction was confirmed by immobilizing cysteine-containing cell adhesion RGD peptides and culturing with fibroblasts to confirm bioactivity maintenance in preparation for the *de novo* IL-4. Finally, with the proposed increase in device lifetime there is an elevated infection risk. Therefore, a method for antibiotic incorporation was developed for the insulin catheter. The extended release of the drug was measured over time and a concentration model was developed to predict the antibiotic concentration around the catheter to ensure minimum inhibitory concentration (MIC) was maintained. The approaches investigated here may significantly reduce the effects of the FBR, aiming to extend insulin catheter longevity or other implantable medical devices.

TABLE OF CONTENTS

List of Figures viii

List of Tables xiii

Chapter 1. INTRODUCTION 17

1.1 Reducing Protein Adsorption with Zwitterionic pSBMA Coatings 21

1.2 Investigating the Effects of pSBMA Chain Length and Density on Non-Specific Protein Adsorption 22

1.3 Guiding the Immune Response with Surface-Immobilized *De Novo* Proteins 24

1.4 Reducing the Risk of Bacterial Infection with Antibiotic Extended Release and Concentration Modeling 25

Chapter 2. Methods 27

2.1 Materials 27

2.2 Surface Functionalization 28

2.2.1 Radio frequency plasma deposition (RFPD) 28

2.2.2 Self-assembled monolayers 30

2.2.3 Immobilizing ATRP initiator to hydroxyl-functionalized surfaces 30

2.2.4 Full factorial of methyl 3-bromopropionate 31

2.3 Synthesizing nonfouling coatings 32

2.3.1 ARGET ATRP with SBMA 32

2.3.2 Full factorial of SBMA coating 33

2.3.3 CBMA surface-grafted hydrogel 34

2.4 Immobilizing biomolecules using an S_N2 reaction 34

2.5 Levofloxacin impregnation, extended release, and concentration modelling 36

2.5.1 Levofloxacin Impregnation 36

2.5.2 Release Profile Assay 36

2.5.3 Bacterial Inhibition Assay 37

2.5.4 Levofloxacin Concentration Model 37

2.5.5 Nonfouling Coating 39
2.6 Surface Characterization 39
2.6.1 X-ray photoelectron spectroscopy (XPS) 39
2.6.2 Attenuated total reflectance Fourier transform infrared spectroscopy (ATR FTIR) 40
2.6.3 Radiolabeled protein adsorption assay 40
2.6.4 Sum frequency generation (SFG) 42
2.6.5 Quartz crystal microbalance with dissipation (QCM-D) 42
2.6.6 Contact Angle 44
2.6.7 Fibroblast adhesion assay 44
2.6.8 Scanning electron microscopy (SEM) 46
2.6.9 Cytotoxicity assay 46
Chapter 3. Reducing protein adsorption with zwitterionic pSBMA coatings 47
3.1 Introduction 47
3.2 Results and Discussion 51
3.2.1 Synthesizing the SBMA polymer brush coatings 51
3.2.2 The catheter polyurethane contains hydroxyl groups. 53
3.2.3 BIBB coating validation and bromine density 53
3.2.4 M3BP coating validation and bromine density 54
3.2.5 Plasma full factorial and optimization of initiator density 55
3.2.6 SBMA coating validation 60
3.2.7 ATRP Full Factorial Design 61
3.2.8 SBMA on polyurethane protein adsorption and validation 64
3.2.9 Surface-grafted CBMA hydrogel 64
3.3 Conclusions 66
3.4 Acknowledgments 67
Chapter 4. Investigating the effects of pSBMA chain length and density on non-specific protein adsorption 69
4.1 Introduction 69
4.2 Results and Discussion 74

4.2.1 The effect of water structure on protein resistance 74
4.2.2 The Hofmeister series and the effect of salt addition during ATRP 75
4.2.3 XPS reveals successful coating of pSBMA and surface density 76
4.2.4 Coating thickness due to varying grafting densities and use of polymerization salt 79
4.2.5 Contact angle due to varying grafting densities and coating thicknesses 80
4.2.6 In situ ATRP of pSBMA and BSA adsorption in QCM-D 81
4.3 Conclusions 85
4.4 Acknowledgments 86

Chapter 5. Guiding the immune response with surface-immobilized *de novo* proteins 88

5.1 Introduction 88
5.2 Results and Discussion 92
5.2.1 L-cysteine was conjugated to an M3BP surface using the S_N2 reaction. 92
5.2.2 Cysteine-containing peptides were conjugated to pHEMA hydrogels. 95
5.2.3 Surface-immobilized peptides remain bioactive 97
5.3 Conclusions 100
5.4 Acknowledgments 100

Chapter 6. Reducing risk of bacterial infection with antibiotic extended release and concentration modeling 102

6.1 Introduction 102
6.2 Results and Discussion 104
6.2.1 S. epidermidis inhibition 104
6.2.2 Levofloxacin release profile 105
6.2.3 Levofloxacin concentration around the insulin catheter 106
6.2.4 Suitable levofloxacin release after nonfouling coating treatment 108
6.3 Conclusions 110
6.4 Acknowledgements 111

Bibliography 112

LIST OF FIGURES

Figure 2.1. Ratner Lab plasma reactor in Foege Hall, University of Washington.....29
Figure 3.1. Molecular structure of SBMA 47
Figure 3.2. Schematic of the ARGET ATRP reaction.....49
Figure 3.3. ATRP initiator molecules (left) α-bromoisobutyryl bromide and (right) methyl 3-bromopropionate 50
Figure 3.4. ATR-FTIR spectra of insulin catheter outer polymer 53
Figure 3.5. Composition of the plasma-deposited HEMA film and the BIBB anchored to the HEMA measured by XPS survey scan 54
Figure 3.6. Composition of plasma-deposited M3BP measured by XPS survey scan after 1 hour soak period.....55
Figure 3.7. Percentage of bromine on the surface. XPS results from the M3BP full factorial experiment after soaking the samples. Since there is an obvious distinction in bromine amount, the samples from the middle of the electrodes is labeled in green and downstream is in blue.....56
Figure 3.8. Amount bromine lost after soaking. Measured by XPS, the amount of bromine lost was calculated for each run in the full factorial experiment for M3BP plasma. Samples from the middle of the electrodes are green and downstream is in blue.....57
Figure 3.9. Amount excess bromine than theoretical. Measured by XPS, the amount of bromine excess compared to the theoretical stoichiometric amount was calculated for each run in the full factorial experiment for M3BP plasma 58
Figure 3.10. Pareto charts reporting the effect of selected variables on **a)** the excess bromine, **b)** amount of bromine loss after soaking, **c)** amount excess bromine with regards to interactions of factors, and **d)** amount bromine loss after soaking with regards to interactions of factors.....59
Figure 3.11. XPS results for the SBMA coating grown using Scheme 1 60
Figure 3.12. XPS results for the SBMA coating grown using Scheme 2 61
Figure 3.13. Albumin adsorption on SBMA samples for the full factorial design.....62

Figure 3.14. Full Factorial DOE results for the ATRP. (Top) singular effects and (bottom) effects including interactions between factors 62
Figure 3.15. Effect of ATRP initiator density on albumin adsorption for the ATRP full factorial 63
Figure 3.16. Protein adsorption of samples prepared using the process in Scheme 3 64
Figure 3.17. Surface composition of surface-grafted CBMA hydrogel from XPS results 65
Figure 3.18. Albumin adsorption measured on the surface-grafted CBMA hydrogel compared to the polyurethane control 66
Figure 4.1. Proposed balance for surface-grafted polymer brushes. Chain density and chain length should be balanced to achieve maximum chain mobility. 69
Figure 4.2. Process diagram for pSBMA coating on gold surfaces and characterization techniques. First, gold is deposited by electron beam deposition onto a substrate such as a prism or glass slide. Second, the ATRP initiator is immobilized onto the gold using thiol chemistry. Then, the ATRP occurs on the surface. Finally, surfaces are characterized using XPS, ellipsometry, SFG, and QCM-D. 72
Figure 4.3. Diagram of sample varying chain lengths and densities. Chain length is modified by adding sodium chloride to make the coating thicker. Chain density is modified with varying initiator densities on the surface of the substrate prior to ATRP. 73
Figure 4.4. a) Albumin adsorption counted using the I-125 label on SBMA coatings and polyurethane control and **b)** ppp polarized SFG spectra of SBMA polymer brush on (top) HEMA and (bottom) M3BP 75
Figure 4.5. Thicknesses of pSBMA coating with varying salts and concentrations during ATRP, n=3. 76
Figure 4.6. Surface composition for BIBB and BIBB-BME on gold surfaces, measured using XPS. 79
Figure 4.7. pSBMA coating thickness for varying grafting densities and chain lengths, n=3. 80
Figure 4.8. Water droplet imaged with goniometer during contact angle measurement on the dense pSBMA coating where NaCl was used during ATRP. 80
Figure 4.9. Contact angle for pSBMA coatings of varying grafting densities and coating thicknesses. 81

Figure 4.10. Mass measured by QCM-D over time at 37°C of in situ ATRP of pSBMA and subsequent BSA adsorption. Time segments: 1) air, 2) PBS wash, 3) in situ ARGET ATRP of pSBMA 4) PBS wash, 5) DI water wash, 6) PBS wash, 7) 1 mg/mL BSA in PBS nonspecific protein adsorption, 8) PBS wash, 9) DI water wash. The 100% Br graphs represent the mass for sensors loaded with ATRP initiator in ethanol [1.4 mM BIBOED]. The 50% Br graphs represent sensors loaded with a 1:1 mole ratio of ATRP initiator and diluent [0.7 mM BIBOED]. 82

Figure 4.11. Nonspecific protein adsorption as measured by QCM-D on various pSBMA surfaces 84

Figure 4.12. Surface composition of sensors post-QCMD, measured by XPS 85

Figure 5.1. Workflow for preparing to immobilize immune-directing de novo molecules. First, L-cysteine was conjugated using the proposed S_N2 reaction. Then, two different cysteine-containing peptides were immobilized. Next, to confirm immobilized molecules remain biologically active, a cysteine-containing cell adhesion (contains RGD sequence) peptide was immobilized and cultured with fibroblasts to determine extent of bioactivity. Finally, the reaction has been established and may be used to conjugate the de novo IL-4. 90

Figure 5.2. Schematic of cysteine/peptide/protein conjugation to plasma-brominated surface using S_N2 reaction. In the first step, M3BP is plasma-deposited onto a bare surface, such as a catheter, functionalizing the surface with reactive bromine. In the next step, the S_N2 reaction is used to conjugate the thiol from a cysteine, thereby immobilizing the cysteine/peptide/protein to the surface....91

Figure 5.3. Process diagram for immobilizing cysteine-containing peptides onto pHEMA hydrogel disks. First, BIBB is conjugated to the available hydroxyl groups in the pHEMA hydrogel. Second, the thiol from the cysteines in the peptides is used to substitute in an S_N2 reaction with the bromine on the hydrogel surface, thereby immobilizing the peptide. 92

Figure 5.4. Molecular structure of L-cysteine....92

Figure 5.5. Surface composition of cysteine conjugated by the SN2 reaction, measured by the S-Probe XPS. 93

Figure 5.6. Amount of sulfur on the surface of the cysteine-conjugated surface using the SN2 reaction, measured with the Kratos XPS at various takeoff angles. 94

Figure 5.7. Surface composition of the cysteine-conjugated surface using the SN2 reaction, measured during the angle-dependent study at 0º takeoff angle using the Kratos XPS. 95

Figure 5.8. a) Surface composition of hydrogel after BIBB conjugation, measured with the Kratos XPS and **b)** the BIBB molecule. There is a small about of bromine found on the surface of the hydrogel that should be enough to immobilize thiolated biomolecules. 95

Figure 5.9. Surface composition of cysteine-containing peptides after conjugation to brominated hydrogel using the S_N2 reaction, measured with the Kratos XPS. 96

Figure 5.10. RGD peptide pHEMA hydrogel surfaces after 24 hours culture with fibroblasts at a) 680x and b) 1500x. 97

Figure 5.11. pHEMA surfaces after 24 hour culture with fibroblasts at a) 84x and b) 450x. 98

Figure 5.12. Cells attached to the surfaces of the incubated hydrogels with 3T3 fibroblasts. Bare pHEMA controls should acquire minimal cell adhesion. After the immobilization of the cell adhesion RGD peptide, more than 3 times the number of cells were attached to the surface as counted. 99

Figure 6.1. Bacterial Inhibition Assay. Levofloxacin-treated tubing implanted in LB agar with S. epidermidis after total release time of **a)** 3 days, **b)** 12 days, **c)** 20 days, and **d)** 31 days with a visible inhibition zone for all time points 104

Figure 6.2. Total levofloxacin released. For different initial treatment solution concentrations, the total drug released was measured over time with n=3. 106

Figure 6.3. Schematic of concentration modeling in a control volume of 2 diameters of bacteria. The levofloxacin diffuses out of the catheter (tan) in the direction of *J*. C_0 was measured with the extended release assay. 106

Figure 6.4. Levofloxacin concentration. The plot shows the drug concentration around the catheter within 2 diameters of bacteria using the semi-empirical model for samples treated at different initial treatment solution concentrations, the MPC, and the MIC for levofloxacin.....107

Figure 6.5. Total levofloxacin released after nonfouling treatment. The plot shows the total drug released for catheter impregnated with levofloxacin and for tubing that experienced the nonfouling coating treatment with n=3. 109

Figure 6.6. Total levofloxacin extended release. Catheter tubing was treated with levofloxacin for extended release in either water or 0.9% NaCl. Over the years, the concentration remained over the MIC for both release mediums. Less antibiotic was released into the NaCl solution most likely due to the partition coefficient or higher osmotic pressure. 110

LIST OF TABLES

Table 2.1. Factorial design of plasma-deposited M3BP 31
Table 2.2. List of run descriptions for full factorial design of plasma-deposited M3BP.....32
Table 2.3. Factorial Design of ARGET ATRP conditions.....33
Table 2.4. List of run descriptions for full factorial design of ARGET ATRP conditions.....34
Table 2.5. Order of solution flown through the QCM-D channels. 43
Table 4.1. Surface composition of pSMBA and brominated glass slides, measured by XPS (atom %).....76
Table 4.2. ATRP rate and albumin adsorption as measured by QCM-D for in situ-prepared pSBMA surfaces. 83
Table 5.1. Theoretical percentages of each atom in each of the cysteine-containing peptides. Of note: the cyclical peptide contains 5% sulfur whereas the other peptide contains just 1% sulfur. 97

ACKNOWLEDGEMENTS

Firstly I'd like to acknowledge and thank my family who never stopped supporting me. Thank you to my mom for answering all of my phone calls and loving me no matter what. Also, thanks for signing me up for chemical engineering—I'm still doing it! Thank you to my dad for being my first engineering mentor, instigating my curiosity for science and technology. It helps that he works with roller coasters. Thank you to my brother, Bradley, for being so cool, always. I'm so proud of you. I'd also like to acknowledge my aunt, Prof. Yanling Wang, who helped me come up with a plan to graduate and showed me so much kindness. Last but not least in any way in the universe, thank you to Mike for keeping me grounded. I very honestly would not have finished this without you.

I feel so fortunate to have had such an amazing companion through these rough times. Dr. Prabhleen Kaur is the best person I have ever had the honor of working with. She is just as responsible for the work presented in chapter 3 as I am. We have consistently developed these nonfouling coatings for ~5.5 years together; so much of what I have learned is from her. She is also such a delightful and cheery person and I am so lucky to have worked so closely with her. I could not have imagined a better partner to do grad school with. Thank you Prabhleen!

As for general scientific development, Prof. Lei Ye, Dr. Marvin Mecwan, Dr. Patrik Johansson, Dr. Le Zhen, Dr. Lars Crawford, Dr. Kan Wu, Dr. Drew Day, Ross Bretherton, and Dr. Anna Galperin have been critical in helping me become an independent researcher. Sanjay Srinivasan has helped with my professional development and writing skills since undergrad.

Thank you to Sharon Creason, Kyung-Hoon Kim, Sherry Liu, Meghan Wyatt, Winston Ciridon, Gerry Hammer, and Samantha Young, PhD for assisting in data collection and providing expertise.

I'd like to thank my committee for their guidance over the years. Thank you Prof. Dave Castner for all of the technical expertise. Thank you very much Prof. Elizabeth Nance for your final thoughts on wrapping up my PhD and being an inspiration! A special thanks to my grad school representative, Prof. David Shechner, for your encouragement and very difficult questions, encouraging true interdisciplinary thinking. Thank you also to Prof. Cole DeForest, who served on my committee for my first two exams. You've been great to talk to and a great mentor!

Finally, thank you to my advisor, Prof. Buddy Ratner, for taking me on as a graduate student, continually finding funding for me, and providing exciting projects. I truly appreciate how diverse my work has been, spanning so many areas in biomaterials research over the years. You are continuously an inspiration.

DEDICATION

As commonly expressed, “research takes a village”. This work is dedicated to that village.

Chapter 1. INTRODUCTION

The work presented here intends to limit the extent of the foreign body reaction (FBR), your body's immune response and rejection of an alien material—in this case, a medical device. For implantable medical devices, the FBR may reduce or even eliminate the device's therapeutic effect. In the case of insulin catheters, the tip becomes entirely occluded and hence cannot deliver insulin. The trigger of the FBR is tenacious and immediate protein adsorption to the surface of the material which instigates a cascade of events[1]. Those adsorbed proteins send signals to neutrophils which release cytokines that activate tissue-resident macrophage cells, triggering them into an M1, pro-inflammatory, phenotype[2]. Macrophages send their own signaling molecules to recruit fibroblasts which in turn deposit excess collagen, eventually forming foreign body giant cells which are ultimately responsible for device failure and occlusion[3–5]. For biomaterials with a therapeutic purpose, the FBR inhibits functionality. We hypothesize that by reducing the FBR, fibrous encapsulation will be delayed or eliminated, thereby extending the duration of device function and overall lifetime.

Diabetes affects a very large number of people. As of 2020, 10.5% of Americans suffered from diabetes[6]. This percentage rose from 5% in 2000[7]. Management of this epidemic ranges everywhere from diet and exercise to medications. The most direct medication is insulin which is most traditionally administered by injection with a needle and syringe. However, needle use has general safety and sterility concerns and is an inconvenience, as well as endorses other societal and environmental health issues. Insulin infusion by pump and catheter is preferable and mimics the pancreatic function more effectively, providing an alternative to injections[8]. However, through the mechanisms of the FBR, the catheter tip becomes occluded 2-3 days after implantation. At this point, the patient must remove and discard the occluded

catheter and insert a new device into fresh tissue. After many years, there is much scarred tissue, leaving no unscarred insertion sites for a new catheter. Consequently, diabetic patients must revert to insulin injection by needle for disease management. For this reason, it is imperative that the insulin catheter lifetime be extended.

In this work, I have investigated 2 approaches to inhibiting the FBR. The first is the traditional method of reducing initial protein attachment to the surface of the material. "If the reaction isn't initiated, it can't happen." -me. This is an appropriate quote since much of this work revolves around a particular reaction and how it is initiated. Our star material here is sulfobetaine methacrylate (SBMA), a zwitterionic molecule that is relatively inexpensive, easily polymerized into biomaterial coatings, and highly hydrophilic. The SBMA's strong affinity for water rejects FBR-triggering protein attachment due to tightly-bound interfacial water[1,9]. We have utilized atom transfer radical polymerization (ATRP) using alternative initiators to robustly cover any implantable medical device in any material, shape or geometry. In a novel method, initiator is immobilized to the surface using radio frequency glow-discharge plasma deposition which is a stable and robust method for making the polymer coatings. Using this initiator coating, we have significantly reduced protein adsorption.

SBMA itself is a well-characterized, highly-researched, and creatively-incorporated material however the tunability of its nonfouling character remains formally uninvestigated. High hydration of SBMA has been often reported[10,11]. Complementarily, the water structure at the SBMA-water interface has been studied, demonstrating the nonfouling mechanism. For pSBMA polymer brush coatings, we hypothesize that the chain length and chain density play a critical role in surface hydration and may be tuned to modify the degree of surface hydration. Here, we have varied these parameters and measured differences in the amount of protein

adsorbed as well as the water structure using sum frequency generation spectroscopy and quartz crystal microbalance with dissipation (QCM-D). In future work, we would like to systematically measure the water structure at the interface of a wider range of formulations to understand how to make a 'perfect' nonfouling pSBMA coating.

The second approach to inhibiting the FBR is to polarize macrophages to an alternative phenotype (M2) thereby preventing the cells from sending signal molecules to fibroblasts and ultimately occlude a device with a foreign body capsule. With recent dramatic increases in computing power, algorithm development, and machine learning, synthetic therapeutic molecules have been designed and synthesized successfully with extreme and tailored biologic function[12,13]. Our collaborator has computationally designed a synthetic version of interleukin-4 (IL-4)—a stimulus for M2[14,15]—and successfully synthesized the protein in the lab[16]. The protein is ultra-stable with extremely high binding affinity and contains a cysteine featured on the opposing side to the binding site of the receptor. In my work, I have designed a method to immobilize this synthetic version of IL-4 to the surface of a biomaterial. Traditionally, a thiol-ene reaction is used to conjugate cysteine to another material. Here, I have used a much simpler S_N2 reaction which is safer, less expensive, and can be accomplished ambiently. In future work, I would like to immobilize the *de novo* IL-4 to observe macrophage differentiation—or coactivation—and investigate the response of the FBR with the addition of a surface-immobilized synthetic therapeutic. Notably, these methods are not limited to just IL-4. With the advent of computationally-designed molecules, the methods described here may be used to immobilize many engineered cysteine-containing therapeutics.

Finally, I have developed a method for reducing the risk of biofilm formation since the risk of infection increases with extended device lifetime[17]. For devices such as insulin catheters,

skin is continually punctured during use of the insulin pump management system. Here I have developed a method to incorporate antibiotic into the outer polymeric matrix of insulin catheter tubing and have quantified the extended release. Since most antibiotics clear the body very quickly before getting the chance to treat an infection, frequent administration is required to maintain antimicrobial activity. Under-dosed infections—antibiotic concentrations less than the minimum inhibitory concentration (MIC)—lead to antibiotic resistance[18]. Maintaining a drug concentration above the MIC is critical and therefore mechanisms and materials are developed to extend the release of antibiotics to prevent antibiotic resistance[19]. Extended release also provides means for better patient compliance. The development of polymers and even inorganic materials have been inspired by the need for extended release and are tailored to control the release rate[20]. For this work, an antibiotic was incorporated for extended release to prevent biofilm formation over an extended period. Additionally, I have developed a model to predict the concentration of the antibiotic around the catheter to ensure maintenance of the minimum inhibitory concentration and therefore biofilm prevention. This method was demonstrated *in vitro* and inhibited bacterial growth visibly.

The projects presented here aim at extending medical device longevity. From a global health standpoint, prolonged lifetime proposes less overall material waste. For population health, longer use means less time managing medical problems and suggests higher patient compliance and quality of life. This variety of methods and their broad range of applications have potential to improve medical device longevity, benefitting the entire field of implantable devices.

1.1 Reducing Protein Adsorption with Zwitterionic pSBMA Coatings

The triggering event in the FBR is immediate protein attachment. Here, multiple coatings have been developed to inhibit protein attachment to a biomaterial. The bulk of this work uses methods that utilize the radio frequency glow discharge plasma deposition of surface-functionalizing molecules to create a robust coating regardless of substrate material or shape. In this work, pSBMA coatings were synthesized using activators regenerated by electron transfer (ARGET) ATRP to limit protein attachment. Hydroxyethyl methacrylate (HEMA) or methyl 3-bromopropionate (M3BP) were plasma-deposited onto the substrate surface. To the hydroxyl groups from the HEMA surface, α-bromoisobutyryl bromide (BIBB)—the traditional ATRP initiator—was immobilized. The bromine from the plasma-deposited M3BP coatings was used as an alternative initiator. In these methods, 5.6% Br was measured on the HEMA-R-Br surfaces and between 15-34% Br was measured on the M3BP surfaces. The differing amount of surface bromine determines the density of the polymer brush coatings of pSBMA and is therefore a critical factor in the coating synthesis. The coatings of M3BP were soaked to determine stability. After 1 hour of soaking, the coatings remained in-tact with 14-30% Br. To optimize the M3BP deposition, a full factorial design of experiment was used and it was determined that for the levels and factors probed, only the position had a significant effect on bromine density as measured by XPS. Then, a full factorial design of experiment was used to determine significant factors in the ARGET ATRP. For the levels and factors investigated, only the bromine density had a significant effect on protein adsorption. Here, higher density coatings—30% Br—limited protein adsorption better than less dense coatings. The SBMA coatings were confirmed using XPS and the wettability of the surfaces with pSBMA increased—the contact angle for the

pSBMA coatings was 12.7 ± 1.9° with a coating thickness of 34 ± 8.6 nm. Nonspecific protein adsorption as low as 17.5 ± 2.9 ng/cm^3 was achieved from pSBMA coatings on the M3BP surfaces. In another approach, BIBB was immobilized directly to the hydroxyl groups inherent in the catheter material. A coating of pSBMA was grown on this surface and achieved 43% less protein adsorption than the control. In a final approach, a carboxybetaine methacrylate (CBMA) hydrogel was synthesized on the surface and achieved 46% less protein adsorption. While promising, these methods present the potential to synthesize a robust nonfouling coating on any material and geometry. However these methods should be optimized further to introduce a superior ultra-nonfouling coating method for any biomaterial, creating great potential for clinical impact.

1.2 Investigating the Effects of pSBMA Chain Length and Density on Non-Specific Protein Adsorption

Most commonly, higher-density nonfouling polymer brush coatings are preferred as they seem to demonstrate superior nonfouling performance as compared to less-dense coatings[11,21]. Rarely is the chain length of the coating evaluated. Alternatively, it has been reported that for some materials in particular situations, less dense or shorter chain lengths reduce protein attachment to a higher degree[22]. Since we understand that water structure is the mechanism behind nonfouling character, we hypothesize that chain mobility is critical to synthesizing an ultra-hydrophilic, ultra-low fouling polymer brush coating to eliminate protein adsorption. In this work, the density and length of pSBMA polymer brush coatings were modified to examine the effect on interfacial water structure using sum frequency generation vibrational spectroscopy

(SFG) and protein adsorption. Coatings were synthesized using 2 methods. In the first method, surfaces were functionalized using the radio frequency plasma deposition of poly(hydroxyethyl methacrylate) (pHEMA) or M3BP. The traditional ATRP initiator, α-bromoisobutyryl bromide (BIBB), was immobilized to the hydroxyl groups on the pHEMA surfaces. At this point, the pHEMA-BIBB surfaces were measured using x-ray photoelectron spectroscopy (XPS) to contain 5-6 atomic % bromine while the M3BP surfaces were measured to contain 29-35% bromine. This large change in surface bromine controls the pSBMA brush density. From here, ATRP was used to synthesize the polymer brush coatings. SFG spectra were taken in water to measure the varying water structure for varying brush densities. In the second method, gold surfaces were used to take advantage of certain characterization techniques requiring model surfaces. Self-assembled monolayers of 2-mercaptoethanol (BME) and a varying nonreactive diluent were used to control the surface density. BIBB was immobilized to BME on the surface and then pSBMA coatings were grafted using ATRP. For these coatings, the chain length of pSBMA was modified using the addition of sodium chloride which raised the critical solution temperature, allowing higher molecular weight chains to remain soluble in the reaction solution and therefore grow longer than without the salt. Surfaces were evaluated using XPS to confirm the coating. Ellipsometry was used to measure the coating thicknesses and confirm varying chain length. For the particular systems observed, the ratio of tightly-bound water and loosely-bound water (3200 cm^{-1} and 3400 cm^{-1}, respectively) was 2.5 and 1.7 for M3BP and pHEMA-BIBB initiators, respectively. The higher ratio implies more tightly-bound water than loosely-bound. Correspondingly, the M3BP-inititated pSBMA coating had 26 ± 3 ng/cm^2 of bovine serum albumin (BSA) adsorption while the pHEMA-initiated coating had 117 ± 46 ng/cm^2 BSA adsorption. These results are consistent with most literature in that higher density nonfouling

coatings reduce protein adsorption to a higher degree than for less dense coatings. The corresponding SFG results confirm the nonfouling mechanism—water structure at the interface. To further-investigate the effect of polymer brush density versus chain length, various densities and lengths were grown *in situ* on QCM-D gold-coated sensors. The polymerization rate and overall mass was measured in real-time as well as the rate and mass of albumin adsorption. These experiments revealed low protein adsorption for moderately-low surface densities of pSBMA brushes and high adsorption for very high density, long brushes. These methods may be utilized to fully-optimize the pSBMA nonfouling coating and pair with information from SFG measurements to completely characterize the nonfouling mechanism.

1.3 GUIDING THE IMMUNE RESPONSE WITH SURFACE-IMMOBILIZED *DE NOVO* PROTEINS

The FBR ultimately occludes a rejected medical device due to collagen accrual and foreign body giant cells[4]. Macrophages are highly responsible for signaling fibroblasts into producing excess collagen. Previously, interleukin-4 (IL-4) has been shown to polarize macrophages to the M2 phenotype[5,23,24] in which anti-inflammatory cytokines are released and therefore pro-inflammatory cytokines are *not* released—the signals to fibroblasts[2]. With current advances in computational protein design, compute power, and machine learning, our collaborator computationally designed and then physically synthesized a *de novo* version of IL-4, adding ultra-stable features and an additional cysteine to the opposing side of the IL-4 receptor binding site. Native proteins most often denature on surfaces, triggering an immune response. This computationally-designed protein has been measured to be ultra-stable after extreme applied stresses and maintain very high binding affinity. In this work, I have proposed the use of

an S_N2 reaction to immobilize this *de novo* protein to the surface of a biomaterial based on a method reported by M. Simon et. al[25]. In this work, pHEMA hydrogels were made and used as a substrate. BIBB was conjugated to the hydroxyl groups in the pHEMA, functionalizing the pHEMA with a substitution-reactive alkyl bromide group. This brominated substrate was used to conjugate the thiol in the cysteine. L-cysteine and cysteine-containing peptides have been immobilized and confirmed using XPS. To confirm maintenance of bioactivity post-surface immobilization, a cysteine-containing cell adhesion peptide—containing the RGD sequence—was immobilized onto pHEMA hydrogels which otherwise resist cell adhesion. Fibroblasts were be cultured with the gels with pure pHEMA gels as controls. The surfaces were reviewed using optical and scanning electron microscopy to determine the extent of adhesion. Adhered fibroblasts suggest that the peptide remains biologically active and that this S_N2 reaction may be used to successfully immobilize the *de novo* IL-4 with the potential to encourage macrophage cells to the M2 phenotype. Since the field of computationally-designed therapeutics is growing, we predict that the need for surface immobilization chemistries will continue to rise and this study will provide a simple immobilization method useful for most cysteine-containing biomolecules.

1.4 Reducing the Risk of Bacterial Infection with Antibiotic Extended Release and Concentration Modeling

Increasing the lifetime of percutaneous insulin delivery catheters to minimize painful needle sticks increases the risk of infection. To combat surface-adherent bacteria and potential biofilm formation, we developed a method to impregnate levofloxacin antibiotic into the outer polymer of the catheter so that it can leach into the external medium. Complementarily, we

developed a method to quantify the concentration of antibiotic to ensure the minimum inhibitory concentration (MIC) is maintained throughout the duration of catheter use. Additionally, we have investigated the extent of antibiotic resistance after a zwitterionic nonfouling coating treatment to ensure suitable release after further surface modification. Levofloxacin was incorporated into the catheter through the swelling of the outer polyurethane of the bilayer catheter and subsequent solvent evaporation. The zone of inhibition was measured over time with S. *epidermidis* on LB agar plates. The release of levofloxacin was measured using optical absorbance spectroscopy in water and quantified against a linear standard curve at 292 nm. We developed a model using Fick's second law of diffusion to calculate the concentration around the catheter. Visible inhibition of bacterial growth and biofilm formation was shown for up to 38 days. A total of 8-45 μg of antibiotic was released over 26 days and a concentration of 820,000 μg/mL in the 0.17 μL control volume was reached at day 26 for the minimally-loaded samples, an amount many orders of magnitude greater than the MIC. After the nonfouling treatment, the lowest concentration reached was 16 μg/mL after 26 days. In conclusion, we have demonstrated a suitable method to induce antibacterial activity for insulin catheters, maintain the MIC, and sustain antibacterial character following further surface coatings.

Chapter 2. METHODS

2.1 MATERIALS

Insulin catheter tubing was separated from the Medtronic Quick-Set® Paradigm® insulin pump infusion set and was washed separately by 2-times sonication in each hexane, acetone, and methanol for 15 min and dried by vacuum in dessicator. 2-hydroxyethyl methacrylate (ophthalmic grade, Cat. No. 04675) was purchased from Polysciences, Inc (Pennsylvania, USA). Pyridine (CAS No. 110-86-1) and HEPES buffer (Cat. No. 15-630-106) were purchased from Fisher Scientific (Massachusetts, USA). Copper(II) bromide (CAS No. 7789-45-9, 2,2'-bipyridyl (CAS No. 366-18-7), α-bromoisobutyryl bromide (CAS No. 20769-85-1), L-ascorbic acid (CAS No. 50-81-7), [2-(Methacryloyloxy)ethyl]dimethyl-(3-sulfopropyl)ammonium hydroxide (CAS No. 3637-26-1), 2-mercaptoethanol (CAS No. 60-24-2), 1-heptanethiol (CAS No. 1639-09-4), bis[2-(2′-bromoisobutyryloxy)ethyl]disulfide (CAS No. 817637-79-9), L-cysteine (CAS No. 52-90-4), guanidinium chloride (CAS No. 50-01-1), D/L-methionine (CAS No. 59-51-8), D/L-dithiothreitol (CAS No. 3483-12-3), chloroform, methanol, n-hexanes, dichloromethane, LB broth with agar as powder, and methyl 3-bromopropionate (CAS No. 3395-91-3) were purchased from Sigma-Aldrich (Missouri, USA). Gly-Arg-Gly-Asp-Ser-Pro (GRGDSP) peptide was purchased from Vivitide (Massachusetts, USA). The Cys-Met-His-Cys-Met-His-Cys-Met-His (CMHCMGCMH) peptide was gifted from the Baker Lab at the University of Washington. The Gly-Cys-Arg-Gly-Pro-Gln-Gly-Ile-Trp-Gly-Gln-Leu-Pro-Glu-Ser-Gly-Gly-Arg-Cys-Gly (GCRGPQGIWGQLPESGGRCG) peptide was gifted from the DeForest Lab at the University of Washington. Staphylococcus epidermidis RP62A and NIH3T3 fibroblasts were used from lab stock. Carboxybetaine methacrylate and carboxybetaine

dimethyacrylate were gifted by the Jiang Lab at the University of Washington. Ultrapure (type 1) water was used throughout all work, deionized to a resistivity of 18.2 MΩ·cm at 25ºC using the Synergy® Water Purification System from MilliporeSigma. All reagents were used without further purification.

2.2 SURFACE FUNCTIONALIZATION

2.2.1 *Radio frequency plasma deposition (RFPD)*

Poly(hydroxyethyl methacrylate) (pHEMA)

Our lab's in-house radio frequency plasma reactor (**Figure 2.1**) was used to deposit poly(2-hydroxyethyl methacrylate) (HEMA) onto the surface of the substrate. A round-bottom flask was filled with 20 mL of HEMA. Keeping the valves closed, the reactor was pumped down to base pressure—less than 10 mTorr. The HEMA was degassed using 3 freeze/thaw cycles. To freeze, the molecule in the flask was frozen using a liquid nitrogen bath. The flask was then evacuated by vacuum by opening the valve of the flask to the reactor. Once base pressure was achieved, the flask was warmed with a mildly warm blow dryer from a distance so as to not polymerize the HEMA prematurely. Bubbles were released into the reactor under vacuum. When the molecule was thawed, the valve was closed, and the process was repeated until no bubbles were visible during the thaw process.

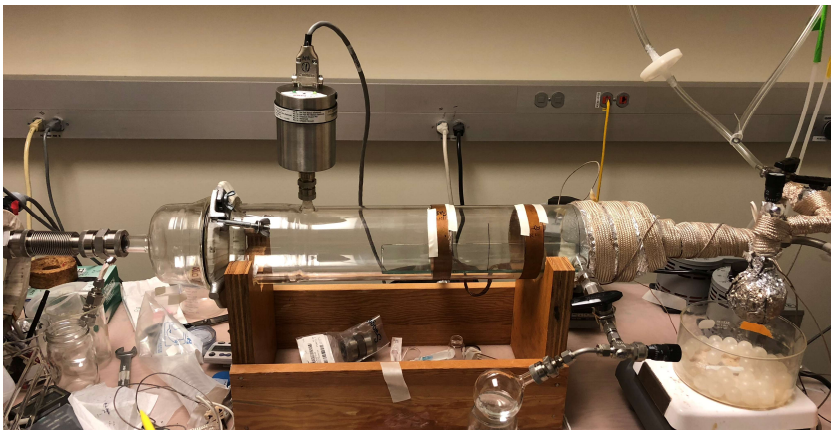

Figure 2.1. Ratner Lab plasma reactor in Foege Hall, University of Washington

After degassing the monomer, the reactor was vented and the substrates were inserted into the main chamber on a glass plate at a distance relative to the electrodes per experimental conditions. The reactor was sealed and pumped down to base pressure. Argon was added to the reactor to clean the substrates. The pressure regulator adjusted the pressure to 250 mTorr. The electrodes were set to a power of 60 W for 5 min. After the plasma treatment, the argon was evacuated by vacuum from the reactor until the reactor reached base pressure.

Methane was added to the reactor to aid with surface adhesion. The pressure regulator adjusted the pressure to 140 mTorr. The electrodes were set to a power of 80 W for 5 min. After the plasma treatment, the argon was evacuated by vacuum from the reactor until the reactor reached base pressure.

Then HEMA was added to the reactor. The pressure was set to 250 mTorr. Power and time were adjusted per experimental protocol. After the plasma deposition, HEMA was evacuated from the reactor until base pressure was achieved.

Argon gas was used to purge the reactor by opening the valve completely and then closing to return the reactor to base pressure thrice. The reactor was vented and then opened and

the samples were cleanly placed into clean tissue culture polystyrene petri dishes in a desiccator for storage until needed for further use. The samples stayed in the desiccator for at least 12 hours before use to quench excessively reactive surfaces.

Methyl 3-bromopropionate (M3BP)

The procedure for depositing M3BP was similar to that of HEMA in section 2.2.1.1. The only difference was that a pressure of 150 mTorr was used when M3BP was in the reactor. Power and time were adjusted per experiment.

2.2.2 *Self-assembled monolayers*

Gold surfaces, either gold-coated glass slides or QCM-D sensors, were functionalized using self-assembled monolayers (SAMs). For a SAM of 2-mecaptoethanol (BME), the substrate was immersed in 0.1 M of BME in ethanol for 14-24 hours[26]. To dilute the amount of hydroxyl functionalization on the surface, a 1:1 mole ratio was used of BME and a diluent. Either octadecanethiol or 1-heptanethiol was used as the diluent per experiment. In a second approach, a SAM of bis[2-(2'-bromoisobutyryloxy)ethyl] disulfide (BIBOED) was made on gold-coated surfaces. Cleaned gold surfaces (ethanol-washed by sonication 3 times) were immersed in an ethanolic solution of BIBOED (0.1% m/v) for 24 hours at room temperature[27]. Per experiment, the BIBOED was diluted with 1-heptanethiol in a 1:1 mole ratio.

2.2.3 *Immobilizing ATRP initiator to hydroxyl-functionalized surfaces*

For surfaces functionalized with a hydroxyl group—either an immobilized SAM of BME, plasma-deposited pHEMA, pHEMA hydrogel, or hydroxyl-inherent outer insulin catheter

polyurethane—111 mM of BIBB and 643 mM TEA were mixed in methylene chloride. Hydroxyl-functionalized surfaces were added to the solution for 24 hours at 4°C. Usually, 350 μL of BIBB and 350 μL of TEA were mixed in 10 mL of methylene chloride with up to 3 substrates 8mm in diameter. After the reaction, samples were washed with methylene chloride 3 times by sonication for 20 minutes and stored under vacuum until further use or analysis.

2.2.4 *Full factorial of methyl 3-bromopropionate*

A 3 factor by 2 level full factorial design of experiment was utilized to determine the significant factors in synthesizing a M3BP coating on the substrates. The effects of the design were bromine density and bromine stability. **Table 2.1** shows the design of the experiment used. The high power used was 80 Watts and the low power used was 7 Watts. High power is when initial adhesion of the molecule of choice occurs. Low power is used to thicken the coating of the molecule on the substrate and is when the growth occurs.[28] There had been discrepancy in our lab over the stability of a plasma-deposited film due to the location of the deposition in the chamber. Therefore the position of the samples was probed. Thinner films have traditionally been more durable and have hence resisted delamination better than thicker films. The growth period of the film at low power was probed to investigate this effect.

Table 2.1. Factorial design of plasma-deposited M3BP

Factor	Level (-1)	Level (+1)
Location in chamber	Middle of electrodes	Downstream of electrodes
Time at high power (80W)	20 sec	60 sec
Time at low power (7 W)	4 min	8 min

Table 2.2 is a key for each run used to determine the significance of each factor for the experiment and corresponds to the input of high and low levels coded for the design of

experiment software, Minitab®. After synthesizing the films in the plasma reactor per run conditions specified, one of the samples was soaked for one hour in 1:1 methanol:water and dried by desiccator. The samples were then analyzed for atomic surface composition using XPS.

Table 2.2. List of run descriptions for full factorial design of plasma-deposited M3BP

Run	Location	High Power	Low Power
1	Middle	20 sec	4 min
2	Middle	20 sec	8 min
3	Middle	60 sec	4 min
4	Middle	60 sec	8 min
5	Downstream	20 sec	4 min
6	Downstream	20 sec	8 min
7	Downstream	60 sec	4 min
8	Downstream	60 sec	8 min

2.3 SYNTHESIZING NONFOULING COATINGS

2.3.1 *ARGET ATRP with SBMA*

To make the polymerization solution, 72 mM of [2-(methacryloyloxy)ethyl]dimethyl-(3-sulfopropyl)ammonium hydroxid (SBMA), 74 mM of ascorbic acid, and 36 mM of sodium chloride (NaCl) were dissolved in ultra-pure water per experiment. Some experiments did not include NaCl during polymerization. Separately, 6.6 mM of copper(II) bromide ($CuBr_2$) and 70 mM 2,2'-bipyridyl (bpy) were dissolved in methanol. Both solutions were sonicated for 5 minutes to ensure dissolution. A 3:2 volumetric ratio of methanolic solution to aqueous solution was used. Then, the aqueous mixture was poured into the methanolic mixture to make the ATRP solution. The ATRP solution was degassed for 60-90 minutes by bubbling nitrogen gas. Then, brominated substrates were added to the mixture for 2-4 hours per experiment with gentle

agitation at room temperature. After the polymerization, samples were removed and washed with 1:1 (v/v) methanol and water 3 times by sonication for 20 minutes, dried, and stored under vacuum until further use or analysis.

2.3.2 *Full factorial of SBMA coating*

A 4-factor by 2-level full factorial design of experiment was used to probe significant factors in the ATRP of SBMA using the Scheme 2 preparation. The measured effect of the design was protein adsorption. **Table 2.3** shows the design of experiment used. The levels of the factors probed were the result of our lab's ARGET ATRP protocol for SBMA polymer brushes and other ratios found in literature.

Table 2.3. Factorial Design of ARGET ATRP conditions

Factor	Level (-1)	Level (+1)
Amount SBMA/8mm disk	120 mg	200 mg
Ascorbic Acid: $CuBr_2$	10 (mol/mol)	50 (mol/mol)
Amount bipyridine	5 mg	30 mg
Water: MeOH	1:4	1:1

Table 2.4 is a key for each run used to determine the significance of each factor for the experiment. After synthesizing the samples per run experimental conditions, the samples were analyzed by XPS for surface composition and by radiolabeled protein adsorption assay. The statistical analysis was carried-out using Minitab®.

Table 2.4. List of run descriptions for full factorial design of ARGET ATRP conditions

Run	SBMA	Ascorbic Acid: $CuBr_2$	Bipyridine	Water:MeOH
1	120	10	5	1:4
2	120	10	5	1:1
3	120	10	30	1:4
4	120	10	30	1:1
5	120	50	5	1:4
6	120	50	5	1:1
7	120	50	30	1:4
8	120	50	30	1:1
9	200	10	5	1:4
10	200	10	5	1:1
11	200	10	30	1:4
12	200	10	30	1:1
13	200	50	5	1:4
14	200	50	5	1:1
15	200	50	30	1:4
16	200	50	30	1:1

2.3.3 *CBMA surface-grafted hydrogel*

The same molar ratios and surface preparation steps were used for the grafting of the CBMA hydrogel. After 5 minutes of polymerization, 1 mol% of the CBMAX crosslinker was added to the polymerization solution. After 4 hours of polymerization by gentle agitation at room temperature, the samples were removed, washed with 1:1 (v/v) water to methanol, and stored under vacuum until further use or analysis.

2.4 IMMOBILIZING BIOMOLECULES USING AN S_N2 REACTION

For surfaces brominated with either a tertiary alkyl bromide or RFGD plasma-deposited M3BP, cysteine-containing molecules were immobilized using a simple and fast S_N2 reaction[25]. First the alkylation buffer was prepared (1 M HEPES pH 7.8, 4 M guanadinium chloride, 10 mM D/L-methionine; 980 ml), and dithiothreitol (DTT) was added (20 ml of 1 M) immediately before use.

In 1 mL of the alkylation buffer per experiment, either 5 mg L-cysteine, 1.5 mg of the GCRGPQGIWGQLPESGGRCG peptide, 0.8 mg of the CMHCMGCMH peptide, or 0.5 mg of the GRGDSPC peptide were added to the alkylation buffer. The reaction reduced for 1 hour at 37°C in the dark in an incubator. Then, the brominated substrates were added to the solution and heated to 50°C for 2.5 hours. After that time 20 μL of the 1 M DTT was added and the reaction continued at 50°C for another 2.5 hours. The reaction was quenched with 100 μL of 2-mercaptoethanol (BME). A washing solution was made of 3 mM BME in HEPES. Samples were washed 3 times by sonication for 20 minutes with the washing solution. Solid samples were stored under vacuum until analysis. pHEMA hydrogel samples were stored in PBS overnight. The PBS was changed every day until further use.

To the substrate surface, methyl 3-bromopropionate (M3BP) was plasma-deposited to functionalize the surface with chemically available bromine. A protocol similar to that described by M. Simon et. al. was used to conjugate the cysteine[29]. To conjugate cysteine, 5 mg of cysteine was dissolved in alkylation buffer (1 M HEPES pH 7.8, 4 M guanadinium chloride, 10 mM D/L-methionine; 980 ml), and dithiothreitol (DTT) was added (20 ml of 1 M) immediately before use. The cysteine was reduced for 1 hr at 37ºC. Brominated substrates were added and the reaction was heated to 50ºC with occasional mixing. After 2.5 hr, DTT was added (10 mL of 1 M) and the reaction was allowed to proceed for another 2.5 hr. The reaction was quenched with 2-mercaptoethanol (BME) (50 mL, 14.2 M) and then washed with ultra-pure water. The samples were stored under vacuum until analyzed with XPS for surface composition.

2.5 LEVOFLOXACIN IMPREGNATION, EXTENDED RELEASE, AND CONCENTRATION MODELLING

2.5.1 *Levofloxacin Impregnation*

Tubing was cut into 1.5 cm length pieces—a length chosen to be similar to the portion inserted into a diabetic user—washed by sonication in hexane, acetone, and then methanol twice for 10 minutes, and dried under vacuum overnight. Similar to processes described previously[30–32], Levofloxacin was dissolved into a 1:4 (v/v) mixture of chloroform:methanol. Methanol was added to reduce the drastic swelling and separation of the inner layer of polyethylene from the rest of the catheter. The catheter pieces were added to the solution at room temperature, gently agitated, removed after 30 min, and dried in a fume hood overnight at ambient pressure so as to not break polymeric crosslinks and to maintain the polymer structure and elasticity.

2.5.2 *Release Profile Assay*

A single piece of tubing was placed in 5 mL of release solution. At time points, the tubing piece was transferred to a new release solution and the optical absorbance at 292 nm was measured, all occurring at room temperature. Our own calibration

$$C = 12.14 \cdot A - 0.052 \tag{2.1}$$

where C is the concentration of levofloxacin in the release solution (mg/L) and A is the optical absorbance—where the R^2 value is 0.9987—was used to determine the concentration of levofloxacin in the 5 mL of release solution at each time point.

2.5.3 *Bacterial Inhibition Assay*

A 1.5 cm piece of catheter was implanted into a plate of LB agar until flush with the surface, resulting in no change of topography. An inoculum of Staphylococcus epidermidis RP62A was deposited onto the plate and spread evenly. After 2-3 days of incubated growth at 37ºC, the zone of inhibition was measured—an average of at least 10 measurements—around the catheter and the piece was explanted from the agar and re-plated into a fresh plate of agar followed by the spreading of a fresh inoculum of S. *epidermidis*.

2.5.4 *Levofloxacin Concentration Model*

Diffusion of levofloxacin through ECM is 2-dimensional and can be described by Fick's second law[33], equation 2.2

$$\frac{\partial C}{\partial t} = -D\frac{\partial^2 C}{\partial x^2} \tag{2.2}$$

Using a function defined as

$$y = \frac{x}{2\sqrt{Dt}} \tag{2.3}$$

equation 2.2 was solved with the first boundary conditions as:

$$C_x = C_0 \text{ for } y = 0 \text{ at } t > 0 \text{ and } x = 0$$
$$C_x = C_{bulk} \text{ for } y = \infty \text{ at } t = 0 \text{ and } x > 0$$

the second boundary conditions as:

$$C_x = C_x \text{ at } y < \infty$$
$$C_x = C_{bulk} \text{ at } y = \infty$$

and assuming that $C_{bulk} = 0$ at $y = \infty$. This resulted in a solution to equation 2.2[34]

$$C_x = C_0\left[1 - erf\left(\frac{x}{2\sqrt{Dt}}\right)\right] \tag{2.4}$$

Represented for the following numerical calculations for the data collected, equation 2.4 can be written as

$$C_x(t) = C_{x=0}(t)\left[1 - erf\left(\frac{x}{2\sqrt{Dt}}\right)\right] \tag{2.5}$$

The diffusivity was calculated using the Stokes-Einstein relation

$$D = \frac{kT}{6\pi\eta R} \tag{2.6}$$

where *k* is the Boltzmann constant, *T* is the temperature of 37°C, η is the dynamic viscosity (note: the viscosity of water at 37°C was used as 0.6913 mPa·sec), and *R* is the radius of the levofloxacin molecule (approximated as 9Å)[35]. The diffusivity was therefore calculated as 3.65 X 10^{-6} cm^2/sec which is consistent with the diffusivity of levofloxacin in a biofilm of Pseudomonas aeruginosa calculated experimentally to be 2.28 X 10^{-6} cm^2/sec [36] and to levofloxacin in agarose hydrogels between 4.2 and 5.1 X 10^{-6} cm^2/sec [37]. Using the experimental total drug released over time data, the numerical slope of the line was calculated at each time point using forward differentiation and these values were used as C_0 for each time point. From here, the concentration over time was calculated with respect to distance from the catheter/adipocyte interface with

$$C_{total}(x) = \int_0^{2\pi}\int_0^{l}\int_0^{2d} C_{x=0}(t)\left[1 - erf\left(\frac{x}{2\sqrt{Dt}}\right)\right] dx\, dl\, d\theta \tag{2.7}$$

where *d* is approximated as 1 μm for the diameter of 1 bacteria, *l* is 15 mm for the length of tubing inserted into the patient, and C_{total} has units of μg/mL·15 mm piece of tubing. The total

concentration around the catheter within 2 diameters of bacteria was calculated numerically using the experimental release data.

Numerically, the triple integral in equation 2.7 was evaluated for each concentration calculated at each time point as

$$C_{total}(t) = \sum_{x=0}^{1\,cm} C_{x=0}(t)\left[1 - erf\left(\frac{x}{2\sqrt{Dt}}\right)\right] \cdot \pi[(x+i)^2 - x^2] \tag{2.8}$$

Rings around the catheter were defined incrementally to calculate the concentration at each interval away from the centerpoint of the cylindrical catheter with circular symmetry.

2.5.5 *Nonfouling Coating*

After the catheter was impregnated with levofloxacin, HEMA was polymerized by radio frequency plasma deposition onto all surfaces. The atom transfer radical polymerization (ATRP) initiator, BIBB, was attached by reaction for 24 hours with pyridine in dichloromethane and methanol at 5°C. Activator regenerated by electron transfer (ARGET) ATRP was conducted for 3 hours at room temperature as per previously published by D. Hong et. al.[21]

2.6 SURFACE CHARACTERIZATION

2.6.1 *X-ray photoelectron spectroscopy (XPS)*

A Surface Science Instruments S-Probe was used for surface analysis. The instrument was equipped with a monochromatic Al Kα x-ray source. The samples were non-conducting and a low energy electron flood gun was used for charge neutralization. A spot size of 800 μm

diameter was used. Pressure during analysis in the chamber was less than 5×10^{-9} Torr. For low resolution survey scans, a pass energy of 150 eV was used from 0 to 1100 eV with a 1 eV step size. The data were analyzed with the Service Physics HAWK version 7 data analysis software to fit peak areas and determine relative surface composition. All binding energies were calibrated with reference to the carbon 1s line at 285.0 eV. A linear background was used for all spectra.

2.6.2 *Attenuated total reflectance Fourier transform infrared spectroscopy (ATR FTIR)*

A Vertex 70 ATR FTIR was used to observe the composition of the catheter outer polymer. Transmittance spectra were taken from 4500 to 400 cm^{-1} with a resolution of 2 cm^{-1} with respect to the background of air.

2.6.3 *Radiolabeled protein adsorption assay*

Materials

Albumin from human serum (Cat. No. 70024-90-7), sodium azide (Cat. No. S2002), and sodium iodide (NaI) (Cat. No. 383112) were purchased from Sigma-Aldrich. Boric acid (Cat. No. A73-500), sodium phosphate monobasic (Cat. No. S369-500), and sodium hydroxide (Cat. No. S399-500) were purchased from Fisher Scientific. Sodium chloride crystals (Cat. No. SX0420-3) was purchased from EMD Millipore. Citric acid, monohydrate (Cat. No. 0115-01) was purchased from J.T. Baker. Iodine-125 radionuclide (Specific Activity: ~17Ci/mg, 10-5M NaOH (pH 8-11)) was purchased from Perkin-Elmer (Cat. No. NEZ033A).

Protein iodination using ICl method

Albumin was radiolabeled using the iodine monochloride (ICl) method.[38] Briefly, 1mCi of Iodine-125 radionuclide was added to a prepared 0.5 mL 2x borate solution. 0.5 mL of 2:1 ICl:NaCl solution and 1 mL of a 10 mg/mL albumin in a citrate phosphate buffered saline solution with sodium azide (cPBSz) were added. The iodination reaction occurred for 20 min on ice. After the reaction, the solution was run through a size exclusion chromatography column. Fractions—more than 30—were collected and measured using a gamma counter to capture the fractions with the greatest activity. The ratio of the intensity of the first peak—radiolabeled albumin—to the second peak—free protein—was used to evaluate the iodination efficiency. The fractions with the greatest activity from the first peak were combined and run through a second chromatography column, adding more cPBSz, repeating fraction collection and peak identification. Purified radiolabeled protein fractions were combined, kept on dry ice, and used within the next day for the adsorption assay.

I-125 radiolabeled albumin from human serum protein adsorption

The samples to be analyzed (n = 4) were soaked in 0.5 mL cPBS solution and 10mM NaI (cPBSzI) for at least 2 hours. During this pre-adsorption period, the radiolabeled albumin was thawed and added to a 0.2 mg/mL solution of albumin in cPBSzI to create a 'hot protein' mixture with an activity of ~200 CPM/ng. 0.5 mL of the hot protein was then added to each sample collection cup and allowed to adsorb for 2 h. After this time, the samples were washed 3 times for 3 seconds each with cPBSzI with a continuous flow rinsing system. The samples were transferred to a gamma counter tube and the radioactivity of each sample was measured for 1 min along with protein standards using a Perkin Elmer Wizard 2 Gamma Counter. From the

activity of each sample, the original activity of the hot protein along with the concentration was used to calculate the amount of protein on each sample.

2.6.4 *Sum frequency generation (SFG)*

In this work, a picosecond Nd:YAG laser system was used to determine the extent of water order at the nonfouling coating interface with buffered water. A CaF_2 prism was cleaned with an ozone cleaner and one face was prepared with a nonfouling coating which would sit face-down onto a sample stage. A sample stage was available with a small reservoir under the prism for the phosphate buffered saline (PBS) solution. For the SFG system, the pulse length of the visible beam (532 nm, frequency doubled from the 1064 nm fundamental wavelength of the Nd:YAG) was about 32 ps. The IR beam was generated by an OPG/OPA/DFG unit pumped by a 1064 nm beam and a frequency doubled beam at 532 nm from the Nd:YAG laser. For the visible beam, the temporal overlap was adjusted manually with a delay stage. The power and polarization state were each controlled with 2 half-wave plates on each side of a polarizer. For the IR beam, the polarization was controlled by a polarization stage and the SFG signal was filtered with a polarizer and notch filters. The incidence beams of the IR and visible were adjusted to just under the critical angle for total internal reflection at the solid/liquid interface. Full spectra were collected at 50 Hz repetition rate.

2.6.5 *Quartz crystal microbalance with dissipation (QCM-D)*

Quartz crystal microbalance with dissipation (QCM-D) was used to measure the rate of polymerization in real time and the overall nonspecific protein adsorption using the changes in mass and viscoelastic properties[39–44]. In this work, gold QCM-D sensors were cleaned using a

piranha etch. Then, sensors were cleaned with ethanol immediately prior to the immobilization of bis[2-(2'-bromoisobutyryloxy)ethyl] disulfide (BIBOED) and 1-heptanethiol diluent per experiment. These sensors were loaded into separate acoustic sensing chambers in the QCM-D [Q-sense E4, Biolin Scientific, Gothenburg, Sweden].

The QCM-D method is based on the piezoelectric effect where a voltage is applied across a piezoelectric quartz crystal—the gold-coated sensor. The material oscillates and the frequency of oscillation is dependent on the amount of material on the crystal. When the applied voltage is turned off, the voltage decay is measured as the dissipation. The viscoelasticity is the rigidity of the deposited layer on the crystal and causes the voltage to decay at different rates[45–47].

Here, the ARGET ATRP solution was flown through the QCM-D channels followed by extensive washing in PBS and water (**Table 2.5**). All experiments were conducted with an instrument setting of 25°C and a constant flow rate of 0.1 mL/min was used. Great care was taken to limit air introduced into the lines during the experiments. The protein adsorption was measured using 1 mg/mL BSA in PBS followed by a PBS wash. All sensors have a fundamental frequency of 4.95 MHz, though a baseline reading was taken for each cleaned sensor prior to any surface modifications.

Table 2.5. Order of solution flown through the QCM-D channels.

Number	Reagent	Time (min)
1	Air	10
2	PBS	30
3	Polymerization Solution	200
4	PBS	40
5	DI water	40
6	PBS	20
7	1 mg/mL albumin	40
8	PBS	20
9	Water	10

The mass adsorbed to each sensor was calculated with the Sauerbrey model

$$\Delta f = \frac{2{f_0}^2}{A\sqrt{\rho_q \mu_q}} \Delta m \tag{2.9}$$

where f_0 is the resonant frequency, A is the area of the quartz crystal sensor, ρ_q is the density of quartz, μ_q is the shear modulus of quartz for the AT-cut crystal, Δf is the measured change in frequency, and Δm is the calculated change in mass[48]. This model is only valid when the dissipation change is low—5% of the change in frequency or less. This is considered rigid and applies to the polymer brush coating and the adsorbed protein[49,50].

2.6.6 *Contact Angle*

For dry samples, a static contact angle was measured with a 2 µL drop of ultra-pure water using a FTA200 contact angle goniometer under ambient laboratory conditions. Three or four measurements were taken per sample[51].

2.6.7 *Fibroblast adhesion assay*

In 48 well plates, 5×10^4 cells/well were pre-incubated with media for 15 minutes. pHEMA hydrogel disks with immobilized RGD peptide or pure pHEMA hydrogel disks as a control group were added to the bottom of clean wells. The cells were plated on top of the disks and incubated at 37°C for 2, 6, and 48 hours. At cell harvest, samples were rinsed in the well 3 times with 1x PBS and transferred to a new well. 400 µL trypsin/versine was added and incubated for 5 minutes. The samples were rinsed with trypsin/versine and the wash was transferred to an Eppendorf tube. The samples were then rinsed with PBS twice and the wash was added to an

Eppendorf tube. The tubes were spun-down for 5 minutes in the microfuge. Media was aspirated. The cell pellet was resuspended in 100 µL of media and cells were counted without further dilution.

The samples were then fixed. Karnovsky's solution was prepared fresh using the prepared Karnovsky's fixative from the kit. 5 mL ultra-pure water, 5 mL of 0.2M sodium phosphate buffer, 15 mL of 0.2M sodium cacodylate, and 6 mL of Karnovsky's fixative were mixed to make Karnovsky's solution. Samples were rinsed in-well twice with 0.2M sodium phosphate buffer. Karnovsky's solution was added to each well and samples were fixed for 2 hours at room temperature or overnight at 4°C.

A CaCo rinse was prepared (25 mL ultra-pure water, 25 mL of 0.2M sodium phosphate buffer, and 50 mL of 0.2M sodium caocodylate). Samples were rinsed with the CaCo rinse 3 times for 10 min at room temperature. For SEM, an osmium tetroxide (OsO_4) stain was prepared (2 mL of water, 2 mL of 0.2M sodium phosphate buffer, 8 mL of 0.2M sodium cocodylate, and 4 mL of 4% osmium tetroxide). The samples were stained using 1.5 mL of the OsO_4 stain for 30 min at room temperature and then rinsed with 2 mL of the CaCo rinse 3 times for 10 min at room temperature. Finally, the samples were rinsed in 50% ethanaol twice for 5 min. Then samples were rinsed once in 70% ethanol for 15 min and then stored in 70% ethanol at 4°C.
On the day of SEM imaging, samples were rinsed in 80% ethanol for 15 min, 90% ethanol for 15 min, and then 100% ethanol for 15 min. Samples were then stored in 100% ethanol and critical point dried with 100% ethanol and CO_2.

2.6.8 *Scanning electron microscopy (SEM)*

Samples were sputter coated with gold 3 times for 60 sec at 6.0 mA [MCM-200 Ion Sputter Coater, SEC Co., Gyeonggi-do, Korea] before loaded into the microscope. Images were taken at various magnifications using the SEM [SNE-3200M, SEC Co., Gyeonggi-do, Korea].

2.6.9 *Cytotoxicity assay*

Following the protocols described in ISO 10993-5, the treated tubing was determined to be non-toxic to NIH3T3 fibroblasts.

Chapter 3. REDUCING PROTEIN ADSORPTION WITH ZWITTERIONIC PSBMA COATINGS

3.1 INTRODUCTION

The triggering event in the foreign body reaction (FBR) is instantaneous and tenacious protein adsorption onto a biomaterial.[1,3] We hypothesize that a significant reduction in protein adsorption will lessen the extent of the FBR and therefore prolong the lifetime of the insulin catheter at a single infusion site. To eliminate protein attachment, we have designed a non-fouling coating utilizing the hydrophilic, nonfouling characteristics of zwitterionic polymers, specifically sulfobetaine methacrylate (SBMA) (**Figure 3.1**).

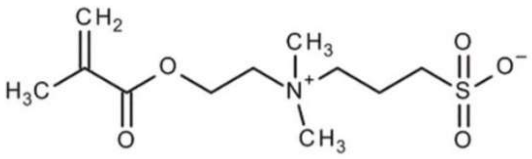

Figure 3.1. Molecular structure of SBMA

In this case, 'nonfouling' refers to the inhibition of protein adsorption to a biomaterial surface. A variety of methodologies have been developed over the last ~70 years to achieve lower protein attachment. Most of these strategies involve hydrophilic materials since it has been well-established that hydrophilic surfaces have better nonfouling character[52]. However, some strategies involve hydrophobic surfaces to purposefully tight-bind albumin and resist subsequent protein adsorption, as described by the Vroman effect, which would trigger the FBR[3]. Nonetheless, engineered nonfouling hydrophobic surfaces are few and far between and most nonfouling surfaces have been designed to achieve considerable hydrophilicity. An array of synthetic hydrophilic surfaces have been designed with the front-runners being poly(ethylene

glycol), poly(2-hydroxyethyl methacrylate), and polymers and copolymers of lactic and glycolic acids. In many cases, combinations of these and other organic components have been engineered into systems for drug delivery, tissue regeneration, and other implantable biomaterials and may even be biodegradable. Methods for assembling these materials into self-assembled monolayers (SAMs) still provide ease for surface coatings. The most popular nonfouling material is poly(ethylene glycol) but more recent studies have shown the material to create immunogenicity issues[53,54]. Some nonfouling materials are bioinspired e.g. SBMA. Cell membranes are composed of the lipid bilayer phenomenon, containing a hydrophilic head. This head is a phosphoryl choline group—a zwitterionic moiety. Phosphoryl choline has been successfully combined with a polymerizable moiety to coat biomaterial surfaces and provide extensive biocompatibility and reduction of the FBR[55]. Other zwitterionic molecules have been developed and synthesized to perform as well as the natural phosphoryl choline. Most commonly, these bioinspired materials are carboxybetaine and sulfobetaine and have been found to eliminate the effects of the FBR in hydrogel form[56,57].

In this work, SBMA is extensively utilized. SBMA has shown to perform well in resisting protein attachment on surfaces[11,58–60]. As a hydrogel, SBMA has been shown to promote complete skin generation[61] and therefore has potential as a surface coating. For this project, I have grafted SBMA to the surface of the catheter by polymerizing the methacrylate into a polymer brush. Activators regenerated by electron transfer (ARGET) atom transfer radical polymerization (ATRP) was used to synthesize the SBMA coating on the surface (**Figure 3.2**)[21]. ATRP is commonly used to polymerize methacrylates[62]. ARGET ATRP is a more convenient and safer version of traditional ATRP because the reaction may be conducted under ambient conditions in the lab and with no pressurized vessels or liquid nitrogen[63] and has been used to

synthesize polymer brush coatings of a similar molecule, carboxybetaine methacrylate, achieving highly-nonfouling success[21]. In ARGET ATRP, the addition of L-ascorbic acid regenerates the catalyst so that a very small amount is used and is not as sensitive to air. In this work, the polymerization protocols have been systematically modified to investigate the effect of the conditions on protein adsorption.

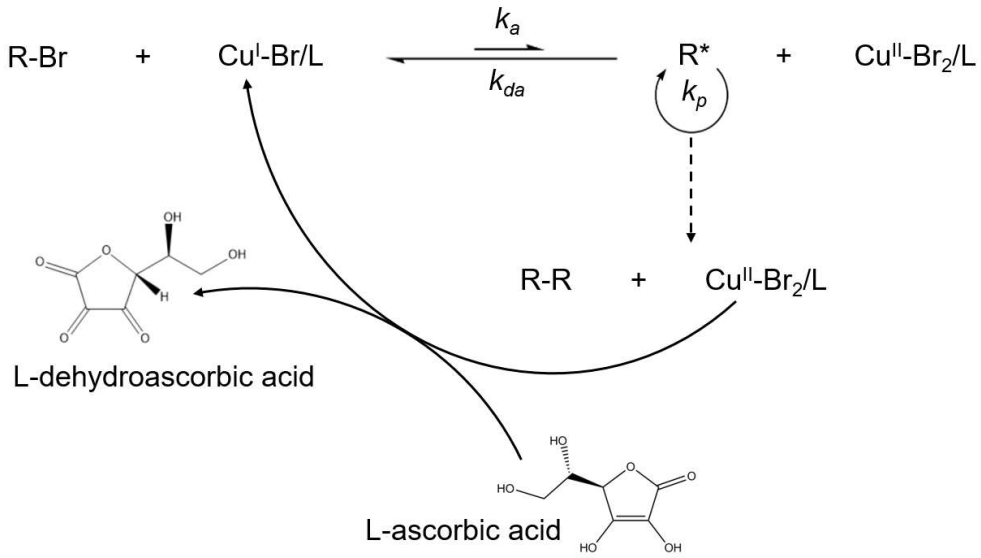

Figure 3.2. Schematic of the ARGET ATRP reaction

Radio frequency plasma deposition of the ATRP halogen initiator via small organic molecules was used to functionalize the catheter surface[64]. The plasma-deposition of the initiator creates a robust surface functionalization for the round geometry of the catheter[28]. I used a full factorial design of experiment (DOE) to determine significant factors on the effect of initiator density and stability. The full factorial DOE is a useful tool—used mostly in manufacturing—to efficiently determine which factors in a process have a statistically significant effect on a given quantifiable outcome. Those factors can then be optimized for a favorable product. For this project, the measured effect is protein adsorption.

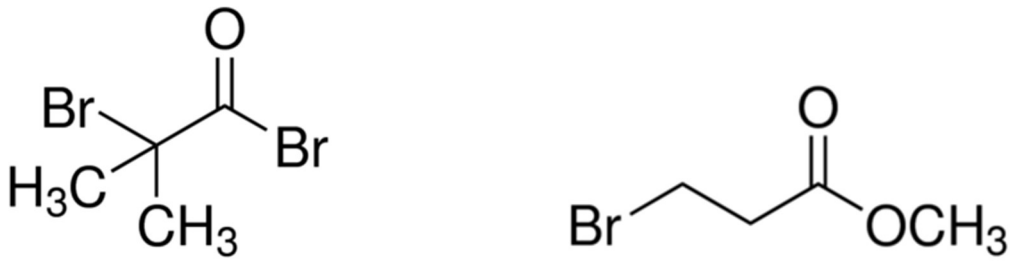

Figure 3.3. ATRP initiator molecules (left) α-bromoisobutyryl bromide and (right) methyl 3-bromopropionate

In this work, I investigated 3 different initiator functionalization methods resulting in 3 different initiator densities. Higher density polymer brush coatings are known to historically resist protein adsorption better than less dense coatings[65,66]. In one method, 2-hydroxyethyl methacrylate (HEMA) was plasma-deposited and subsequently functionalized in a simple reaction with α-bromoisobutyryl bromide (BIBB), the traditional ATRP initiator[67] (**Figure 3.3 left**). HEMA is an FDA-recognized, common biomaterial that has been used commercially since the 1970's for contact lenses with good biocompatibility[68,69]. In the second method, methyl 2-bromopropionate (M3BP) was plasma deposited, directly functionalizing the surface with the halogen initiator (**Figure 3.3 right**). The 2 methods were compared in protein adsorption resistance ability, cytotoxicity, and overall biocompatibility. As a third approach, I attempted to functionalize biomedical polyurethane—containing chemically available hydroxyl groups—with the ATRP-initiating BIBB.

In a more creative attempt to graft the nonfouling zwitterion to the catheter surface, carboxybetaine methacrylate (CBMA) hydrogel success in mice *in vivo* inspired a new method[70]. As a hydrogel, subcutaneously implanted CBMA, a molecule very similar to SBMA, triggered no visible FBR after 3 months[56]. In my work, I attempted to graft the CBMA hydrogel directly to a surface by plasma-depositing the ATRP initiator, starting the ATRP of CBMA, and then

quickly adding the CBMA crosslinker. Surface-grafted hydrogels have shown to be tailored to have specific interfacial and mechanical properties that may be beneficial to preventing protein adsorption on the insulin catheter, ultimately preventing fibrotic deposition and consequential occlusion[71].

3.2 Results and Discussion

3.2.1 *Synthesizing the SBMA polymer brush coatings*

Poly(HEMA) is a common biomaterial which conveniently contains hydroxyl groups to immobilize the traditional ATRP initiator, α-bromoisobutyryl bromide (BIBB). Scheme 1 shows a method for synthesizing the SBMA polymer brush coating using the BIBB functionalization. In the first step, HEMA is plasma-deposited onto the substrate. BIBB is then anchored with a simple substitution reaction. The BIBB was then used as the ARGET ATRP initiator, as it is a widely used, traditional, molecule for ATRP initiation.

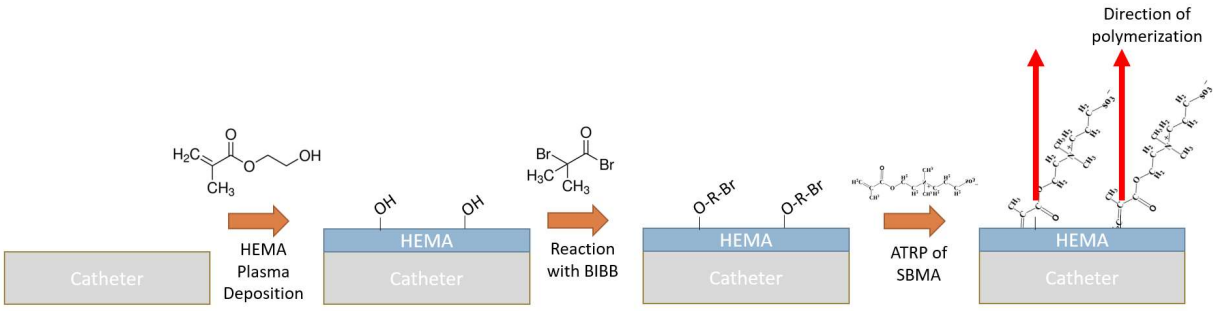

Scheme 1. SBMA brush synthesis using BIBB as the ATRP initiator

To achieve higher initiator density for a better nonfouling coating, methyl 3-bromopropionate (M3BP) was plasma deposited, thereby directly functionalizing the surface with the ATRP

initiating halogen. Scheme 2 shows our method for synthesizing the SBMA polymer brush coating using the M3BP functionalization.

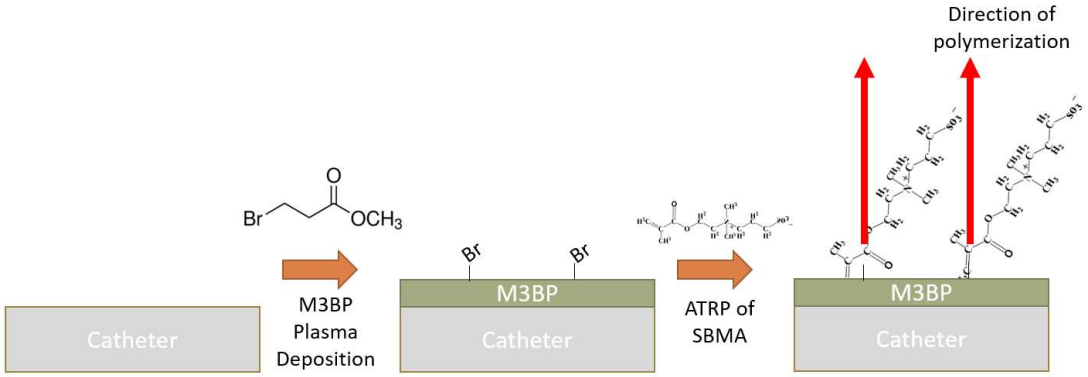

Scheme 2. SBMA brush synthesis using M3BP as the ATRP initiator

In a third approach, the hydroxyls present in the polyurethane of the catheter were used to directly react with the BIBB, thereby functionalizing the surface with the traditional ATRP molecule. Scheme 3 shows our method for synthesizing the SBMA coating directly to a polyurethane substrate.

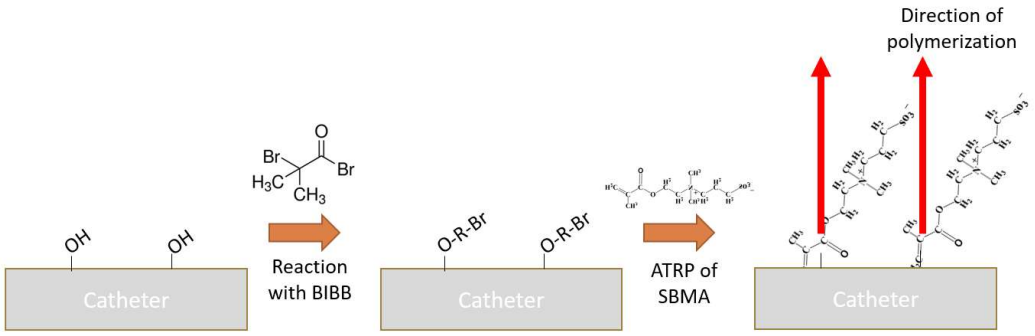

Scheme 3. SBMA brush synthesis using BIBB on a polyurethane substrate as the ATRP initiator

3.2.2 *The catheter polyurethane contains hydroxyl groups.*

Early-on, an ATR-IR spectra of the catheter outer polymer was investigated. A broad peak at 3350 cm^{-1} was observed indicative of hydroxyl groups (**Figure 3.4**). The present hydroxyl groups were used for the anchoring of the ATRP initiator, BIBB, for the synthesis of the SBMA nonfouling coating in Scheme 3.

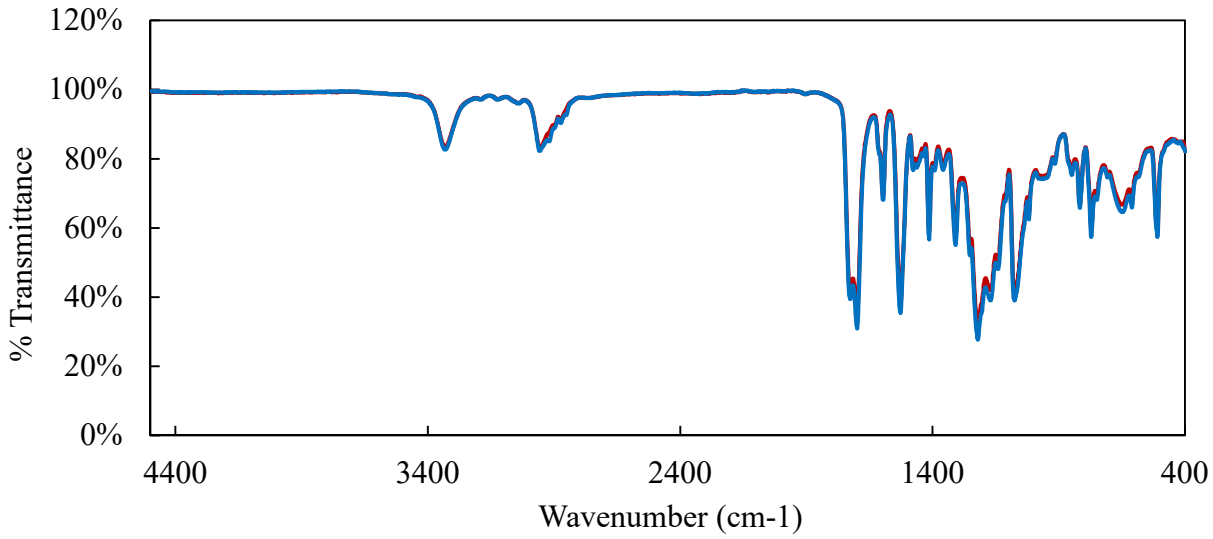

Figure 3.4. ATR-FTIR spectra of insulin catheter outer polymer

3.2.3 *BIBB coating validation and bromine density*

Stochiometrically, the BIBB molecule after reacting with the hydroxyl groups on a surface contains 16.7% bromine. The amount measured is much less than this since the penetration depth of XPS analysis in about 100 Å and therefore the instrument measures atoms present below the level of the anchored BIBB, including the pHEMA film and possibly the polyurethane—which contains nitrogen (**Figure 3.5**). The silicon observed is mostly likely contamination from the surface analysis lab since it is not present in the HEMA coating prior to the BIBB reaction. The nitrogen observed indicates that the HEMA coating was most likely not

stable and partially delaminated since the XPS results for the HEMA coating are very similar to that of theory. From this data, it is observed that 5.6% bromine has been anchored to the surface. It is assumed that 100% of that bromine is available to function as the ATRP initiator to synthesize the nonfouling coating. Therefore, for Scheme 1, it is assumed that the polymer brush density will be close to 5.6% on the surface.

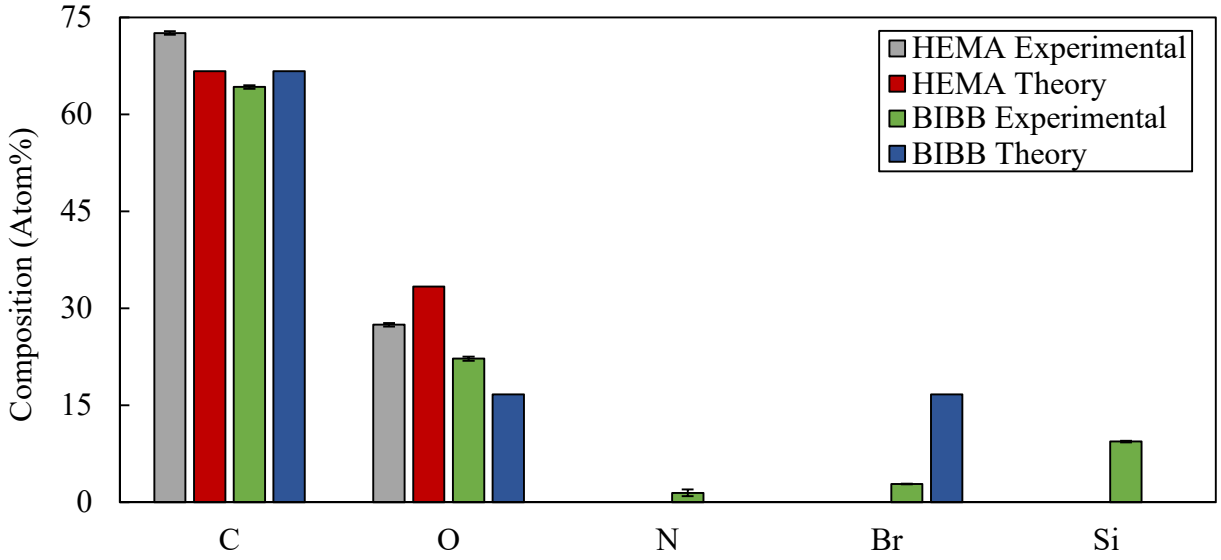

Figure 3.5. Composition of the plasma-deposited HEMA film and the BIBB anchored to the HEMA measured by XPS survey scan

3.2.4 *M3BP coating validation and bromine density*

Stoichimetrically, M3BP contains 14.3% bromine. During the plasma deposition, the molecule is fragmented resulting in a surface that contains more than double the amount of theoretical bromine (**Figure 3.6**). Depending on experimental conditions, the amount of stable bromine differs. The data shown is for a partially-optimized protocol for the plasma deposition. These conditions have been used for the majority of noteworthy work presented in this document,

assuming a 31% polymer brush density due to the 31% bromine recognized by the XPS spectra as the ATRP initiator and uniformity throughout the M3BP film.

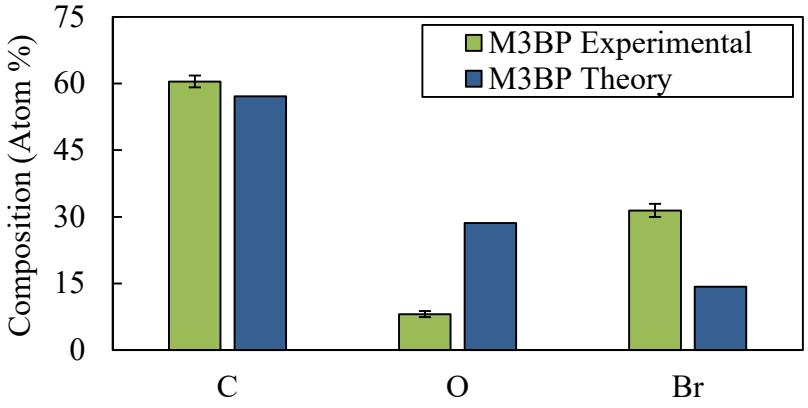

Figure 3.6. Composition of plasma-deposited M3BP measured by XPS survey scan after 1 hour soak period

3.2.5 *Plasma full factorial and optimization of initiator density*

High polymer brush density is required for minimized protein adsorption.[65] Our lab has used plasma deposition of M3BP to functionalize biomaterial surfaces for ATRP successfully but has not optimized for dense polymer brush coatings[28]. I used a 3 factor by 2 level full factorial design of experiment to probe which factors in the plasma deposition process were significant for the effects of bromine density and bromine stability. It is thought that the M3BP is torn apart in the plasma state, allowing for larger bromine composition than is theoretically possible stoichiometrically based on the initial molecule.[28] The percentage of bromine on the surface for each run is shown to be greater than the theoretical amount of 14.3% (**Figure 3.7**). The first 4 runs have much higher bromine than runs 5-8 corresponding to the middle of the electrodes and downstream of the electrodes, respectively. This is especially noteworthy since bromine can be easily pulled from the surface in ultra-high vacuum, of which XPS is performed.

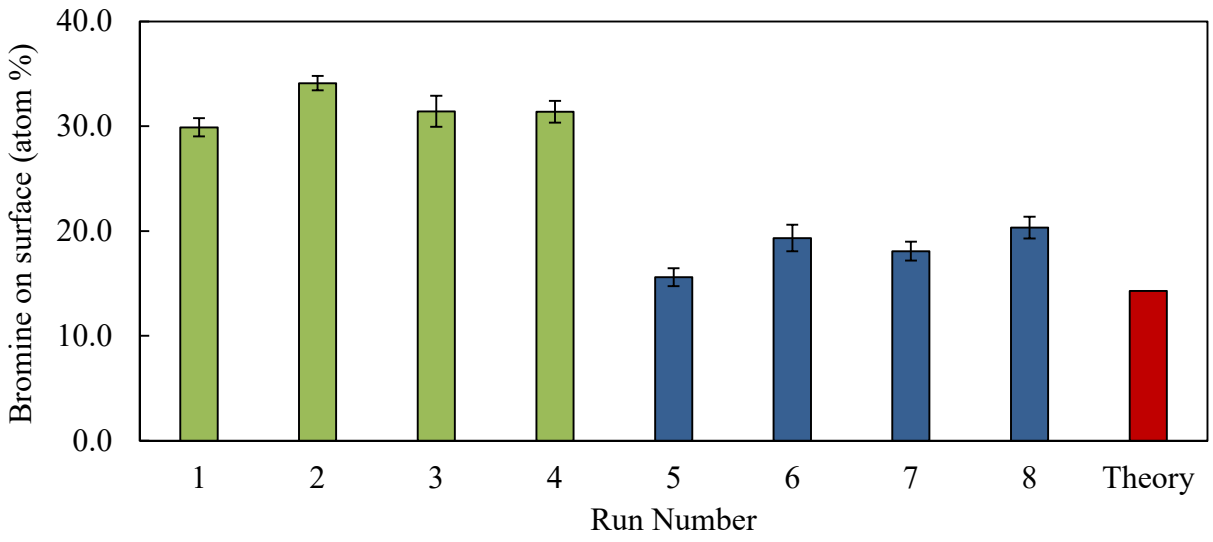

Figure 3.7. Percentage of bromine on the surface. XPS results from the M3BP full factorial experiment after soaking the samples. Since there is an obvious distinction in bromine amount, the samples from the middle of the electrodes is labeled in green and downstream is in blue.

High bromine percentage is important for synthesizing a nonfouling coating but so is the stability after soaking. The amount of bromine lost after soaking was calculated as a percentage with respect to the bromine amount on the surface before soaking from the same experimental run and use of the plasma reactor

$$amount\ Br\ lost = \frac{Br\ before\ soaking - Br\ after\ soaking}{Br\ before\ soaking} \times 100\% \quad (3.1)$$

Runs 2-4 show very low bromine lost compared to the other runs **(Figure 3.8)**. These runs were all performed in the middle of the electrodes.

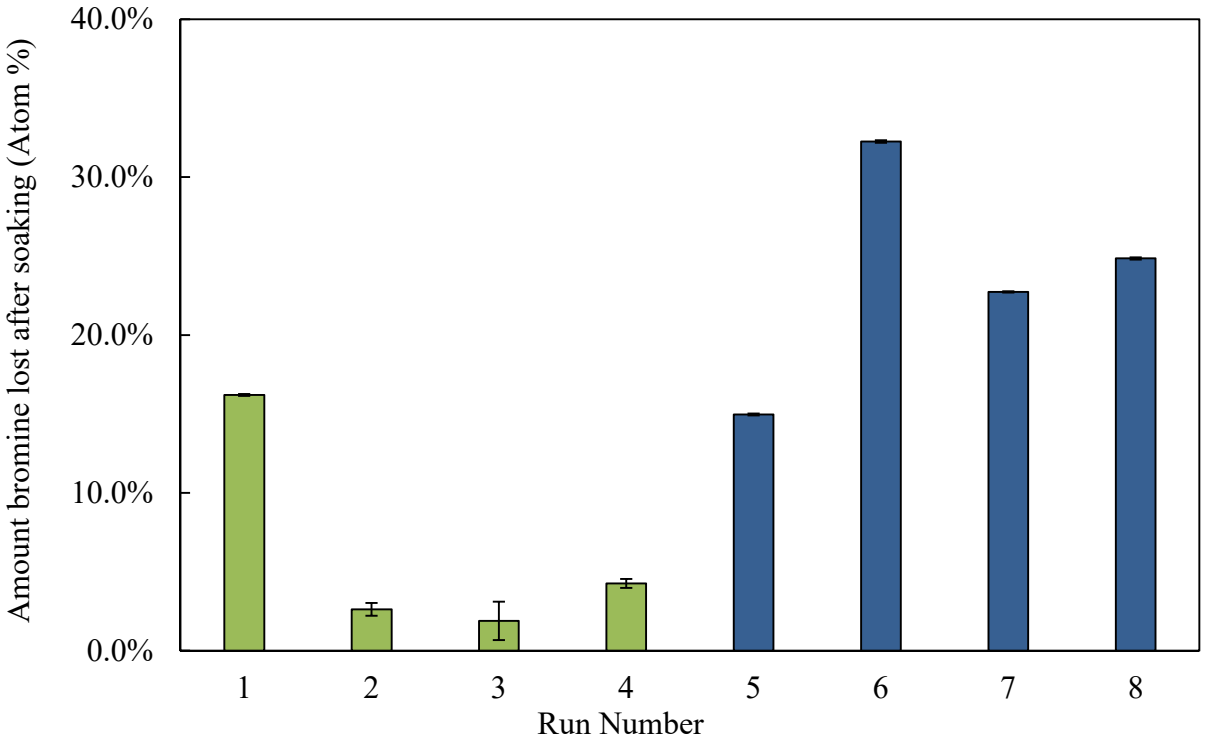

Figure 3.8. Amount bromine lost after soaking. Measured by XPS, the amount of bromine lost was calculated for each run in the full factorial experiment for M3BP plasma. Samples from the middle of the electrodes are green and downstream is in blue.

The theoretical amount of bromine for the M3BP molecule, stoichiometrically, is 14.3 percent (**Figure 3.3**). The amount of excess bromine was calculated using

$$amount\ excess\ bromine = \frac{measured\ Br - theoretical\ Br}{theoretical\ Br} \times 100\% \quad (3.2)$$

Runs 1-4 have significantly more bromine after soaking than runs 5-8, corresponding with the middle of the electrode position (**Figure 3.9**). The position significance is apparent but the full factorial statistical analysis is necessary to determine which of the other factors is significant in creating a dense and stable bromine coating for use as the ATRP initiator.

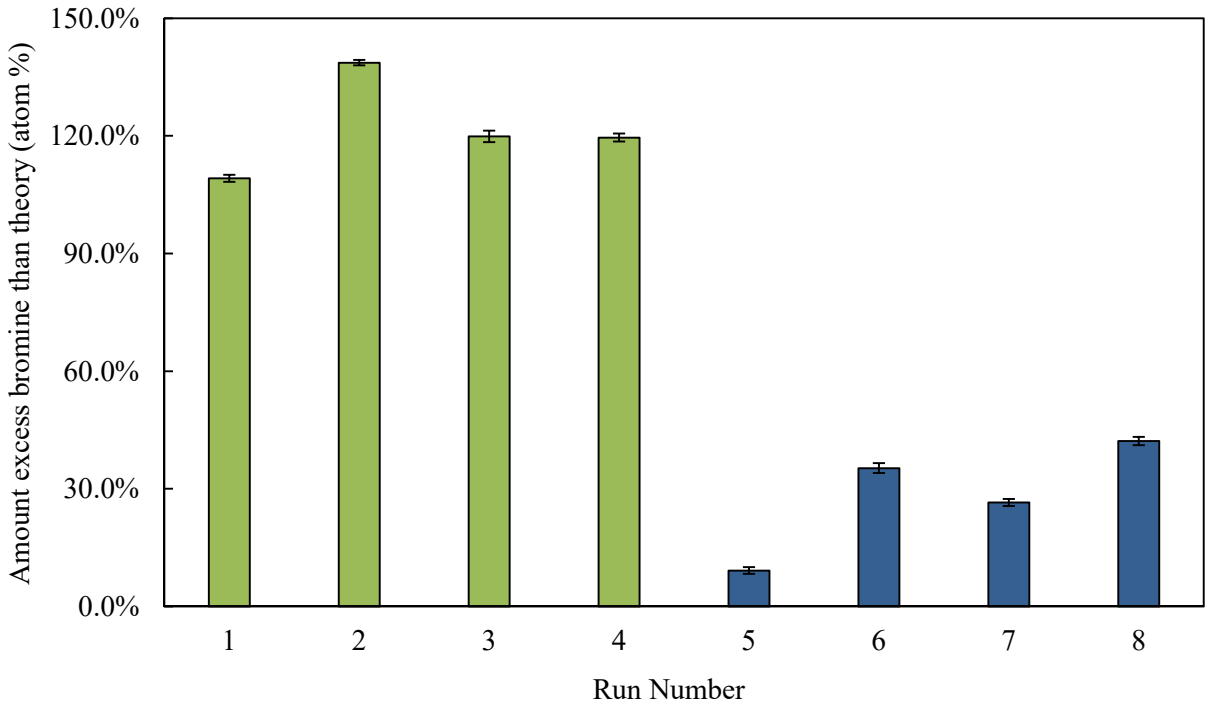

Figure 3.9. Amount excess bromine than theoretical. Measured by XPS, the amount of bromine excess compared to the theoretical stoichiometric amount was calculated for each run in the full factorial experiment for M3BP plasma

Minitab®, a statistical analysis tool for full factorial designs and 'black box' for calculations, was used to determine the significance of each factor for each of the effects—amount bromine loss and amount excess bromine. The software calculates the threshold for statistical significance for the normalized effect values. For both the amount of bromine loss and the amount of excess bromine, only the position was statistically a significant factor for these effects (**Figure 3.10 a and b**). Interactions between each of the factors may be observed as well. For the amount of excess bromine, only the position was statistically significant (**Figure 3.10 c**). For the amount of bromine lost, taking into account interactions, no factors were significant, however the position was close to the threshold of significance (**Figure 3.10 d**).

The position is very difficult to optimize given that the space is small. For production purposes, the space between the electrodes produces highly regular and predictable high amounts of stable bromine to act as the ATRP initiator. From this point in time, the conditions from run 3 were used to functionalize the substrates with the ATRP initiator. The conditions result in high amounts of stable bromine similar to those from run 4. However, for durability on the flexible insulin catheter, a thinner film is desired. The conditions for run 3 have a shorter growth period at low power resulting in a thinner film.

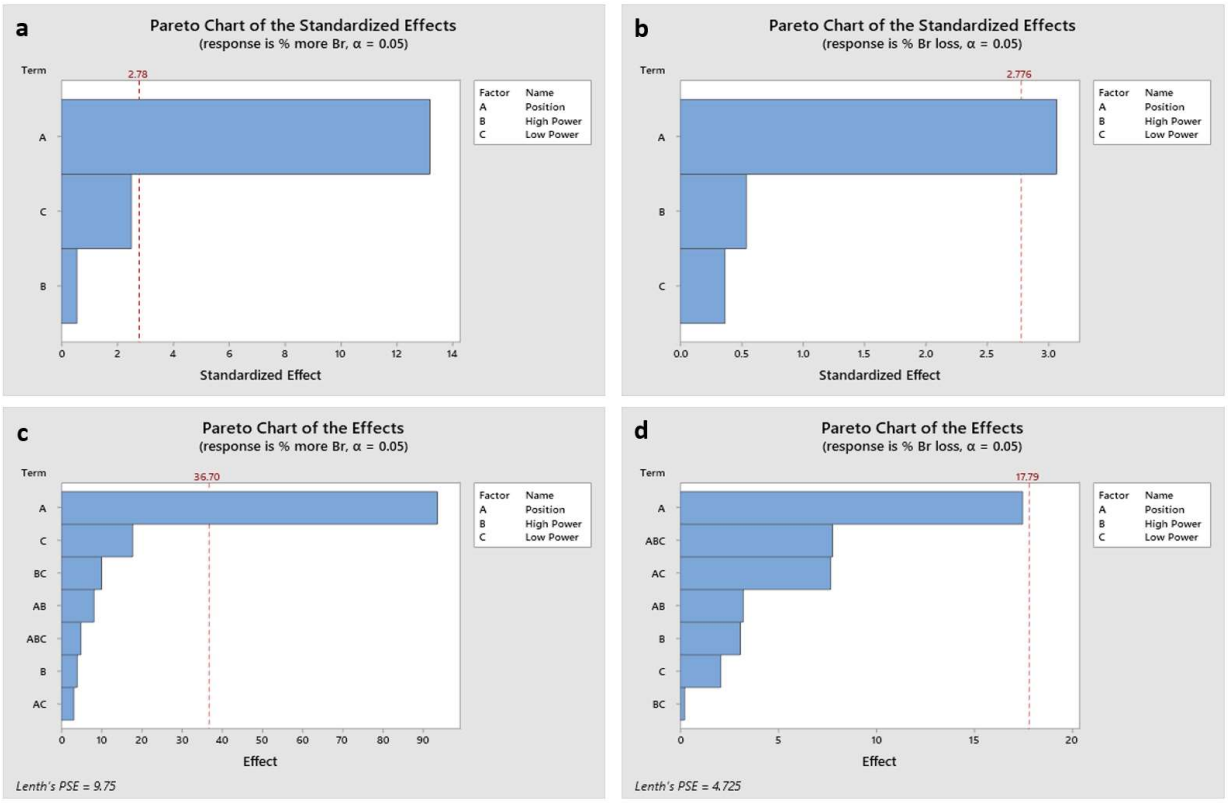

Figure 3.10. Pareto charts reporting the effect of selected variables on **a)** the excess bromine, **b)** amount of bromine loss after soaking, **c)** amount excess bromine with regards to interactions of factors, and **d)** amount bromine loss after soaking with regards to interactions of factors.

3.2.6 *SBMA coating validation*

XPS was used to confirm the presence of SBMA on the substrate using the ARGET ATRP protocol. Using Scheme 1, some contamination was measured by way of silicon with trace amounts of residual bromine (**Figure 3.11**). The bromine may be left from washing after the polymerization—of which contains a bromine catalyst. A very small amount of nitrogen and sulfur as compared to the theoretical percentages were present indicating a poor coverage of SBMA on the surface. This could be due to the small amount of polymerization initiator on the surface. It could also be due to delamination of the HEMA coating.

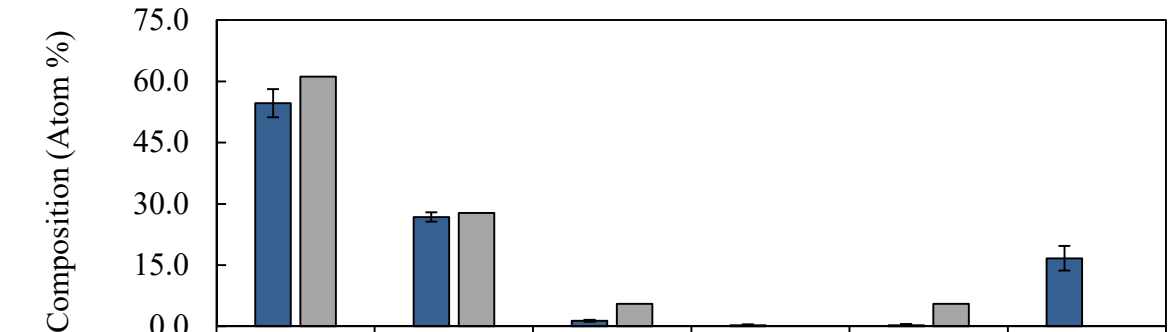

	C	O	N	Br	S	Si
Experimental	54.6	26.8	1.4	0.3	0.3	16.7
Theoretical	61.1	27.8	5.6		5.6	

Figure 3.11. XPS results for the SBMA coating grown using Scheme 1

The SBMA coating synthesized on the M3BP coating of Scheme 2 contained larger amounts of sulfur and nitrogen (**Figure 3.12**). No contamination was observed using XPS, however this could be due to increase of lab hygiene practices with experience over time. The theoretical amount of sulfur and nitrogen, stoichiometrically, is 5.6%. A thick and dense coating

of SBMA should result in these values. The coating synthesized on M3BP is very close to the theoretical amounts, indicating a coating that has better nonfouling potential.

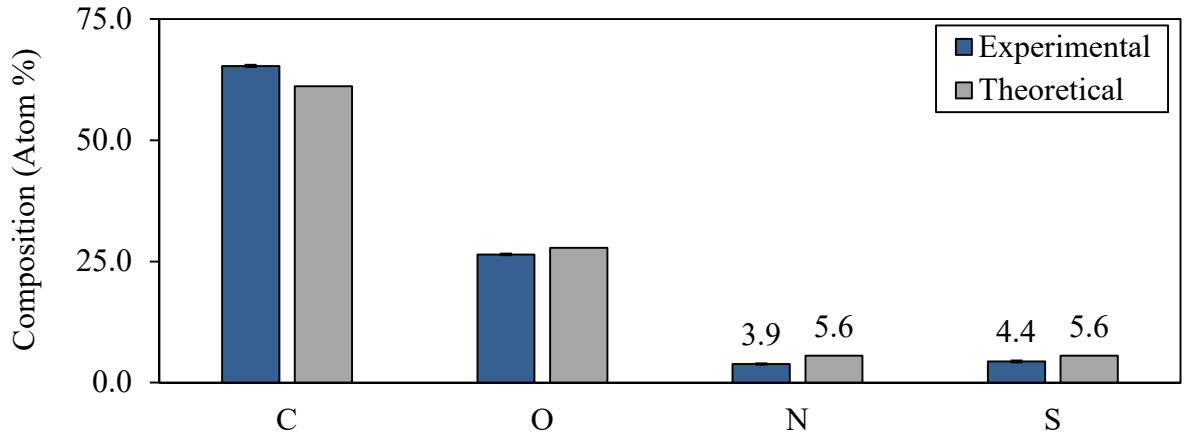

Figure 3.12. XPS results for the SBMA coating grown using Scheme 2

3.2.7 *ATRP Full Factorial Design*

One definition of a biocompatible material limits the extent of the FBR[72]. For *in vitro* tests, the widely accepted threshold for protein attachment to indicate a material performing well *in vivo* is less than 5 ng/cm^2. To optimize the polymer brush coating to achieve protein adsorption less than 5 ng/cm^2, I started by determining the significant factors in the polymerization using a full factorial design. The first half of runs have been completed in the experiment, omitting the fourth factor—water-to-methanol ratio. The presence of SBMA on the surface was confirmed with XPS. Albumin adsorption was measured and compared to adsorption on the polyurethane control (**Figure 3.13**). While adsorption was high, and for some sample groups greater than that on the control, some sample groups resisted protein adsorption well. Run 2 achieved 79% less albumin adsorption than the control, which would most likely have a significant increase in lifetime of the insulin catheter.

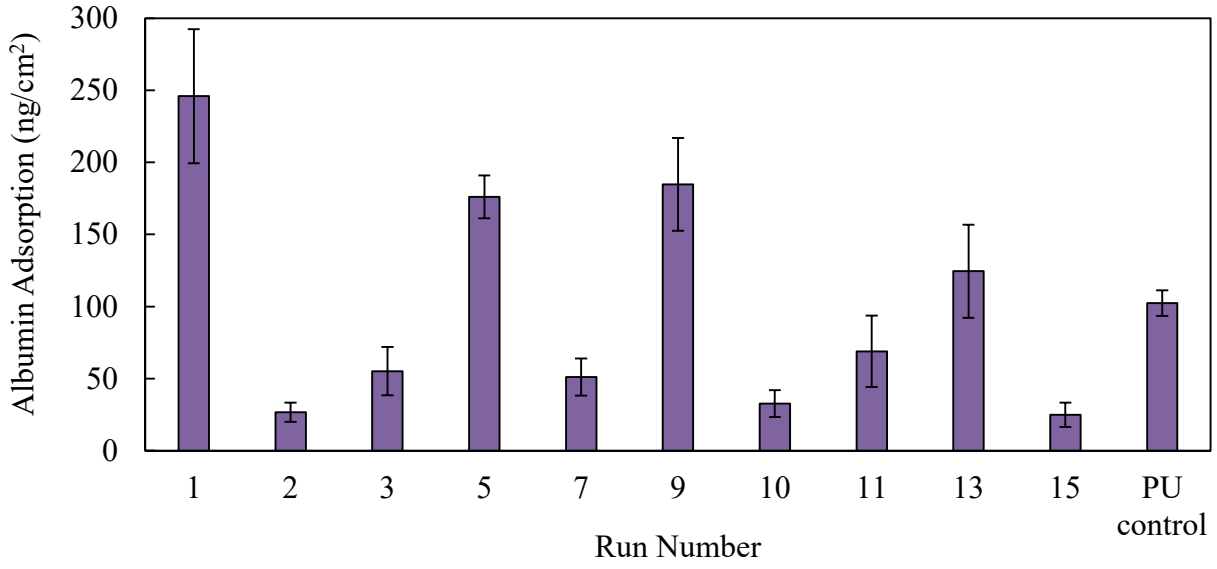

Figure 3.13. Albumin adsorption on SBMA samples for the full factorial design

Protein adsorption was the effect in the full factorial design. For this design, none of the factors were significant to the effect (**Figure 3.14**). This could be due to poor design of the high and low experimental values of the 4 factors probed. More likely, it could be due to initiator density which was later investigated.

Source	LogWorth	PValue
Amount Bipyridine(5,30)	1.205	0.06240
Ascorbic Acid:CuBr2(10,50)	0.822	0.15083
Amount SBMA(120,200)	0.656	0.22084

Source	LogWorth	PValue
Amount Bipyridine(5,30)	1.025	0.09437
Ascorbic Acid:CuBr2(10,50)	0.869	0.13535
Amount SBMA(120,200)	0.784	0.16440
Amount SBMA*Amount Bipyridine	0.738	0.18263
Ascorbic Acid:CuBr2*Amount Bipyridine	0.703	0.19833
Amount SBMA*Ascorbic Acid:CuBr2	0.578	0.26400

Figure 3.14. Full Factorial DOE results for the ATRP. (Top) singular effects and (bottom) effects including interactions between factors

The bromine density of each batch of plasma-deposited M3BP substrates was measured using XPS. The bromine density is assumed to be similar to that of the polymer brush density which is associated with nonfouling capabilities. For the samples prepared for the full factorial design, the bromine density was not consistent (**Figure 3.15**). The samples prepared with higher bromine density substrates had significantly lower protein adsorption than the samples prepared with substrates of lower bromine density. There was a broad distribution of albumin adsorption for the samples prepared with lower bromine density substrates. From this analysis, a quality control experiment was performed to investigate differences in washing procedures and exact positioning in the reactor. It was concluded that substrates would be analyzed with XPS for surface bromine density before use in finishing the full factorial design of experiment to determine significant factors in the ATRP.

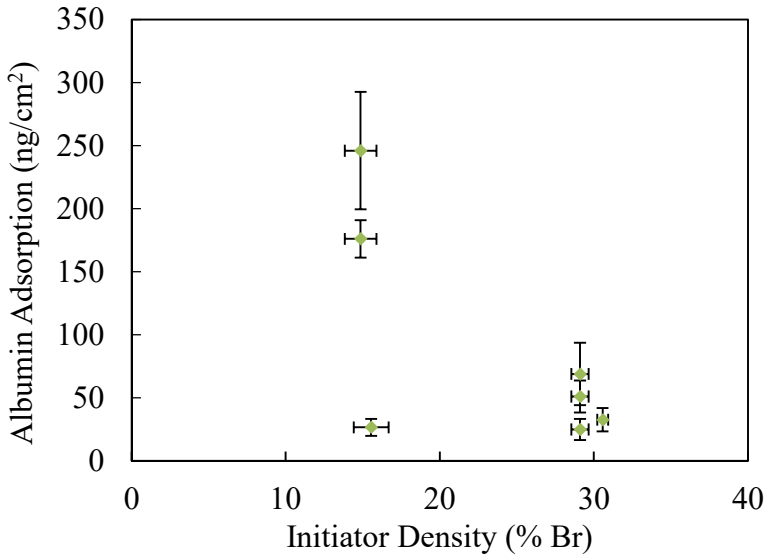

Figure 3.15. Effect of ATRP initiator density on albumin adsorption for the ATRP full factorial

3.2.8 *SBMA on polyurethane protein adsorption and validation*

Utilizing the inherent hydroxyls available in the catheter polyurethane, Scheme 3 was used to fabricate a SBMA polymer brush coating. This method should be more durable given that there is not a plasma-deposited film used that may be prone to delamination and consequential 'holes' in the nonfouling coating, which may in-turn promote protein attachment and the FBR. While the coating did not achieve the ultralow protein adsorption target of less than 5 ng/cm^2, the coating did resist protein adsorption better than the catheter control by 43% (**Figure 3.16**). This experiment was performed early-on and the ARGET ATRP protocols have been tuned since. This method may have potential to synthesize a durable nonfouling coating.

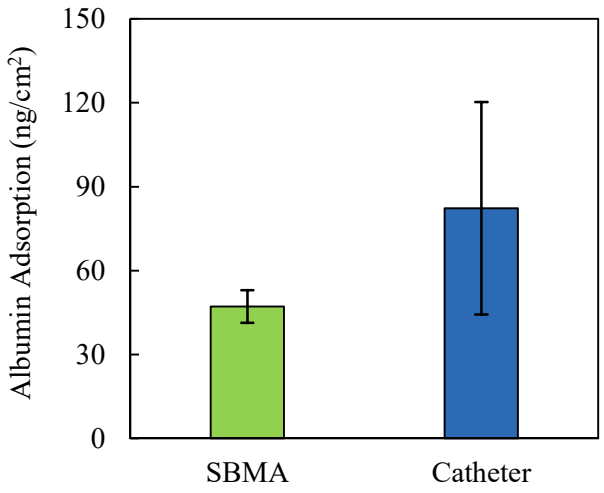

Figure 3.16. Protein adsorption of samples prepared using the process in Scheme 3

3.2.9 *Surface-grafted CBMA hydrogel*

As previously published, CBMA hydrogel provokes no visible FBR after 2 months of subcutaneous implantation.[56] The CBMA hydrogel was synthesized on the surface of the substrate with plasma-deposited M3BP as the ARGET ATRP initiator. The surface composition was

observed using XPS (**Figure 3.17**). Small amounts of bromine contamination was observed. This could be due to poor washing or bromine trapped in the hydrogel after drying and analysis under ultra-high vacuum in the XPS analysis chamber. The other elements—carbon, oxygen, and nitrogen—were present in amounts close the theory.

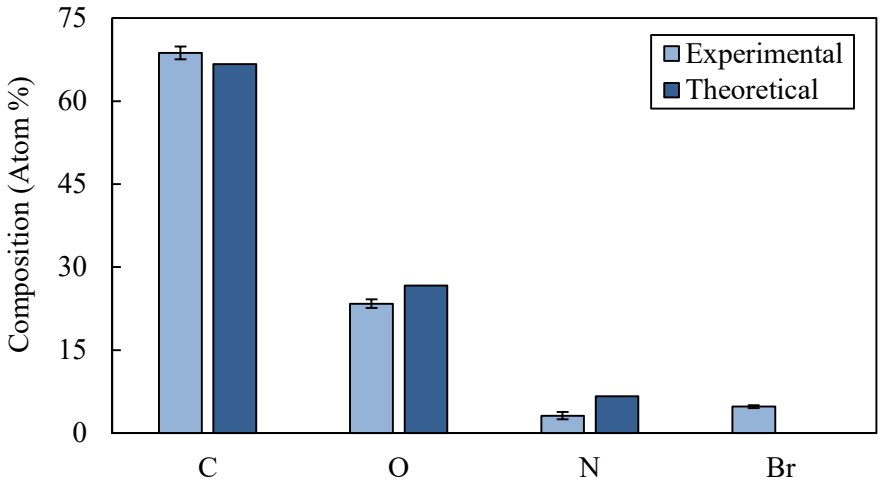

Figure 3.17. Surface composition of surface-grafted CBMA hydrogel from XPS results

The surface-grafted CBMA hydrogel did not perform as well limiting protein attachment as the implanted hydrogels (**Figure 3.18**). This is most likely due to unoptimized reaction conditions and formation of the hydrogel as grafted to the stiff biomaterial surface. The CBMA reduced albumin attachment by 46% from the control. With optimization, this method shows some potential for improving biocompatibility of the insulin catheter.

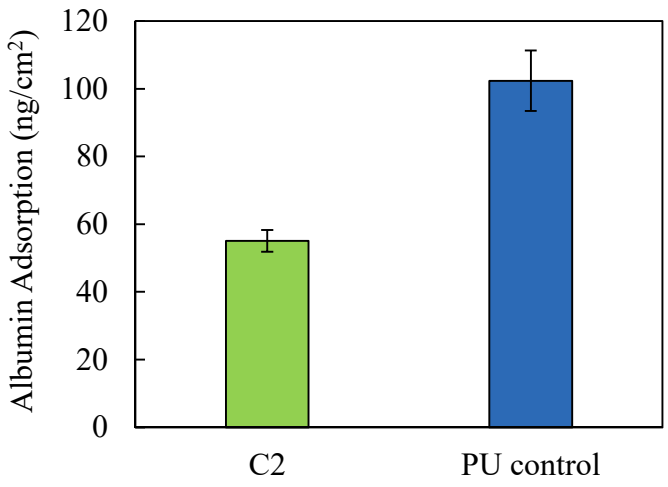

Figure 3.18. Albumin adsorption measured on the surface-grafted CBMA hydrogel compared to the polyurethane control

3.3 CONCLUSIONS

Nonfouling coatings of SBMA polymer brushes may be robustly synthesized to the biomaterial surface using a variety of processes. Surface-grafted SBMA polymerizes on a variety of ARGET ATRP initiators, including the traditional ATRP initiator—α-bromoisobutyryl bromide—and a plasma-deposited, higher density initiator—methyl 3-bromopropionate. The M3BP plasma-deposited intiator can reach a surface density as high as 31% bromine. Using HEMA as an anchor for the BIBB initiator, a polymer brush density of 5.7% is achieved, resulting in much higher protein attachment. It has been confirmed that higher ATRP initiator surface density leads to lower albumin adsorption for the conditions investigated. Consistency in initiator density has been found to be critical in comparing conditions of the polymerization of the nonfouling coating. With an SBMA coating of 31% density as synthesized using the M3BP initiator, protein adsorption as low as 22 ng/cm^2, which is 79% less than the polyurethane

control, was achieved and is suspected to reduce the rate of the FBR and consequential insulin catheter occlusion.

Other methods for grafting nonfouling zwitterionic SBMA have shown some potential in reducing protein adsorption; Grafting SBMA directly to a polyurethane containing hydroxyls using the BIBB initiator and grafting a CBMA hydrogel to the substrate are methods that have significantly reduced protein adsorption with respect to the polyurethane control. To achieve true biocompatibility—'invisibility' to a living system—less than 5 ng/cm^2 of protein adsorption *in vitro* is desired. Steps to optimize and improve the zwitterionic nonfouling coatings should be made to reduce *in vitro* protein adsorption to amounts below the established threshold.

3.4 ACKNOWLEDGMENTS

I would like to acknowledge Lei Ye, PhD [leiyeuw@gmail.com, Shandong University] for his mentorship and initial design of the coating for this project. Prabhleen Kaur, PhD [pkaur@uw.edu, University of Washington] has contributed significantly to the ARGET ATRP protocols and consistent discussion regarding the chemistries and procedures. Sharon Creason [screason@uw.edu, University of Washington] has provided initial laboratory mentorship and designed the animal use protocol as well as performed the initial mouse surgeries. Gerry Hammer [Molecular Analysis Facility, retired] has provided expertise in XPS. Marvin Mecwan, PhD [mmecwan@uw.edu, University of Washington] has provided mentorship and plasma reactor and protein adsorption expertise. Priyesh Jain, PhD [jainp2@uw.edu, University of Washington] from Prof. Shaoyi Jiang's group has provided the CBMA crosslinker. The Molecular Analysis Facility (MAF) [Molecular Engineering and Sciences, University of Washington] has been instrumental (pun intended) in providing analysis equipment and expertise

for this work, including the XPS, ellipsometer, and the SFG system. I would like to acknowledge Prof. Buddy Ratner [ratner@uw.edu, University of Washington] for the design of the project and persistent mentorship. I would like to acknowledge the generous funding from the Juvenile Diabetes Research Fund to support this work.

Chapter 4. INVESTIGATING THE EFFECTS OF PSBMA CHAIN LENGTH AND DENSITY ON NON-SPECIFIC PROTEIN ADSORPTION

4.1 INTRODUCTION

In chapter 3, nonfouling graft-from polymer brush coatings of poly(sulfobetaine methacrylate) (SBMA) were widely investigated using an alternative initiator. The purpose of the work in this chapter is to observe the nonfouling mechanism—interfacial water structure. Here I hypothesize that SBMA grafting density and chain length influence chain mobility which is responsible for the degree of hydration for the nonfouling coating (**Figure 4.1**).

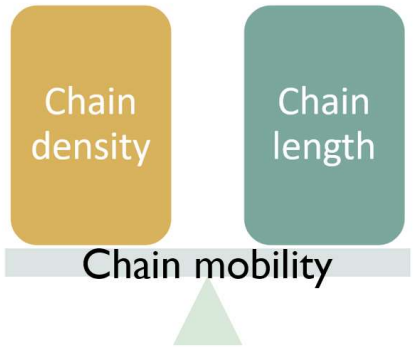

Figure 4.1. Proposed balance for surface-grafted polymer brushes. Chain density and chain length should be balanced to achieve maximum chain mobility.

In the period, 1989-1992, Jeon and Andrade were investigating self-assembled monolayers (SAMs) of poly(ethylene oxide) (PEO) and the effects on protein adsorption. They found that there is a weak, long-range hydrophobic attraction between the PEO and protein that is competitive with the repulsion and is responsible for determining the protein adsorption resistance of the surface. They also concluded that the concentration of PEO chains required to resist adsorption is inversely proportional to protein size and that densely packed surfaces may

not resist adsorption at all[73,74]. Famously, Prime and Whitesides followed-up on this work and observed that for surfaces, comprised of oligomer and polymer chains of ethylene oxide (PEO) with varying end groups—hydroxyls or methyls—the packing and length of the SAM influenced protein adsorption[22]. Specifically, they concluded that high surface concentrations of PEO resisted protein adsorption. They found that longer chains resisted adsorption better than shorter chains. Surprisingly, they measured that the terminal group—either a methyl or a hydroxyl—had no effect on protein adsorption. Of note: both sets of scientists set an unknown threshold for resisting protein adsorption. They report that either 1) surfaces resisted protein adsorption or that 2) surfaces adsorbed a sometimes-quantified amount protein. Often XPS or ellipsometry was used to quantify protein adsorption which we now would consider unsuitable techniques[75]. Today, we are concerned with the amount of protein attached to a surface and aim for less than 3-5 ng/cm^2 nonspecific protein adsorption[76].

Nonfouling surfaces have come a long way with zwitterionic materials, specifically with carboxybetaine and sulfobetaine—materials based on the hydrophilic head group of the lipid bilayer in a cell membrane, phosphoryl choline[58–60]. Many groups have measured the effects of protein adsorption resistance using these surface-grafted polymers and report that higher surface density is critical for lower protein adsorption[11,21,66,77–85]. Often, it is reported that high-density polymers with "appropriately high chain length" or polymer chains of "appropriate surface density" are a contributor to lowered protein adsorption and I still have yet to determine what this means exactly because usually no further detail is explicit. Most of these papers report how high packing density is critical. Z. Zhang was one of the first to report that for carboxybetaine acrylic acid, the degree of polymerization is more important than the packing density[86].

As in Prime and Whitesides' work, we hypothesize that nonfouling ability is related to chain mobility. Better, or "appropriate", chain mobility leads to more flexibility for interfacial water molecules to arrange and become orderly. This is called the water barrier theory—tightly-bound surface water provides a barrier to a foreign surface so that proteins cannot adsorb and trigger the foreign body reaction (FBR). Surface water may be so highly-structured that the energy required to dislodge a bound, interfacial water is greater than the entropy of its release. Thermodynamically, this event is unfavorable for a surface of extremely high surface hydration as shown by

$$\Delta G = \Delta H - T\Delta S \tag{4.1}$$

where G is Gibb's free energy, H is enthalpy, T is temperature, and S is entropy. The event will occur if ΔG is negative. The change in entropy for releasing surface-bound water is positive, but if ΔH is large enough for structured interfacial water—water bound tightly to the nonfouling surface, ΔG remains positive and water will not dislodge.

This interfacial water structure can be measured using sum frequency generation (SFG) vibrational spectroscopy. The SFG signal is a result of the nonlinearly-polarized combination of visible and infrared (IR) beams at the interface of structured bonds, such as the bonds of structured water at a biomaterial surface[87,88]. This has been shown for SBMA[77,78,89]. The SFG signal is more intense for higher-ordered interfaces, which has been shown to correspond with better nonfouling surfaces, aligning with the water barrier theory. Additionally, SBMA hydrogels have shown to have stronger bond strengths than other nonfouling, hydrophilic hydrogels, as indicated by SFG peak intensity and wavelength shift[56]. Here, we have explored the relationship between our SBMA coatings on CaF_2 prisms with the corresponding protein adsorption as measured by a radiolabeled protein adsorption assay.

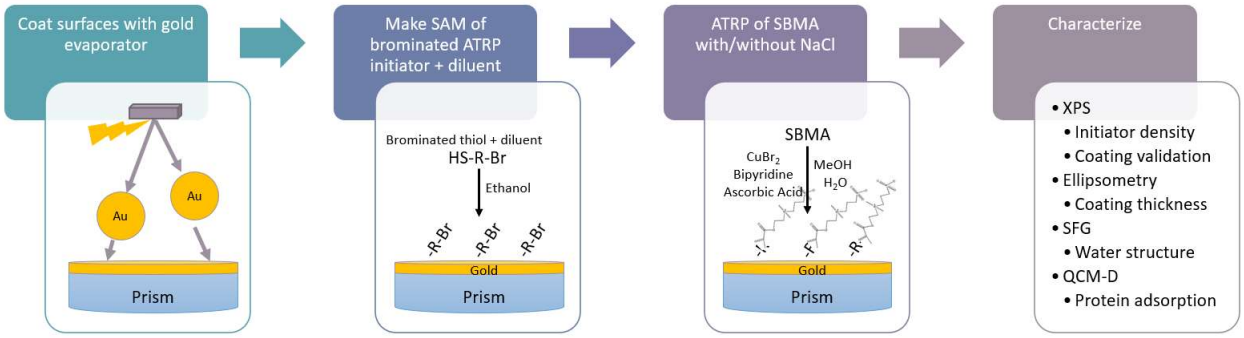

Figure 4.2. Process diagram for pSBMA coating on gold surfaces and characterization techniques. First, gold is deposited by electron beam deposition onto a substrate such as a prism or glass slide. Second, the ATRP initiator is immobilized onto the gold using thiol chemistry. Then, the ATRP occurs on the surface. Finally, surfaces are characterized using XPS, ellipsometry, SFG, and QCM-D.

In this work, I have systematically investigated the effects of zwitterionic chain density and length on protein adsorption and interfacial water structure with SBMA (**Figure 4.2**). We attempted using the surface plasmon resonance (SPR) in our department but it did not work; thus I could not measure protein adsorption with this well-documented method. Instead, I have measured nonspecific protein adsorption using radiolabeled protein and quartz crystal microbalance with dissipation (QCM-D) and a radiolabeled protein adsorption assay. The interfacial water structure was measured using SFG. The SFG results shown here are preliminary and further SFG investigations are recommended. Activators regenerated by electron transfer (ARGET) atom transfer radical polymerization (ATRP) was used to ambiently polymerize coatings of SBMA on surfaces, as described in chapter 2[63]. The addition of sodium chloride during the polymerization raises the lower critical solution temperature so that pSBMA remains soluble at higher molecular weights, resulting in thicker coatings as compared to pSBMA polymerized without the polymerization salt (**Figure 4.3**). The grafting density of polymer chains was controlled using multiple methods. The first was through the difference in the amount of surface bromine, as measured with x-ray photoelectron spectroscopy (XPS), of

plasma-deposited poly(hydroxyethyl methacrylate) (pHEMA) with immobilized α-bromoisobutyryl bromide (BIBB) and plasma-deposited methyl 3-bromopropionate (M3BP). The M3BP surfaces achieve bromine densities up to 6 times higher than the pHEMA-BIBB surfaces, resulting in higher grafting densities. The second method was through self-assembled monolayers (SAMs) on gold for the purposes of QCM-D and surface plasmon resonance (SPR) as well as allowing for highly-tunable and accurate surface density. Here, thiolated molecules with either a tertiary alkyl bromide[27] or a hydroxyl which was used to immobilize α-bromoisobutyryl bromide (BIBB) were used to make a SAM as the initiator for ATRP. A diluent of 1-heptanethiol was used to modify the concentration of bromine on the surface to achieve varying grafting densities. For the QCM-D experiments, the initiator was added prior to QCM-D and the ATRP was carried out *in situ* in the device chamber. Further experiments of varying chain lengths and densities are recommended to fully characterize the pSBMA nonfouling coatings.

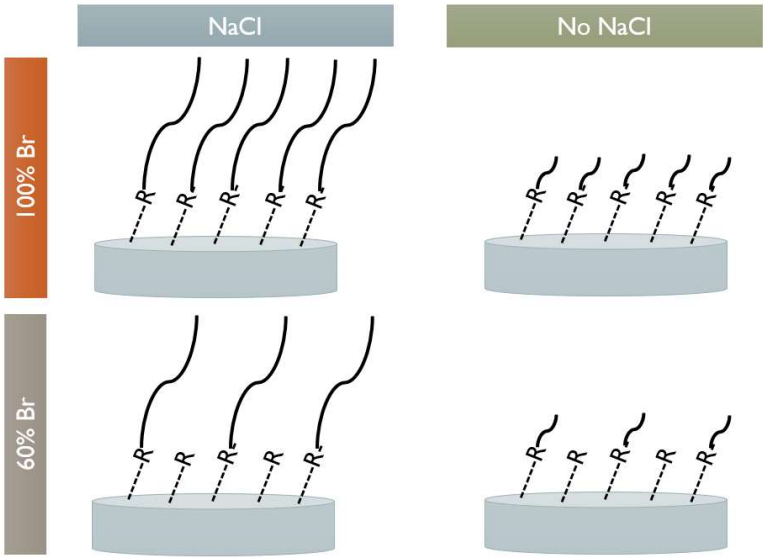

Figure 4.3. Diagram of sample varying chain lengths and densities. Chain length is modified by adding sodium chloride to make the coating thicker. Chain density is modified with varying initiator densities on the surface of the substrate prior to ATRP.

4.2 RESULTS AND DISCUSSION

4.2.1 *The effect of water structure on protein resistance*

Using SFG, a correlation between ATRP initiator density and protein adsorption was explained. For the samples prepared for this experiment, the SBMA coated onto substrates prepared using Scheme 1 with a HEMA film did not reduce protein adsorption significantly from the bare polyurethane control (**Figure 4.4 a**). The samples prepared using the process in Scheme 2 with M3BP as the ATRP initiator significantly reduced albumin adsorption. For these samples, the bromine density using the HEMA layer and the M3BP functionalization was 5.7% and 16.8%, respectively, which is consistent with higher polymer brush density relation to lower protein attachment. The SFG spectrum for the HEMA coating displays 2 peaks whereas the SFG spectrum for the M3BP coating has a weaker second peak (**Figure 4.4 b**). The 2 peaks observed correlate to tightly-bound and loosely-bound water molecules at the coating interface[90]. The tightly-bound water peak is observed on the left at 3200 cm^{-1} and the loosely-bound water peak is observed on the right at 3400 cm^{-1}. The ratio of the tightly-bound to loosely-bound peak intensities is greater for the M3BP coating, corresponding to the significantly less protein adsorption measured for the same SBMA coating. This means that the M3BP-initiated SBMA coating binds interfacial water better than the HEMA-based SBMA coating. The tightly-bound water provides a barrier for proteins to the biomaterial surface. This information suggests that to displace a tightly-bound water molecule would require energy greater than the increase in entropy that would otherwise occur. Water plays a central role in resisting the FBR.

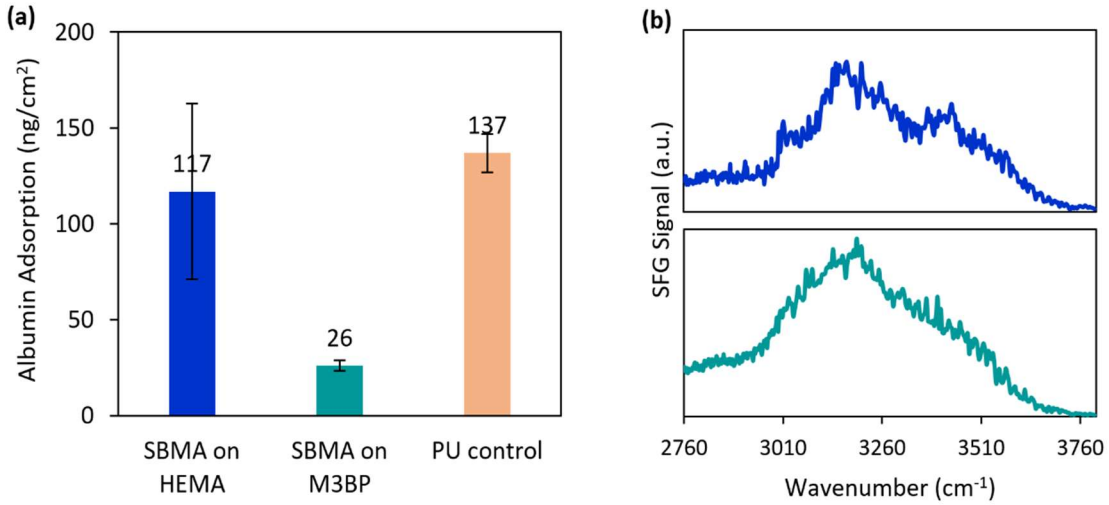

Figure 4.4. a) Albumin adsorption counted using the I-125 label on SBMA coatings and polyurethane control and **b)** ppp polarized SFG spectra of SBMA polymer brush on (top) HEMA and (bottom) M3BP

4.2.2 *The Hofmeister series and the effect of salt addition during ATRP*

To vary the chain length of the pSBMA polymer brush coating, various anions in sodium salts were added during the polymerization and the resulting thicknesses were measured using ellipsometry (**Figure 4.5**). The anions were chosen to represent a broad spectrum of the Hofmeister series. This series of cations and anions and spectra are used to describe a proteins likeliness to 'salt-out'. In order from CO_3^{2-}, Cl^-, I^-, to SO_4^{2-} decreases surface tension, increases solubility of proteins to 'salt-in', increases protein denaturation, and decreases protein stability—CO_3^{2-} being at the side of the spectrum to increase surface tension and SO_4^{2-} at the end to decrease surface tension[91]. This same series describes similar behavior for zwitterionic materials[92]. Adding Na_2SO_4 limits zwitterion solubility, thereby inhibiting polymer brush chain growth whereas adding Na_2CO_3 increases solubility and allows for thicker coatings.

These anions were added in varying concentrations relative to the amount of SBMA monomer and the thickness was measured using ellipsometry. The Na_2SO_4 addition reduced the

thickness of the pSMBA coating. NaCl dramatically increased the thickness. NaI and Na_2CO_3 did not increase the thickness as hypothesized because each reacted with other reagents of the ATRP, limiting the brush growth by using up reagents. The NaI precipitated out with a reaction with the ascorbic acid. These results are still useful. From here, 40% NaCl (mol NaCl/mol SBMA) was added to the ATRP solution when making thicker polymer brush coatings.

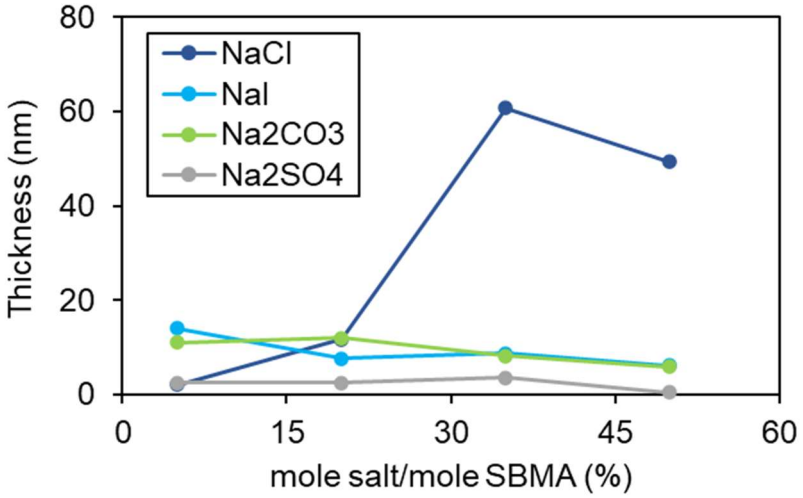

Figure 4.5. Thicknesses of pSBMA coating with varying salts and concentrations during ATRP, n=3.

4.2.3 *XPS reveals successful coating of pSBMA and surface density*

Table 4.1. Surface composition of pSMBA and brominated glass slides, measured by XPS (atom %)

Surface	C 1s	O 1s	N 1s	S 1s	Br 3d	Au 4f
gold-coated glass slide	24.6 ± 4.4	5.4 ± 1.7				70.0 ± 4.5
BIBB on BME on gold-coated glass slide	33.1 ± 2.9	5.0 ± 1.2			1.9 ± 0.2	60.0 ± 2.9
BIBB on 50% BME and ODE on gold-coated glass slide	26.5 ± 1.9	3.8 ± 0.7			1.8 ± 0.1	68 ± 2.6
pSBMA on BIBB on BME on gold-coated glass slide	49.7 ± 2.7	16.6 ± 1.1	3.5 ± 0.4	1.9 ± 0.3		28.4 ± 1.9

Polymer brush density of the pSBMA coating was controlled on gold surfaces using a non-reactive diluent—either 1-octadecanethiol or 1-heptanethiol—in a 1:1 mixture with the reactive thiolated molecule. **Table 4.1** shows the surface composition of various surfaces. The bare gold-coated glass slides have inherent hydrocarbon groups, adventitious carbon adsorbed from the air. In this experiment, 2-mercaptoethanol (BME) and 1-octadecanethiol (ODE) were immobilized to the gold. ODE was used as a diluent in a 1:1 mol ratio with BME. After BME was immobilized, α-bromoisobutyryl bromide (BIBB) was substituted onto the surface using the hydroxyl group from BME. The results here show similar amounts of bromine on the surface after the BIBB immobilization, or the diluted BIBB/ODE immobilization. Post-ATRP, on the BIBB-only surface, gold is still highly-detected but in smaller quantities after the pSBMA polymer brush growth.

The negligible difference in bromine on the brominated surfaces could be due to the size difference between BME and ODE. ODE is much larger than the BME which most likely restricts the steric availability of BIBB to react with the BME on the surface. In another explanation, BME is much more reactive than ODE and may have immobilized onto the gold much better than the ODE. In a third explanation, the ODE found in the lab was from the 1970's and may have been degraded, accounting for the lack of bromination difference after the attempted dilution. Perhaps the ODE was incapable of strongly adsorbing to the gold as the BME does.

To make a brominated surface on gold, new molecules were acquired. The bromination step by BIBB onto BME stripped the gold off of QCM-D sensors due to the corrosiveness of the BIBB. Alternatively, we searched for thiolated alkyl bromide molecules. Here, an alkyl-brominated molecule containing a disulfide bond has been shown to adsorb well to gold and

carry-out ATRP for SBMA for QCM-D purposes[93]. This molecule would eliminate the need for an extra bromination step after the BME immobilization. As an alternative to this molecule, bis[2-(2′-bromoisobutyryloxy)ethyl]disulfide (BIBOED) was purchased due to its pricetag and reported ATRP-initiating capabilities, again, for QCM-D[27]. In our lab, 1-heptanethiol was found and used to be a diluent in a 1:1 ratio for these experiments for QCM-D. However, XPS spectra were not taken to quantify the bromination degree and differentiation of these surfaces due to lack of funding. QCM-D was carried out.

In an exploratory side experiment, we wondered if the BIBB would immobilize on a gold surface without a thiol group. Based on the XPS results, BIBB did become immobilized onto the gold surface and in slightly greater amounts than for with the BME anchor (**Figure 4.6**). Sulfur was measured for the BME surface, and not for the BIBB-only surface, further-confirming the validity of these results. This is meaningful because loosely-bound bromine is readily removed under ultra-high vacuum that XPS runs under. The bromine measured is tightly-bound to the surface. Whether or not the bromine would remain as a viable chemical anchor for ATRP is unknown without further investigation.

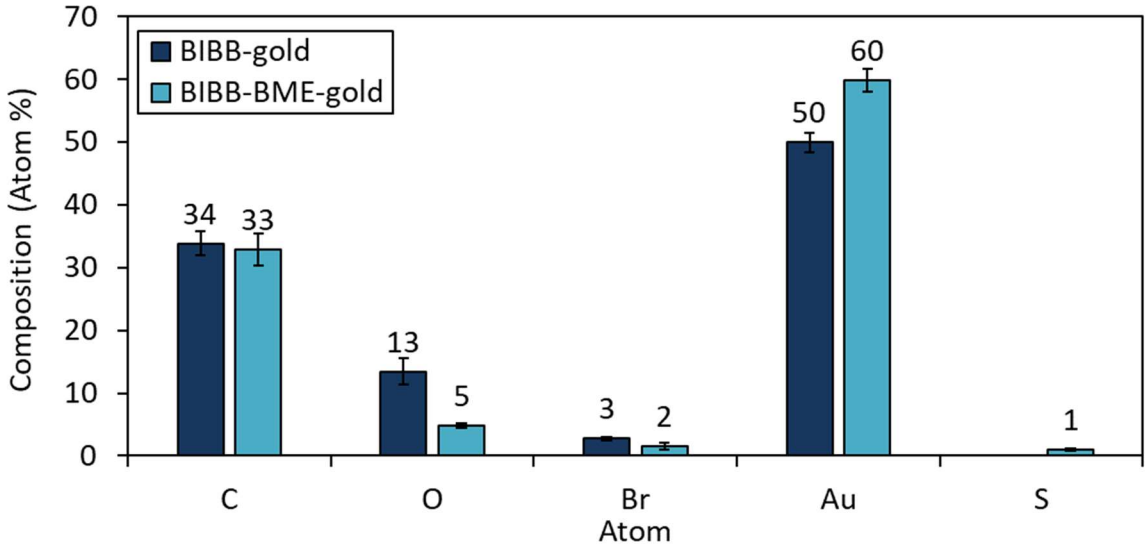

Figure 4.6. Surface composition for BIBB and BIBB-BME on gold surfaces, measured using XPS.

4.2.4 *Coating thickness due to varying grafting densities and use of polymerization salt*

Surfaces of pSBMA were synthesized on gold-coated glass substrates. Ethanolic mixtures of either 100% BME or 1:1 BME:1-heptanethiol (mol:mol) were used to functionalize the gold followed by BIBB immobilization. The addition of sodium chloride was added during the ATRP to allow for longer chains of SBMA to grow, thereby synthesizing thicker coatings. The thickness was measured using ellipsometry since the coatings were very uniform. Cauchy models were used to model the refractive indices for both the functionalization layers and the pSBMA. As compared to their saltless counterparts, the coatings where NaCl was used during ATRP were significantly thicker (**Figure 4.7**). The denser coatings were thicker than the less dense coatings. The less dense coating where NaCl was used was thicker than the dense coating without salt. These results are as predicted. It should be noted that these are dry thicknesses. It is possible that the thicknesses would greatly differ for the surfaces in wet conditions.

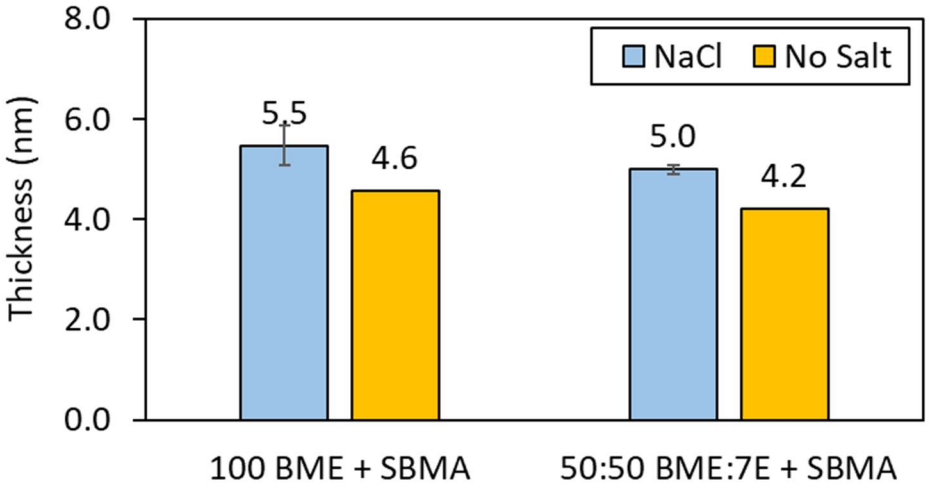

Figure 4.7. pSBMA coating thickness for varying grafting densities and chain lengths, n=3.

4.2.5 *Contact angle due to varying grafting densities and coating thicknesses*

Figure 4.8. Water droplet imaged with goniometer during contact angle measurement on the dense pSBMA coating where NaCl was used during ATRP.

A goniometer was used to measure the water-air contact angle on the prepared pSBMA surfaces of varying thicknesses and grafting densities. A sample image of a water droplet is shown as measured on a dense pSBMA surface where NaCl was used during ATRP (**Figure 4.8**). For the 4 types of surfaces prepared, the less dense pSBMA coating where NaCl was used during ATRP had the lowest contact angle, corresponding to the greatest surface hydration (**Figure 4.9**). The

denser coatings have lower surface hydration than the less dense coatings. There was no statistically significant difference between the use of NaCl or not during ATRP for the less dense coatings. More contact angle measurements and more variations in density and thickness are required for making substantial conclusions about these surfaces.

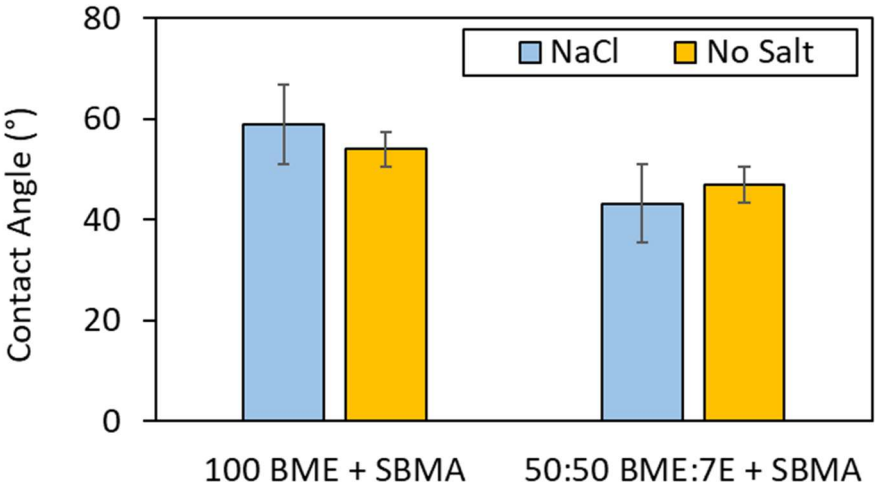

Figure 4.9. Contact angle for pSBMA coatings of varying grafting densities and coating thicknesses.

4.2.6 *In situ ATRP of pSBMA and BSA adsorption in QCM-D*

QCM-D sensors were prepared by immersion in ethanolic solution of bis[2-(2′-bromoisobutyryloxy)ethyl]disulfide (BIBOED) initiator and diluent of 1-heptanethiol per experiment in a 1:1 mole ratio for dilution. These sensors were loaded into the QCM-D chambers for *in situ* ARGET ATRP of the pSBMA coatings (**Figure 4.10**). This allowed us to 1) only make the nonfouling coating on one side of the electrode, keeping the other side clear of polymeric material and maintain a higher potential differential and 2) measure the rate of ARGET ATRP with these conditions and materials.

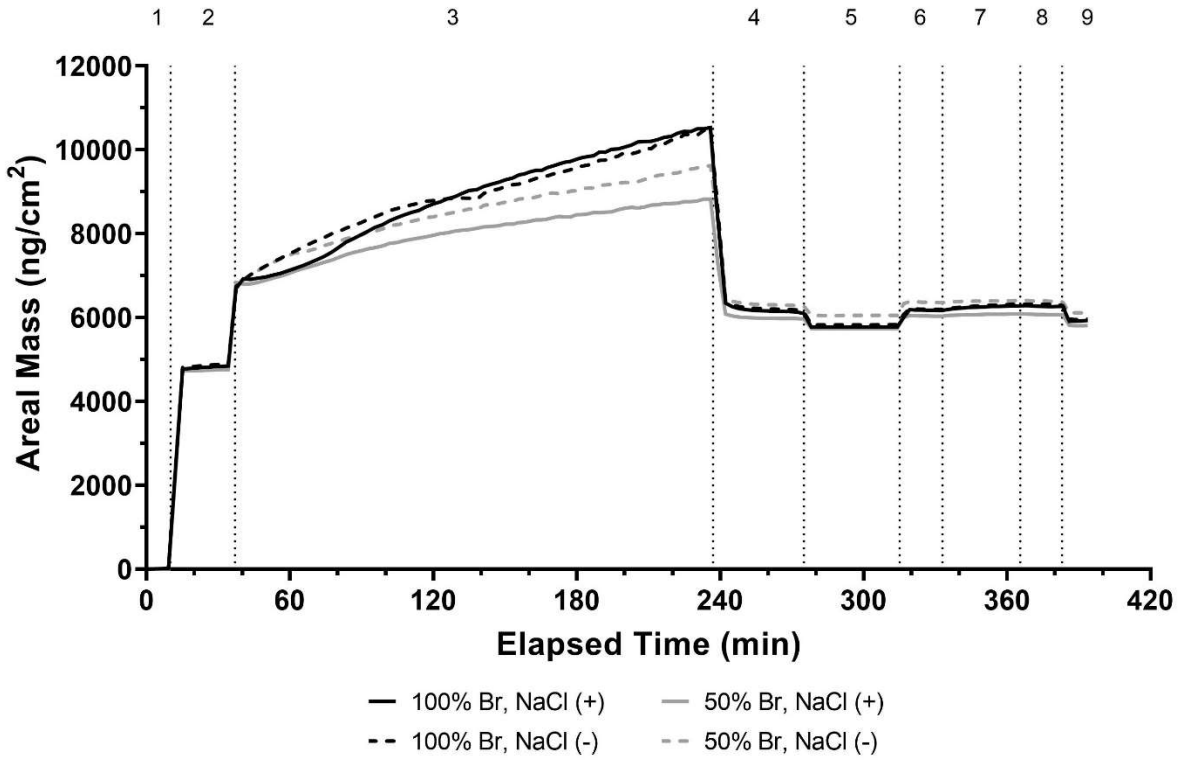

Figure 4.10. Mass measured by QCM-D over time at 37°C of in situ ATRP of pSBMA and subsequent BSA adsorption. Time segments: 1) air, 2) PBS wash, 3) in situ ARGET ATRP of pSBMA 4) PBS wash, 5) DI water wash, 6) PBS wash, 7) 1 mg/mL BSA in PBS nonspecific protein adsorption, 8) PBS wash, 9) DI water wash. The 100% Br graphs represent the mass for sensors loaded with ATRP initiator in ethanol [1.4 mM BIBOED]. The 50% Br graphs represent sensors loaded with a 1:1 mole ratio of ATRP initiator and diluent [0.7 mM BIBOED].

After taking a reading in air, PBS was added to the chamber, prior to polymerization (segment 1) (**Figure 4.10**). The mass increases due to increased sorption to the sensor surface of the added salts and the bombardment of the sensor. Then, the ARGET ATRP solution—either with NaCl or without—was flowed into the chamber, beginning the polymerization (segment 2). The coatings on the dense surfaces (labeled as 100% bromine meaning that only the BIBOED initiator was used during the initiator immobilization) acquired more mass overall and more quickly than the less dense (labeled as 50% bromine, where a 1:1 mole ratio of BIBOED and the

diluent were used for the initiator immobilization) surfaces. This makes sense since there should have been twice the amount of initiator as the less dense surfaces. This portion of the QCM-D mass was zero-ed and a logarithmic plot was fit using least squares regression. The rate constant is reported (**Table 4.2**). Here, it is shown that the dense coating with salt has the largest growth rate and the less dense coating with salt has the slowest growth rate. Further experiments are required to clarify these phenomena.

Table 4.2. ATRP rate and albumin adsorption as measured by QCM-D for in situ-prepared pSBMA surfaces.

Surface	ATRP log rate (ng/min)	Albumin Adsorption (ng/cm^2)
1.4 mM BIBOED, NaCl	1319	87 ± 3
1.4 mM BIBOED, no salt	1114	118 ± 4
0.7 mM BIBOED, NaCl	691	32 ± 4
0.7 mM BIBOED, no salt	829	23 ± 7

In segment 4 of the QCM-D experiments (**Figure 4.10**), the surfaces were thoroughly washed with PBS post-ARGET ATRP. Segment 5 was an accidental DI water wash. Segment 6 was a PBS wash to re-equilibrate the polymer brush coating post-water wash with physiological pH prior to the nonspecific protein adsorption measurements. Segment 7 is the BSA adsorption. A 1 mg/mL BSA in PBS solution was used. The adsorption was allowed to occur for 35 minutes followed by another PBS rinse as shown by segment 8. Segment 9 was another DI water wash.

The nonspecific protein adsorption was calculated by taking the difference of the average masses from the PBS washes in segments 6 and 8 immediately prior to and post albumin adsorption (**Table 4.2**). Surprisingly, there is no direct correlation between the ATRP log rate and the protein adsorbed. As for trends associated with surface density and coating thickness, the least dense and shortest coating had the least protein adsorption significantly (**Figure 4.11**).

These results can be explained in the same way as Prime and Whitesides[22]: shorter or less dense chains allow for better chain mobility and therefore higher water binding and less protein adsorption. The dense, short pSBMA coating had low protein adsorption as well. It is possible that for the systems investigated here, the density was too high to achieve the ultra-low fouling surfaces reported in previous literature for these surface-grafted pSBMA[11]. It is recommended that further variations on these coatings be investigated. It would be very simple to vary the grafting density by increasing the diluent ratio in the ethanolic bromination step with BIBOED. It is also recommended that the polymerization be left to go until completion in QCM-D to observe the extent of polymerization and the actual effect polymerization salt has on coating thickness. These methods may be used to fully-optimize the pSBMA nonfouling coatings.

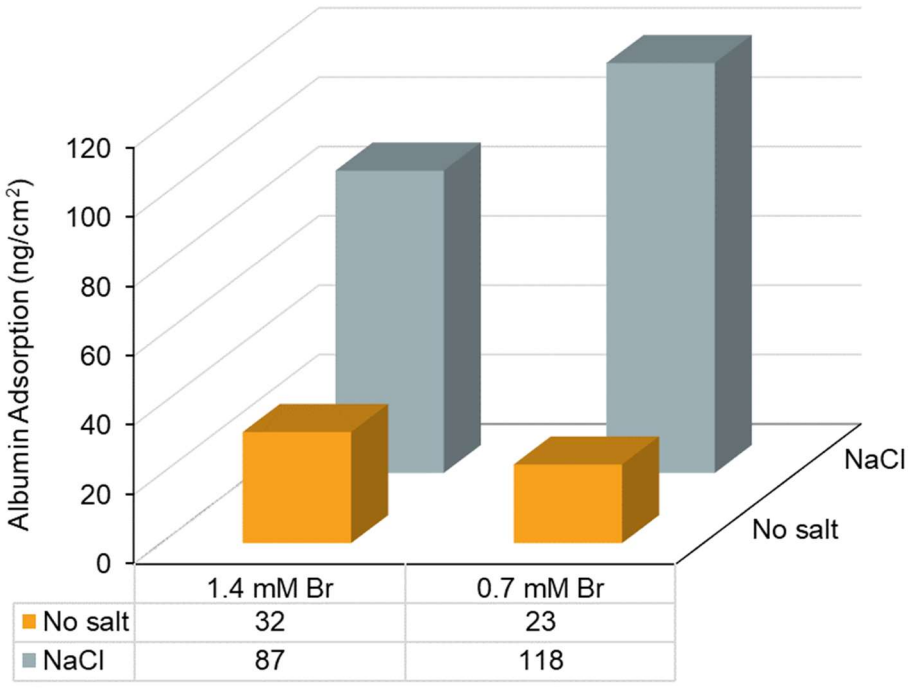

Figure 4.11. Nonspecific protein adsorption as measured by QCM-D on various pSBMA surfaces

As a final check, the surface composition was measured by XPS on the QCM-D sensors post-adsorption to confirm the presence of albumin on the surfaces. All surfaces were very similar in composition (**Figure 4.12**).

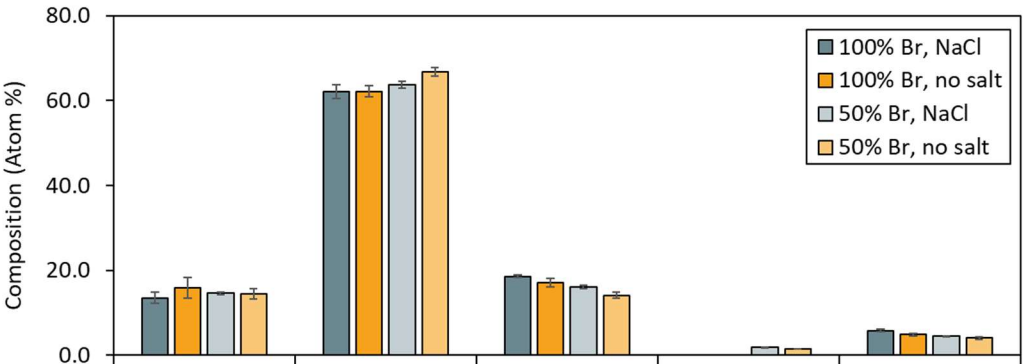

	O	C	Au	S	N
100% Br, NaCl	13.5	62.1	18.6		5.8
100% Br, no salt	15.9	62.1	17.1		4.9
50% Br, NaCl	14.6	63.7	16.1	1.8	4.5
50% Br, no salt	14.5	66.8	14.1	1.6	4.1

Figure 4.12. Surface composition of sensors post-QCMD, measured by XPS

4.3 CONCLUSIONS

In this chapter, the chain length and density of pSBMA polymer brush coatings was varied to aim at optimizing the hydration ability of the surface and ultimately reduce protein adsorption, thereby limiting the FBR. For the surfaces investigated, differences in SFG spectra for tightly-bound and loosely-bound water for the different coatings confirm a higher ratio of tightly-bound to loosely-bound water for the denser SBMA coating, initiated by the M3BP coating and correlating with significantly less albumin adsorption. This information suggests that interfacial water on a nonfouling surface requires more energy to be dislodged from the surface structure to create a binding site for a protein than the entropic gain of the system that would otherwise occur. For the systematically investigated surfaces using QCM-D, the water-air contact angle

suggests high wetting for all surfaces, but especially for the denser surfaces. Contrastingly, the corresponding protein adsorption does not directly correlate to these results. The least dense, shortest coating of pSBMA achieved the lowest protein adsorption. These methods—the use of QCM-D for *in situ* polymerization of the nonfouling coatings and measurement of nonspecific protein adsorption and the highly-tunable grafting density—should be used to further-investigate these pSBMA coatings to fully optimize the nonfouling ability. This information may be coupled with information from corresponding SFG spectra to fully-characterize the nonfouling mechanism.

4.4 ACKNOWLEDGMENTS

Patrik Johansson, PhD [patjo586@gmail.com, Stanford University] has provided SFG expertise and training as well as project inspiration. Kan Wu, PhD [wukansz@gmail.com, University of Washington] has helped with SBMA fundamentals, nonfouling coatings, experimental design, and SPR. Sherry Liu [sherryliu24@gmail.com, University of Washington] has provided expertise in QCM-D. Prabhleen Kaur, PhD [pkaur@uw.edu, University of Washington] has contributed significantly to the ARGET ATRP protocols and consistent discussion regarding the chemistries and procedures. Samantha Young, PhD [Molecular Analysis Facility] has taken great XPS data for me since. Marvin Mecwan, PhD [mmecwan@uw.edu, University of Washington] has provided mentorship and plasma reactor and protein adsorption expertise. Kyung-Hoon Kim [kyunghkim87@gmail.com, University of Washington] has conducted the protein adsorption experiments. Prof. Dave Castner [castner@uw.edu, University of Washington] has provided mentorship, collaboration, and funding for the SFG experiments. The

Molecular Analysis Facility (MAF) [Molecular Engineering and Sciences, University of Washington] has been instrumental in providing analysis equipment and expertise for this work, including the XPS, ellipsometetry, QCM-D, and SFG. I would like to acknowledge Prof. Buddy Ratner [ratner@uw.edu, University of Washington] for persistent mentorship.

Chapter 5. GUIDING THE IMMUNE RESPONSE WITH SURFACE-IMMOBILIZED *DE NOVO* PROTEINS

5.1 INTRODUCTION

Early in the classical foreign body response (FBR), macrophage cells are recruited to aid in the 'fight' against the invader—the implanted biomaterial e.g. an insulin catheter. In the FBR, neutrophils are activated by the endotoxin, lipopolysaccharide (LPS)[94–96], and signal macrophages with interferon gamma (IFN-γ)[97,98] to an M1 phenotype[2]. M1 type macrophages are associated with inflammation and rejection—a response appropriate for a foreign material. These pro-inflammatory macrophages then signal fibroblasts using a range of pro-inflammatory cytokines. Fibroblasts are responsible for the structuring and remodeling of the extracellular matrix and are critical for wound repair. However, stimulation by M1-expressed molecules leads to excessive proliferation and leads to fibrosis[5]—which ultimately occludes the insulin catheter.

On the other hand, macrophages exposed to interleukin 4 (IL-4) are polarized to the M2 phenotype associated with healing[2]. M2 macrophages are critical for wound repair, encourage angiogenesis, and improve insulin resistance[99,100]. It has been suggested that increasing the count of M2 macrophages may accelerate wound closure[100]. For these pro-healing qualities of the M2 macrophages, our collaborator has designed a *de novo* IL-4 to immobilize on the insulin catheter surface, aiming to increase angiogenesis and prevent inflammation by macrophages that otherwise would be polarized to an M1 phenotype.

Using this surface-immobilized molecule, the extent of M2 polarization could be investigated. M2 macrophages express a variety of markers depending on the type of M2 phenotype. All M2 phenotypes express CD206, CD204, and CD163[100]. Conveniently, these

markers may be quantified with commercial ELISA kits. As an alternative approach for immunohistochemistry, rat anti-F4/80 primary antibodies may be used to detect mouse macrophages. Goat anti-macrophage mannose receptor (MMR) may be used as an M2 marker. In the far future, bone marrow derived macrophages should be used in an *in vitro* assay to culture cells in the presence of the IL-4 coated catheter/biomaterial. ELISAs for M2-specific markers should be used to determine the extent of M2 polarization.

From the David Baker lab [Dept. of Biochemistry, University of Washington], the *de novo* IL-4 was computationally designed and physically synthesized with the purpose of surface immobilization to the insulin catheter tip to encourage the M2 phenotype of macrophages. If macrophages around an implanted medical device were triggered into a 'pro-healing' phenotype, the area should heal better while also not triggering a pro-inflammatory phenotype. This *de novo* IL-4 was expertly designed after the *de novo* IL-2[101]. Various features of the protein were modified to make the engineered protein ultra-stable and able to be anchored to a biomaterial surface. Native proteins that come into contact with surfaces tend to denature, thereby triggering their own FBR. This ultra-stable *de novo* version would, in theory, be so stable that it would be capable of moderate chemical reactions and still maintain high bioactivity on a surface. After the *de novo* IL-4 was synthesized, it was subjected to multiple harsh conditions such as solvents and boiling and remarkably maintained an extremely high binding affinity to the native IL-4 receptor. Additionally, it did not bind to the native IL-2 receptor—a concern since the *de novo* IL-2 was used as a blueprint for the *de novo* IL-4. To anchor the *de novo* IL-4 to a biomaterial surface, a single cysteine, added opposite the binding site of the IL-4 receptor, was added without compromising the structural or biological integrity of the protein. However, due to the COVID-19 pandemic, this synthesized protein was not properly stored and degraded over time.

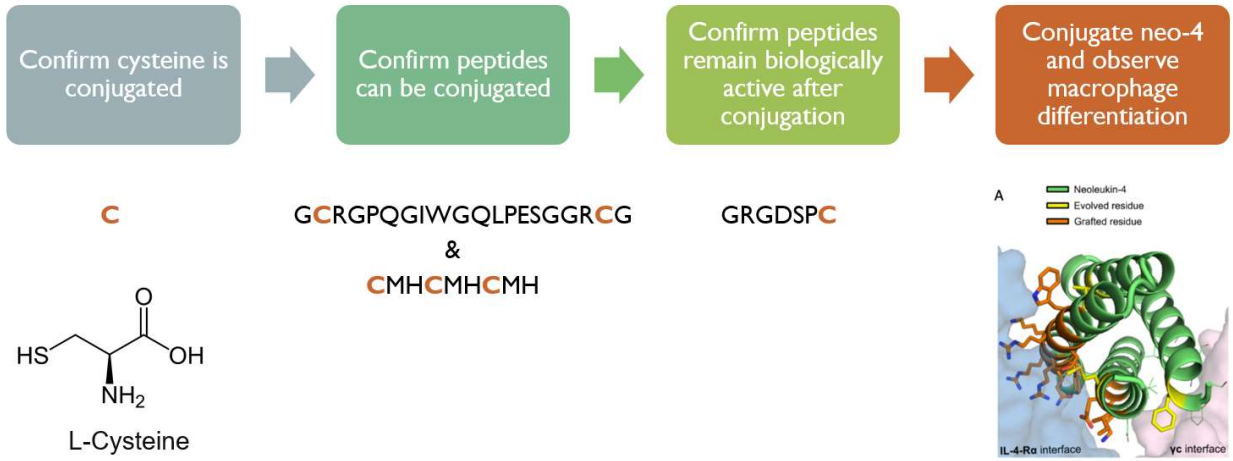

Figure 5.1. Workflow for preparing to immobilize immune-directing de novo molecules. First, L-cysteine was conjugated using the proposed S_N2 reaction. Then, two different cysteine-containing peptides were immobilized. Next, to confirm immobilized molecules remain biologically active, a cysteine-containing cell adhesion (contains RGD sequence) peptide was immobilized and cultured with fibroblasts to determine extent of bioactivity. Finally, the reaction has been established and may be used to conjugate the de novo IL-4.

In this work, I have designed and characterized the immobilization chemistry in preparation for the *de novo* IL-4 and other cysteine-containing surface therapeutics. Most famously, thanks to the most recent 2022 Nobel prize in chemistry, 'click' chemistry is the first method most people think of for the immobilization[102–104]. An alternative to click chemistry might be maleimide chemistry. Click and maleimide chemistries are great for when a system is very complex and the materials used are environmentally- and chemically-sensitive and aren't as tunable due to their biological nature. While robust methods, an alternative and very simple S_N2 reaction was investigated for this project[105]. In this work, we have the luxury of designing the insulin catheter surface so that it may be synthesized in whichever way to make it easiest to reduce the FBR and conjugate the immune-directing molecules, making the simple S_N2 reaction a viable option. Additionally, the reaction has been used between cysteine-containing molecules and brominated proteins to conjugate various side groups[25]. The reaction occurs aqueously and

with little supervision at mildly elevated temperatures making it safer and environmentally friendly. Through the work in chapters 3 and 4, multiple methods of brominating a surface have been established and can be used to functionalize surfaces for the S_N2 reaction. Here, the electrophilic surface bromine may be substituted by the nucleophilic thiol group from the cysteine by a quick backside attack reaction[106].

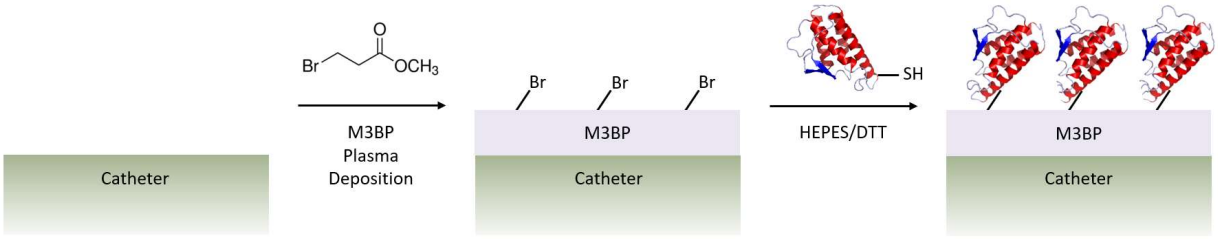

Figure 5.2. Schematic of cysteine/peptide/protein conjugation to plasma-brominated surface using S_N2 reaction. In the first step, M3BP is plasma-deposited onto a bare surface, such as a catheter, functionalizing the surface with reactive bromine. In the next step, the S_N2 reaction is used to conjugate the thiol from a cysteine, thereby immobilizing the cysteine/peptide/protein to the surface.

Since the *de novo* IL-4 is currently unavailable, steps have been taken to prepare for the novel molecule (**Figure 5.1**). First, L-cysteine was conjugated to the surface of poly(tetrafluoro ethylene) (PTFE) with a plasma-deposited methyl-3 bromopropionate (M3BP) surface functionalization coating (**Figure 5.2**). The surface was characterized using just XPS and angle-dependent XPS. Secondly, a few cysteine-containing peptides, generously donated by other labs on campus, were conjugated to α-bromoisobutyryl bromide (BIBB) brominated poly(hydroxyethyl methacrylate) (pHEMA) hydrogel disks (**Figure 5.3**). Since XPS data will not predict biological reactivity, a bioassay was developed. A pro-cell adhesion cysteine-containing peptide (containing the RGD sequence) was conjugated to the brominated pHEMA hydrogel and characterized with XPS[103]. The peptide-conjugated hydrogels were cultured with fibroblasts for up to 48 hours, observed optically, and imaged with SEM to observe the extent of cell adhesion

compared to bare pHEMA controls. In future work, the *de novo* IL-4 will be conjugated to a brominated surface using the characterized S_N2 reaction to polarize macrophages to an alternative, M2, phenotype and ultimately limit the extent of the FBR, extending the lifetime for insulin catheters.

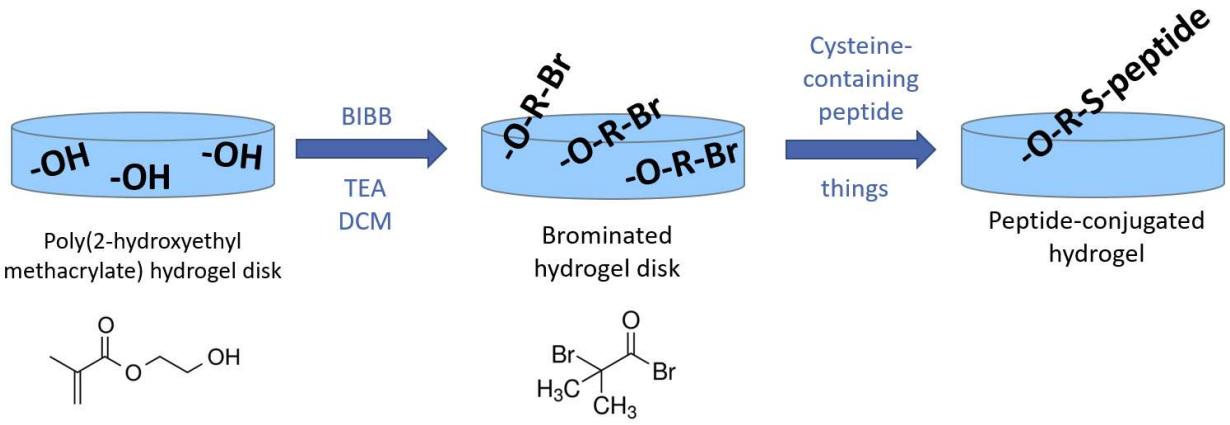

Figure 5.3. Process diagram for immobilizing cysteine-containing peptides onto pHEMA hydrogel disks. First, BIBB is conjugated to the available hydroxyl groups in the pHEMA hydrogel. Second, the thiol from the cysteines in the peptides is used to substitute in an S_N2 reaction with the bromine on the hydrogel surface, thereby immobilizing the peptide.

5.2 Results and Discussion

5.2.1 *L-cysteine was conjugated to an M3BP surface using the S_N2 reaction.*

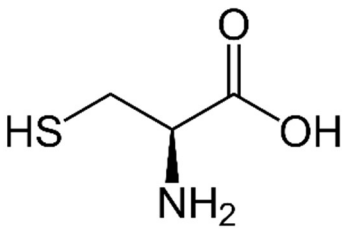

Figure 5.4. Molecular structure of L-cysteine.

To demonstrate that the proposed immobilization chemistry is suitable for the immobilization of a time- and material-expensive *de novo* protein, L-cysteine was first conjugated using the S_N2 reaction protocol proposed for conjugating the full thiolated protein. Since cysteine is small and

contains exactly 1 sulfur and 1 nitrogen (**Figure 5.4**), XPS was used to confirm the presence on the surface (**Figure 5.5**) using the M3BP-functionalizing coating process (**Figure 5.2**). It is assumed that 1) the M3BP film is uniform in atomic composition regardless of depth and 2) 1 cysteine reacts with every 1 bromine on the surface. Equal amounts of nitrogen and sulfur were observed, suggesting limited contamination; the sulfur and nitrogen observed is from the conjugated cysteine. Before the reaction, the M3BP film was measured to have 31% bromine by XPS. This is the maximum density of sulfur and nitrogen on the surface. Since XPS penetrates a depth of about 100 Å, it is expected to measure the M3BP film on the surface of the substrate, as is observed from the XPS results. There is substantial evidence that the cysteine was successfully conjugated to the M3BP coating.

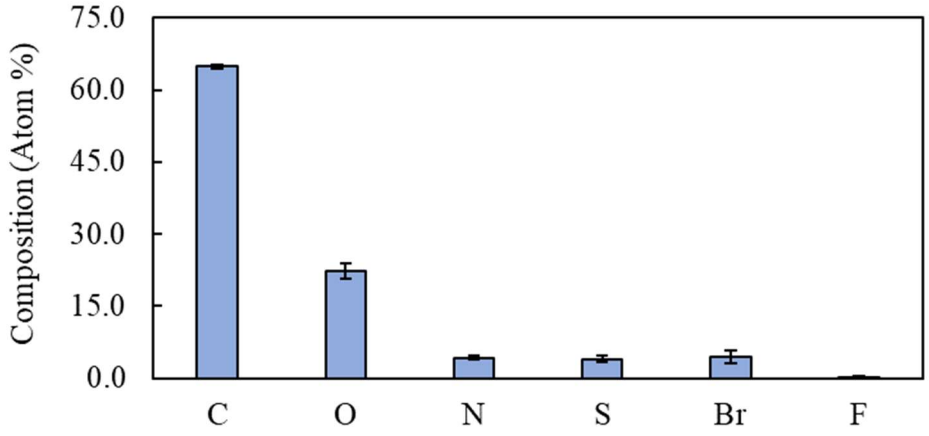

Figure 5.5. Surface composition of cysteine conjugated by the SN2 reaction, measured by the S-Probe XPS.

To investigate the surface coverage of the cysteine on the surface, angle-dependent XPS was used to probe the atomic composition at shallower depths than the traditional 0º takeoff angle for 2 samples coated in the same batch (**Figure 5.6**). Small differences in the amount of sulfur was observed for each sample at each takeoff angle for each sample. There was greater difference between the amounts of sulfur at each angle between sample A and sample B. The

error for each data point was also high, a consequence of the low XPS signal from sulfur and possibly contamination issues.

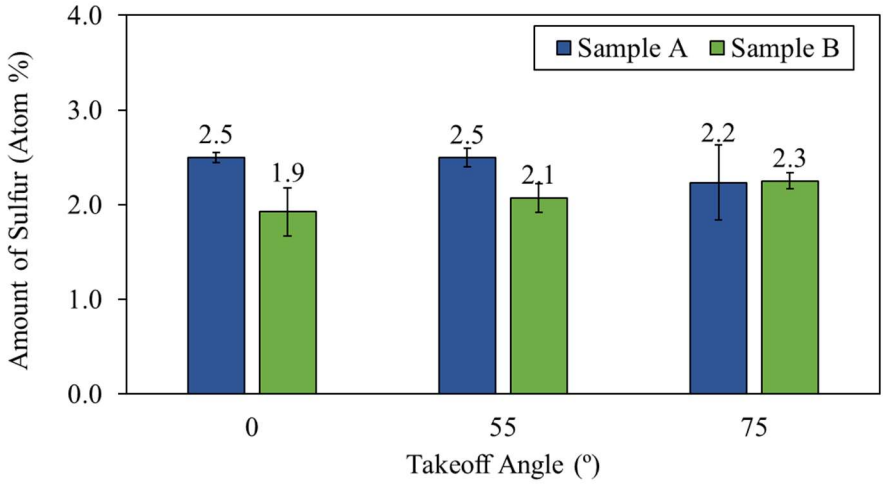

Figure 5.6. Amount of sulfur on the surface of the cysteine-conjugated surface using the SN2 reaction, measured with the Kratos XPS at various takeoff angles.

The full composition from the angle-dependent study verifies contamination by way of excess nitrogen and sodium (**Figure 5.7**). There is also a significant amount of fluorine present, indicating delamination of the coating. The similar amounts of measured fluorine suggest that the same degree of delamination occurred for both samples. The amount of bromine observed varies greatly from sample A to sample B. Both samples were prepared in the same batch and should be nearly identical suggesting contamination or harsh handling during XPS stage mounting. The angle-dependent XPS of the cysteine-conjugated surface using the S_N2 reaction should be repeated to clarify differences in the composition at shallower depths of the coating.

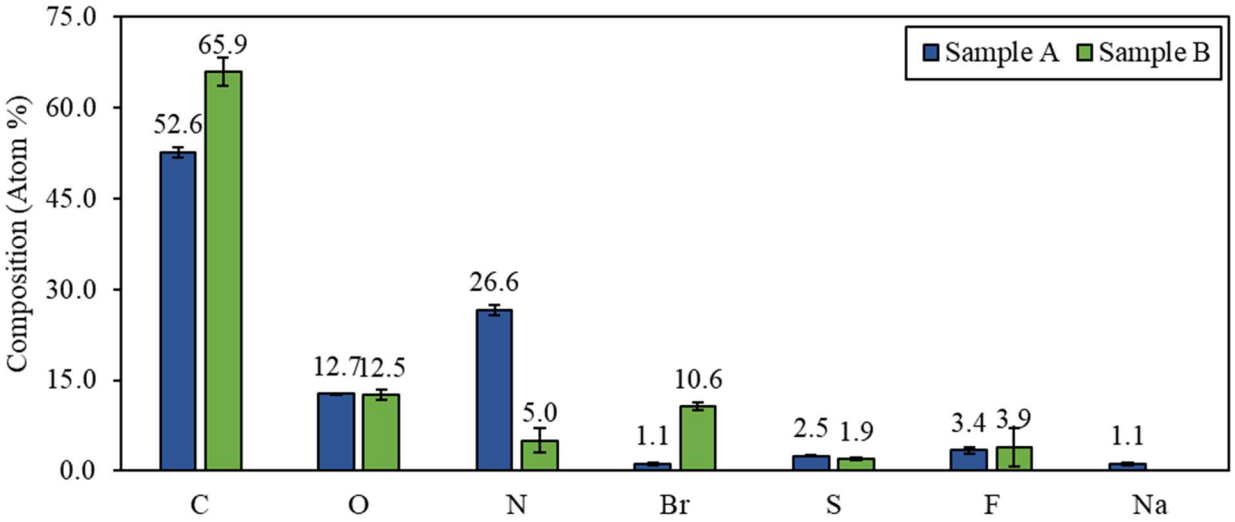

Figure 5.7. Surface composition of the cysteine-conjugated surface using the SN2 reaction, measured during the angle-dependent study at 0º takeoff angle using the Kratos XPS.

5.2.2 *Cysteine-containing peptides were conjugated to pHEMA hydrogels.*

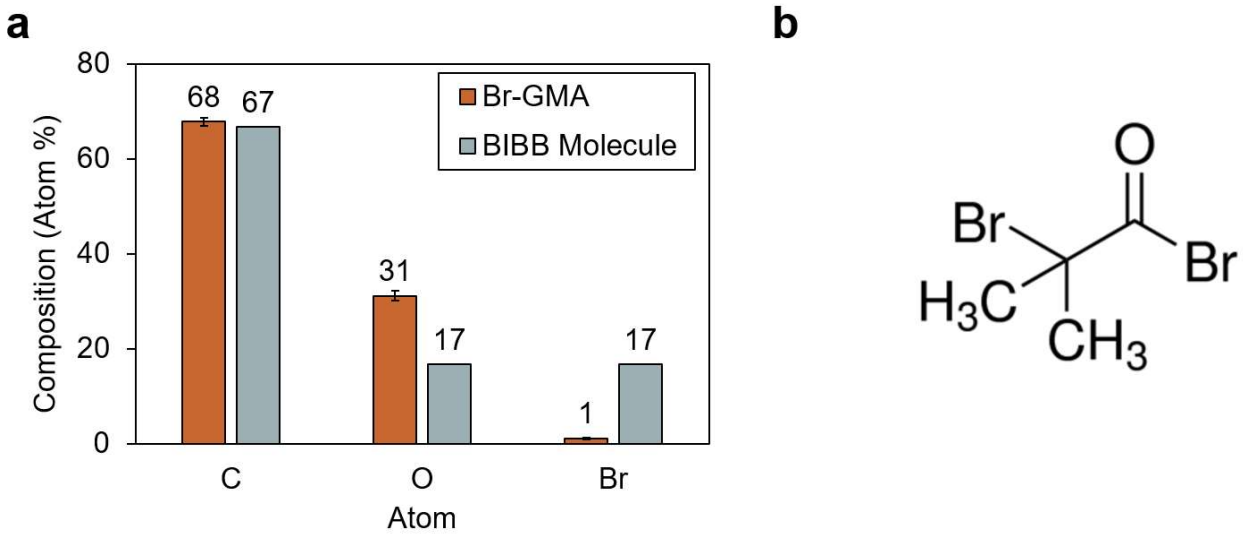

Figure 5.8. a) Surface composition of hydrogel after BIBB conjugation, measured with the Kratos XPS and **b)** the BIBB molecule. There is a small about of bromine found on the surface of the hydrogel that should be enough to immobilize thiolated biomolecules.

Using the S_N2 reaction for conjugating cysteine to a brominated surface, cysteine-containing peptides were conjugated to pHEMA hydrogels (**Figure 5.3**). These peptides were acquired from

other labs' scraps and therefore have no scientific purpose other than being a larger biomolecule containing a cysteine. One of the peptides was cyclical and was from the David Baker Lab [Dept. of Biochemistry, University of Washington]. The other peptide was from the DeForest Lab [Dept. of Chemical Engineering, University of Washington]. Firstly, the hydrogels were synthesized, brominated with BIBB, and characterized with XPS (**Figure 5.8**). After BIBB conjugation, the hydrogels had just 1% bromine on the surface. While this is not a great amount of bromine, it is enough to measure changes in the surface composition due to conjugated peptides and cysteines.

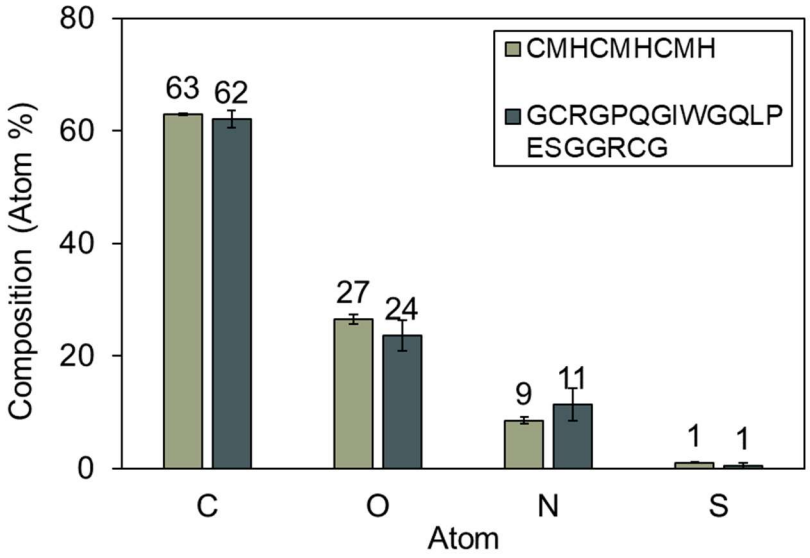

Figure 5.9. Surface composition of cysteine-containing peptides after conjugation to brominated hydrogel using the S_N2 reaction, measured with the Kratos XPS.

On the brominated hydrogels, the 2 donated peptides were conjugated and measured using XPS (**Figure 5.9**). The surfaces increased significantly in nitrogen and both surfaces had a small sulfur signal. The non-cyclical peptide contains just 1% sulfur (**Table 5.1**). Given the initial 1% bromine on the surface, this 1% sulfur could be expected for a 100% conversion. For the cyclical peptide, just 1% sulfur was measured as well, despite having a much larger

percentage of sulfur in the molecule. However, this discrepancy is still within the range of error for the XPS characterization technique. More interestingly, no bromine was measured on the surfaces, suggesting that there was either 1) too weak of a signal to quantify or 2) most of the bromine left during the backside attack of the S_N2 reaction. Either way, techniques with better sensitivity is required for further characterization of the viability of the S_N2 reaction for immobilizing biomolecules.

Table 5.1. Theoretical percentages of each atom in each of the cysteine-containing peptides. Of note: the cyclical peptide contains 5% sulfur whereas the other peptide contains just 1% sulfur.

Atom	CMHCMHCMH	GCRGPQGIWGQLPESGGRCG
C	51	51
O	24	28
N	20	20
S	5	1

5.2.3 *Surface-immobilized peptides remain bioactive*

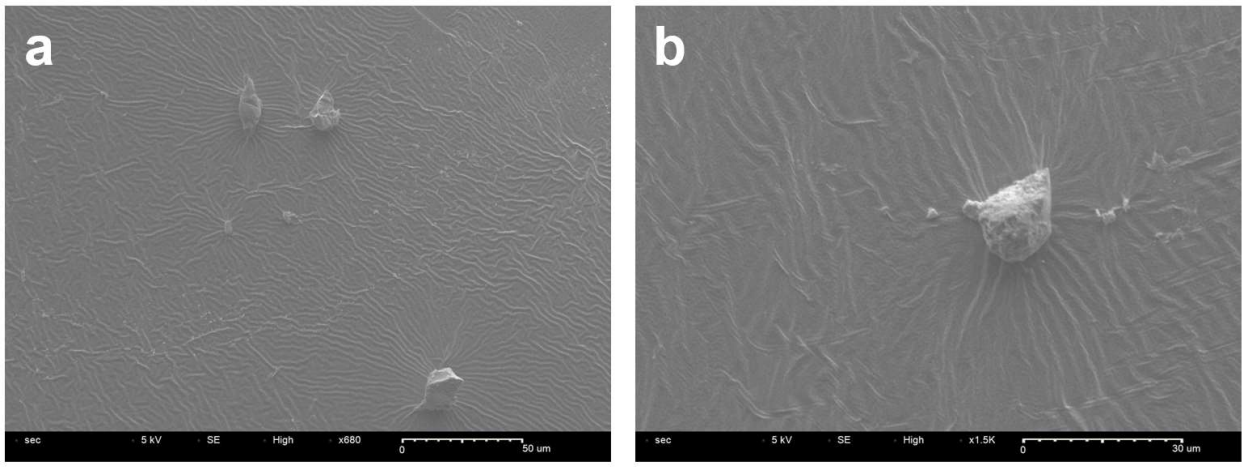

Figure 5.10. RGD peptide pHEMA hydrogel surfaces after 24 hours culture with fibroblasts at a) 680x and b) 1500x.

To demonstrate that immobilized molecules using the proposed S_N2 reaction maintain bioactivity, a simple assay was developed. A peptide containing the RGD sequence that promotes cell attachment was conjugated to the brominated hydrogel using the S_N2 reaction (**Figure 5.3**). The peptide-conjugated hydrogels were cultured with 3T3 fibroblasts for up to 48 hours, fixed, and imaged with SEM. As expected, the pHEMA hydrogels resist cell attachment. Cells were only found on RGD peptide-immobilized pHEMA hydrogels cultured for 24 hours (**Figure 5.10**). The features found on the surfaces roughly-resemble fibroblasts. They are the size of typical fibroblasts. The surface ridges that have formed radially from the cells might have been from a turbulent critical point dry process and poor sample management. In any account, these experiments should be repeated. No cells were found on the control pHEMA hydrogels (**Figure 5.11**). These results suggest that the RGD-containing peptides were immobilized to a small extent to the pHEMA hydrogels, demonstrating that the S_N2 reaction is suitable for cysteine-containing biomolecules and brominated surfaces. Upon further exploration, this method may be used extensively to conjugate cysteine-containing *de novo* molecules and proteins for many therapeutic purposes.

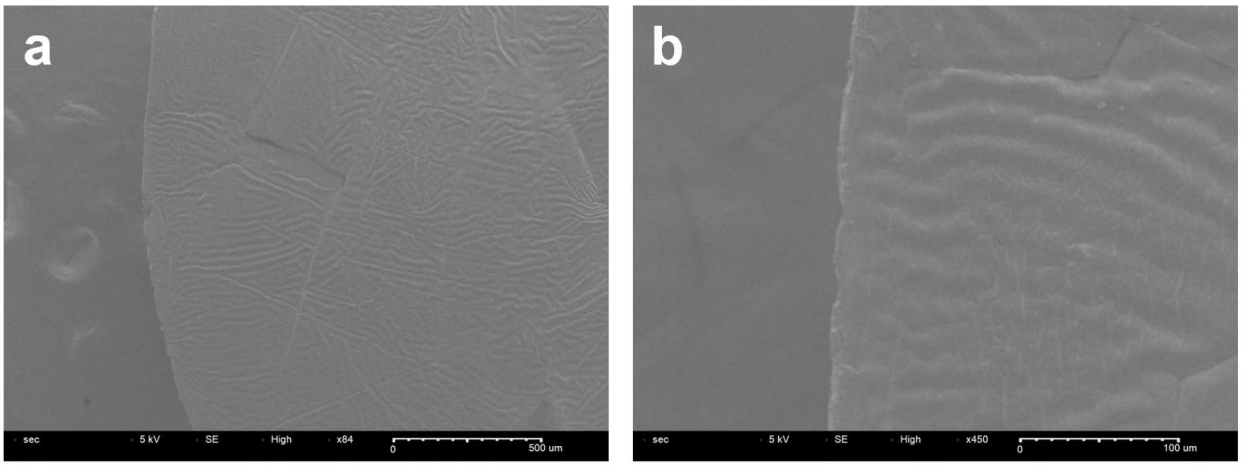

Figure 5.11. pHEMA surfaces after 24 hour culture with fibroblasts at a) 84x and b) 450x.

Additionally, cells were harvested from the surface of the hydrogels and counted after 2 and 6 hours of incubation (**Figure 5.12**). The bare pHEMA hydrogels should have minimal cell adhesion as shown by the low cell count in green. To verify that the proposed S_N2 reaction immobilizes the cysteine-containing biomolecule while retaining biofunctionality, the RGD cell adhesion peptide was immobilized to the pHEMA hydrogel. After washing, there were 3 times as many cells on the RGD-immobilized pHEMA hydrogels as the control bare pHEMA hydrogels, confirming that the peptides were immobilized to the surface. There was very little difference in cell immobilization at 2 hours of incubation versus 6 hours. In future work, the assay will only be run for 2 hours of cell incubation. Overall, the proposed S_N2 reaction has shown to be a promising method of immobilizing cysteine-containing biomolecules while retaining bioactivity and may be used to immobilize the *de novo* IL-4.

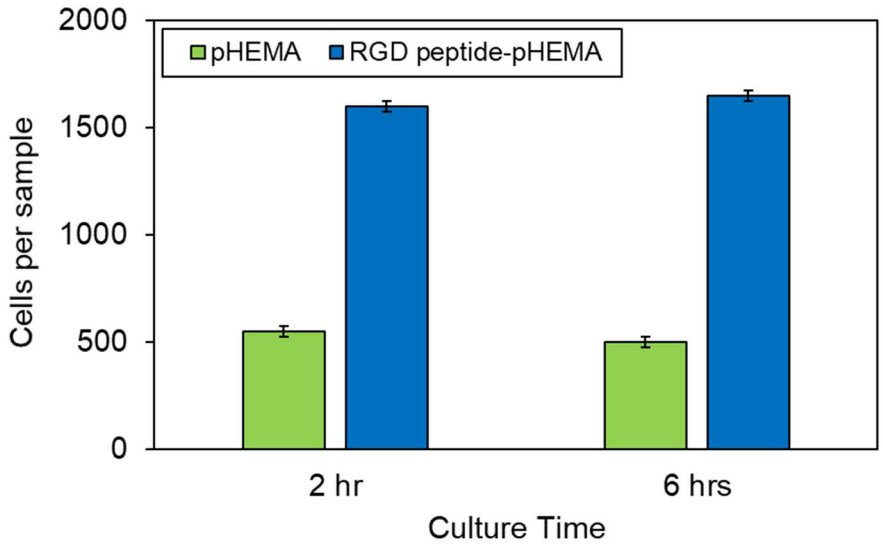

Figure 5.12. Cells attached to the surfaces of the incubated hydrogels with 3T3 fibroblasts. Bare pHEMA controls should acquire minimal cell adhesion. After the immobilization of the cell adhesion RGD peptide, more than 3 times the number of cells were attached to the surface as counted.

5.3 CONCLUSIONS

To polarize macrophage cells associated with the FBR to an alternative, M2, phenotype, a computationally designed, ultra-stable *de novo* IL-4 will be conjugated to the insulin catheter surface. Here, a simple S_N2 reaction was investigated to conjugate the cysteine anchor on the *de novo* IL-4 to a brominated surface. First, cysteine was conjugated. Then, cysteine-containing peptides were immobilized on brominated pHEMA hydrogels. XPS was used to confirm the presence of these materials on the surfaces. To ensure immobilized molecules remain biologically active, a peptide that promotes cell adhesion—contains the RGD sequence—was immobilized on brominated pHEMA hydrogels and cultured with fibroblasts. After 24 hours, fibroblasts were fixed and imaged with SEM. Cells were found on the RGD-containing peptide hydrogel surfaces but not on the control hydrogel surfaces without the cell adhesion peptide suggesting that the immobilization S_N2 reaction is a viable option for conjugating cysteine-containing biomolecules and therapeutics. In future work, it is suggested that the cysteine-containing *de novo* IL-4 is re-synthesized and immobilized to pHEMA hydrogels. The hydrogels may then be cultured with macrophages and various ELISAs for M1 and M2 markers may be used to quantify macrophage polarization and extent of polarization.

5.4 ACKNOWLEDGMENTS

I would like to acknowledge Umut Ulge, MD, PhD [umutu@uw.edu, University of Washington, Neoleukin Therapeutics] for the design and synthesis of the *de novo* IL-4 and mentorship. Patrick Shelton, PhD [sheltonp@uw.edu, University of Washington] suggested the S_N2 reaction. Lars Crawford, PhD [crawford.lars@gmail.com, University of Washington] provided guidance

in planning *in vitro* macrophage polarization assays. Sharon Creason [screason@uw.edu, University of Washington] has provided initial laboratory mentorship and carried out all of the cell adhesion study with her expertise in cell culture. Samantha Young, PhD [samyoung@uw.edu, Molecular Analysis Facility] provided expertise in XPS. Marvin Mecwan, PhD [mmecwan@uw.edu, University of Washington] has provided mentorship and plasma reactor and protein adsorption expertise. The Molecular Analysis Facility (MAF) [Molecular Engineering and Sciences, University of Washington] has been instrumental (pun intended) in providing analysis equipment and expertise for this work, including XPS. I would like to acknowledge Prof. Buddy Ratner [ratner@uw.edu, University of Washington] for the design of the project and persistent mentorship. I would like to acknowledge the generous funding from the Juvenile Diabetes Research Fund to support this work.

Chapter 6. REDUCING RISK OF BACTERIAL INFECTION WITH ANTIBIOTIC EXTENDED RELEASE AND CONCENTRATION MODELING

6.1 INTRODUCTION

Insulin delivery catheters often are functional for only 2-3 days whereas contemporary glucose sensors can function well for about 2 weeks [107]. Consequently, for a diabetic patient using a closed-loop system to regulate blood glucose levels, these components necessitate separate schedules of device maintenance. Ideally, the components would be merged into a single closed-loop system, requiring increased catheter lifetime to match that of the sensor. Experiments are ongoing in our laboratories to increase catheter lifetimes through mitigation of the foreign body response—briefly described in this paper. However, consider that longer percutaneous penetrations increase the risk of microbial infection and biofilm formation. To combat this risk of infection, we propose a method for the integration of an antibiotic into the outer polymer layer of the catheter tubing for extended release over a 2-week lifetime at the insertion site. We also propose a method for calculation of the concentration of the released drug in the extracellular matrix (ECM) around the catheter tip to ensure bacteria death and biofilm inhibition. This will minimize the development of bacterial antibiotic resistance.

We have chosen to impregnate the catheter with the antibiotic, levofloxacin, due to its broad spectrum antibacterial profile, tolerability, and efficacy[108,109]. It has an apparent volume of distribution of 70 L, meaning that there is minimal uptake by adipose tissue, the typical site of an insulin delivery catheter [110]. Thus, the concentration of levofloxacin calculated by the model should be close to the amount readily available in the ECM to prevent bacterial growth.

The antibiotic is used to prevent the formation of a biofilm which may lead to infection[111]. To prevent the development of antibiotic resistance, it is critical that the concentration of antibiotic around the catheter insertion site is above the minimum inhibitory concentration (MIC). Skin-resident bacteria, Staphylococcus *epidermidis*, are known as the bacterial colonizer of the skin[112]. The highest MIC found in literature is 8 μg/mL for levofloxacin in methicillin-resistant S. *epidermidis* strain 125[113]. The highest MIC found overall is for ofloxacin-resistant S. aureus strain 60171 at 9.38 μg/mL though typical MICs for common bacteria non-resistant strains are less than 1 μg/mL for levofloxacin[109,114]. In this work, we used the experimental data from the release of antibiotic from treated catheters to develop a semi-empirical model utilizing Fick's second law of diffusion to calculate the concentration of drug present in the ECM around the catheter within 2 diameters of a bacterium—the zone assumed to be critical to biofilm formation. The calculated concentration was compared to the MICs found in the literature. Previously, researchers have used methods such as the optical electronic speckle pattern interferometry refractive index method[37], high performance liquid chromatography[115,116], Higuchi method[117–119], Korsmeyer-Peppas method[120], *in vitro* radiolabeling[121], and microvoltammetry[122] to calculate the diffusivity of a drug and consequently the concentration. While these methods have either been found faulty or require extensive optical or chromatography instrumentation, we utilized the Stokes-Einstein equation which has been used previously for levofloxacin with the refractive index method[37].

To increase the *in vivo* lifetime of the insulin catheter to 2 weeks, we have developed a nonfouling coating, a surface-polymerized zwitterionic molecule, sulfobetaine methacrylate (SBMA), to resist protein adsorption and subsequent catheter tip occlusion. Since the nonfouling coating requires solvents that swell the catheter polymer—a polyurethane—we suspected

premature extraction of antibiotic during the coating treatment and hence less antibiotic release. Therefore, we studied the difference in antibiotic release before and after the nonfouling treatment to determine that the levofloxacin impregnation was sufficient to maintain the MIC.

6.2 RESULTS AND DISCUSSION

6.2.1 *S. epidermidis inhibition*

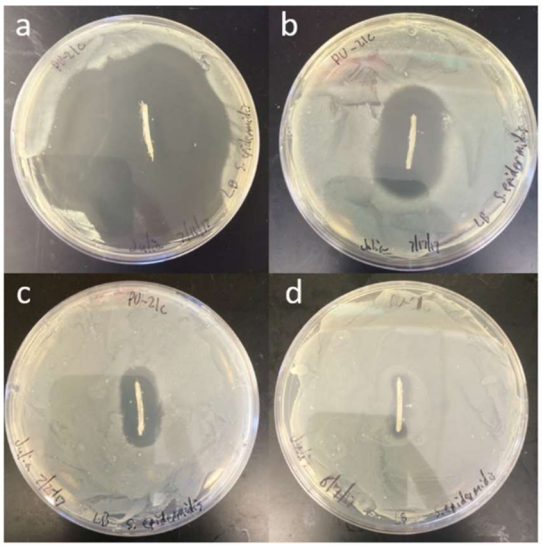

Figure 6.1. Bacterial Inhibition Assay. Levofloxacin-treated tubing implanted in LB agar with S. epidermidis after total release time of **a)** 3 days, **b)** 12 days, **c)** 20 days, and **d)** 31 days with a visible inhibition zone for all time points

The bactericidal character and prevention of biofilm formation by the levofloxacin-impregnated tubing is demonstrated and confirmed with the inhibition of S. epidermidis on LB agar plates post-incubation (**Figure 6.1**). The zone is visible for more than 38 days, displaying an inhibition zone of at least a few millimeters even at day 38. Over time, the inhibition zone became smaller as expected with the decreasing antibiotic release from the catheter. Agar was a satisfactory medium for observing antibiotic diffusion as it is commonly used for drug and protein diffusion

experiments and bacterial inhibition experiments such as the Kirby-Bauer Method[123], specifically with levofloxacin[114,124,125]. The experiment was terminated when the inhibition zone became so small that measurement was difficult. These results verify a significant amount of released antibiotic during this course.

6.2.2 *Levofloxacin release profile*

Quantitatively, the amount of levofloxacin released in water follows logarithmic behavior (**Figure 6.2**). The high concentration of levofloxacin released immediately is favorable for insulin delivery catheters. At the time of insertion there is an increased chance for infections and therefore there are potential benefits from a higher antibiotic dose. For tubing loaded in treatment solutions of higher drug concentration, the tubing released more levofloxacin and at a faster rate. The logarithmic behavior of the release curves can be described by

$$N = \exp[0.23 \cdot ln(t) + 2.9C + 0.25] \tag{6.1}$$

where N is the total amount of levofloxacin released (μg/cm^2), t is the total time of release (hr), and C is the initial concentration of the treatment solution (mg/mL). The numerical constants in equation 2.1 were calculated empirically from collected data for a treatment solution range of 0.2-1.7 mg levofloxacin/mL solution. The model in equation 6.1 could potentially be used to predict overall antibiotic release for other loading concentrations, though we do not use the model itself in the concentration prediction model presented in equation 2.6.

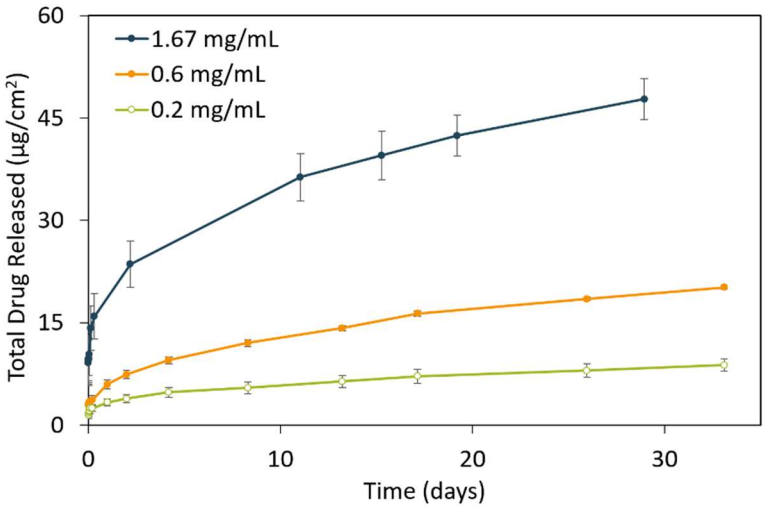

Figure 6.2. Total levofloxacin released. For different initial treatment solution concentrations, the total drug released was measured over time with n=3.

6.2.3 *Levofloxacin concentration around the insulin catheter*

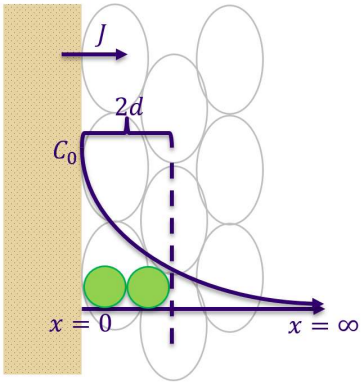

Figure 6.3. Schematic of concentration modeling in a control volume of 2 diameters of bacteria. The levofloxacin diffuses out of the catheter (tan) in the direction of *J*. C_0 was measured with the extended release assay.

From the semi-empirical model, we have determined the concentration of levofloxacin around the catheter was maintained at multiple orders of magnitude greater than the MIC for 4 different initial treatment solution concentrations, even after 3 weeks (**Figure 6.4**). The minimally-loaded—0.2 mg/mL—samples released antibiotic to 820,000 µg/mL at day 26. Our aim is to

maintain a levofloxacin concentration above the MIC. The control volume used to calculate the levofloxacin concentration around the catheter is 2 diameters of bacteria on the surface (**Figure 6.3**).

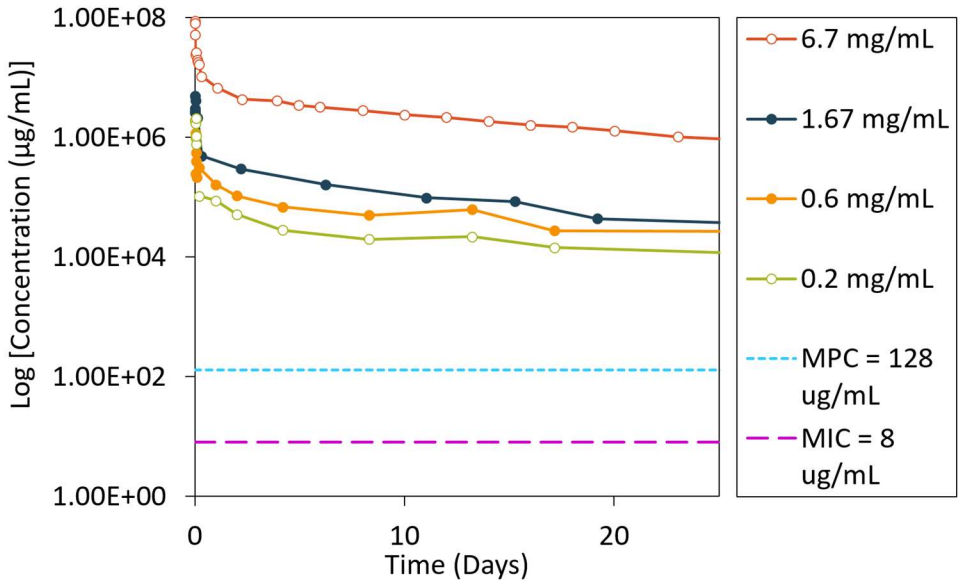

Figure 6.4. Levofloxacin concentration. The plot shows the drug concentration around the catheter within 2 diameters of bacteria using the semi-empirical model for samples treated at different initial treatment solution concentrations, the MPC, and the MIC for levofloxacin

Notably, the highest MIC reported in literature for Staphylococcus was 8 µg/mL[113], though typically the MIC is less than 1 µg/mL[109]. The results of the concentration model on the release data show concentrations multiple orders of magnitude above the MIC. This may seem excessive. However, the release control volume was 0.17 µL. Even though the concentration is much higher than the MIC, the total drug released from the catheter tip ranged from 8-45 µg in 26 days which is 4 orders of magnitude less than the 500-750 mg/day dose commonly administered systemically. Local drug delivery is important for this reason: the drug may be effective in treating an infection at low concentrations when directed at the site of infection

without exposing the whole body, thereby reducing the risk of adverse effects and possible antibiotic resistance.

6.2.4 *Suitable levofloxacin release after nonfouling coating treatment*

Since we plan to extend the longevity of the insulin catheter with a nonfouling coating, we have studied how antibiotic leaching is impacted by the submersion-intensive coating process (**Figure 6.5**). For the minimally-loaded tubing, the total levofloxacin released from the nonfouling coating-treated tubing was 7.4 μg/cm^2 after 26 days whereas 32 μg/cm^2—4.3 times more—was released for the tubing without the nonfouling coating treatment. While the difference in total levofloxacin released is significant, the catheter treated with the nonfouling coating reached a concentration as of 16 mg/mL after 26 days which is still greater than the MIC, confirming sufficient antibacterial activity of the treated tubing. We have concluded that our method for levofloxacin impregnation is sufficient for reducing the risk of biofilm formation for insulin catheters with an additional nonfouling treatment to extend device longevity.

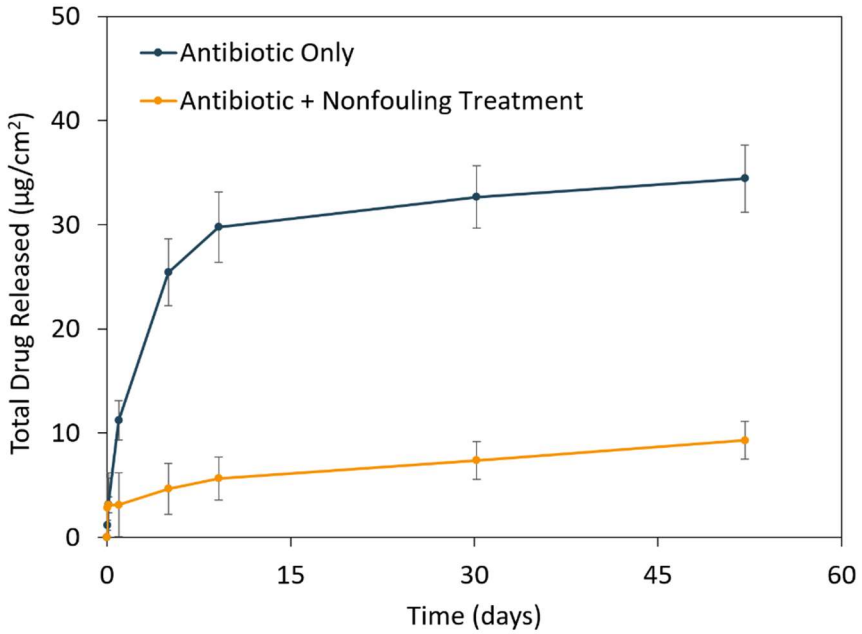

Figure 6.5. Total levofloxacin released after nonfouling treatment. The plot shows the total drug released for catheter impregnated with levofloxacin and for tubing that experienced the nonfouling coating treatment with n=3.

Finally, the amount of levofloxacin released was measured in both water and 0.9% sodium chloride solutions for almost 5 years (**Figure 6.6**). Even though only a total of up to 130 µg was released, the MIC was maintained for 5 years according to the model presented. This method of levofloxacin incorporation into the insulin catheter and extended release has shown to be a sufficient method in preventing infection with the proposed lifetime extension for the device.

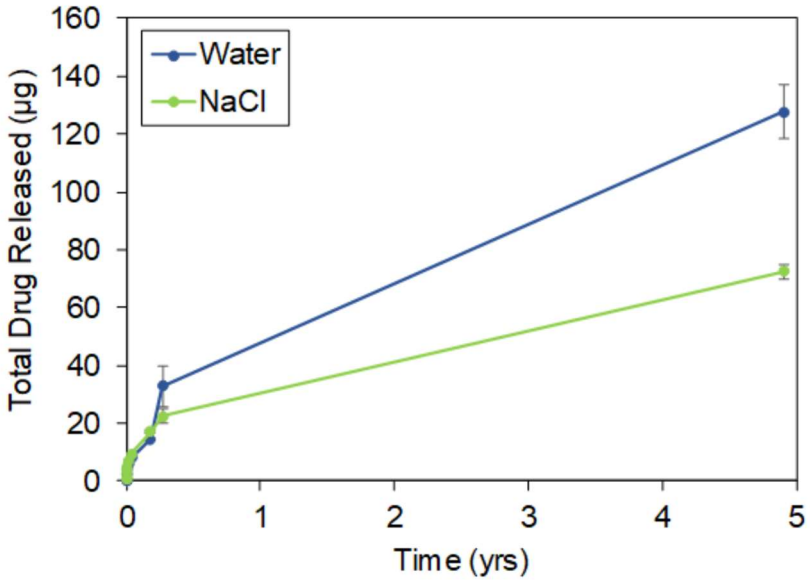

Figure 6.6. Total levofloxacin extended release. Catheter tubing was treated with levofloxacin for extended release in either water or 0.9% NaCl. Over the years, the concentration remained over the MIC for both release mediums. Less antibiotic was released into the NaCl solution most likely due to the partition coefficient or higher osmotic pressure.

6.3 CONCLUSIONS

Swelling infusion for adding levofloxacin to the insulin delivery catheter provides effective antibacterial activity for longer than the 2-week period specified by our design criteria. To assess if we have sufficient antibiotic concentration around the catheter, the semi-empirical model calculates the concentration of levofloxacin in the vicinity of the catheter over time. Concentrations of levofloxacin were multiple orders of magnitude higher than the MIC. After the nonfouling coating treatment for levofloxacin-impregnated catheters, the levofloxacin concentrations were maintained higher than the MIC, confirming sufficient antibiotic to prevent biofilm formation for the nonfouling coating and enhance the longevity of the implanted insulin catheter. Given the similarity in molecular weight and structure of levofloxacin to other

fluoroquinolones, we predict that similar results will be obtained with other antibiotics in this class of molecules.

6.4 ACKNOWLEDGEMENTS

I would like to acknowledge Sharon Creason [screason@uw.edu, University of Washington] for initial laboratory mentorship. The James Bryers lab [Dept. of Bioengineering, University of Washington] supplied lab equipment, training for bacterial experiments, and inoculum of bacteria. Prof. Buddy Ratner [ratner@uw.edu, University of Washington] helped design this project and gave persistent mentorship. JDRF supported this work financially.

BIBLIOGRAPHY

1. Ratner BD. Role of Water in Biomaterials. In: *Biomaterials Science - An Introduction to Materials in Medicine*. 3rd ed. Elsevier; 2013:55-59.
2. Lee KY. M1 and M2 polarization of macrophages: a mini-review. *Med Biol Sci Eng*. 2019;2(1):1-5. doi:10.30579/mbse.2019.2.1.1
3. Anderson JM, Rodriguez A, Chang DT. Foreign body reaction to biomaterials. *Semin Immunol*. 2008;20(2):86-100. doi:10.1016/j.smim.2007.11.004
4. Grainger DW. All charged up about implanted biomaterials. *Nat Biotechnol*. 2013;31(6):507-509. doi:10.1038/nbt.2600
5. Glaros T, Larsen M, Li L. Macrophages and fibroblasts during inflammation, tissue damage and organ injury. *Front Biosci*. 2009;14:3988-3993.
6. Centers for Disease Control and Prevention. *National Diabetes Statistics Report 2020. Estimates of Diabetes and Its Burden in the United States.*; 2020.
7. Centers for Disease Control and Prevention. *Long-Term Trends in Diabetes*.; 2017.
8. Mueller-Godeffroy E, Vonthein R, Ludwig-Seibold C, et al. Psychosocial benefits of insulin pump therapy in children with diabetes type 1 and their families: The pumpkin multicenter randomized controlled trial. *Pediatr Diabetes*. 2018;19(8):1471-1480. doi:10.1111/pedi.12777
9. Fenter P, Lee SS. Hydration layer structure at solid–water interfaces. *MRS Bull*. 2014;39(12):1056-1061. doi:10.1557/mrs.2014.252
10. Ren P-F, Yang H-C, Liang H-Q, Xu X-L, Wan L-S, Xu Z-K. Highly Stable, Protein-Resistant Surfaces via the Layer-by-Layer Assembly of Poly(sulfobetaine methacrylate) and Tannic Acid. *Langmuir*. 2015;31:5851-5858. doi:10.1021/acs.langmuir.5b00920
11. Zhang Z, Chen S, Chang Y, Jiang S. Surface Grafted Sulfobetaine Polymers via Atom Transfer Radical Polymerization as Superlow Fouling Coatings. *J Phys Chem B*. 2006;110:10799-10804. doi:10.1021/jp057266i
12. Moore GE. Cramming more components onto integrated circuits. *Electronics*. 1965;38(8).
13. Coluzza I. Computational protein design: a review. *J Phys Condens Matter*. 2017;29:1-16. doi:10.1088/1361-648X/aa5c76
14. Bosco MC. Macrophage polarization: Reaching across the aisle? *J Allergy Clin Immunol*. 2019;143:1348-1350. doi:10.1016/j.jaci.2018.12.995

15. Wang N, Liang H, Zen K, Lenz LL. Molecular mechanisms that influence the macrophage M1-M2 polarization balance. *Front Immunol*. 2014;5:1-9. doi:10.3389/fimmu.2014.00614
16. Lippow SM, Tidor B. Progress in computational protein design. *Curr Opin Biotechnol*. 2007;18:305-311. doi:10.1016/j.copbio.2007.04.009
17. Zhang L, Cao S, Marsh N, et al. Infection risks associated with peripheral vascular catheters. *J Infect Prev*. 2016;17(5):207-213. doi:10.1177/1757177416655472/FORMAT/EPUB
18. Friedman ND, Temkin E, Carmeli Y. The negative impact of antibiotic resistance. *Clin Microbiol Infect*. 2016;22(5):416-422. doi:10.1016/J.CMI.2015.12.002
19. Frieri M, Kumar K, Boutin A. Antibiotic resistance. *J Infect Public Health*. 2017;10(4):369-378. doi:10.1016/J.JIPH.2016.08.007
20. Gao P, Nie X, Zou M, Shi Y, Cheng G. Recent advances in materials for extended-release antibiotic delivery system. *J Antibiot (Tokyo)*. 2011;64(9):625-634. doi:10.1038/ja.2011.58
21. Hong D, Hung H-C, Wu K, et al. Achieving Ultralow Fouling under Ambient Conditions via Surface- Initiated ARGET ATRP of Carboxybetaine. *Appl Mater Interfaces*. 2017;9:9255-9259. doi:10.1021/acsami.7b01530
22. Prime KL, Whitesides GM. Adsorption of Proteins onto Surfaces Containing End-Attached Oligo(ethylene oxide): A Model System Using Self-Assembled Monolayers. *J Am Chem Soc*. 1993;115:10714-10721. https://pubs.acs.org/doi/pdf/10.1021/ja00076a032. Accessed February 5, 2018.
23. Park S-J, Lee K-P, Kang S, Lee J, Sato K, Chung HY. Sphingosine 1-phosphate induced anti-atherogenic and atheroprotective M2 macrophage polarization through IL-4. *Cell Signal*. 2014;26:2249-2258. doi:10.1016/j.cellsig.2014.07.009
24. Gao S, Zhou J, Liu N, et al. Curcumin induces M2 macrophage polarization by secretion IL-4 and/or IL-13. *J Mol Cell Cardiol*. 2015;85:131-139. doi:10.1016/j.yjmcc.2015.04.025
25. Simon MD, Chu F, Racki LR, et al. The Site-Specific Installation of Methyl-Lysine Analogs into Recombinant Histones. *Cell*. 2007;128(5):1003-1012. doi:10.1016/J.CELL.2006.12.041
26. Mashazi PN, Ozoemena KI, Maree DM, Nyokong T. Self-assembled monolayers (SAMs)

of cobalt tetracarboxylic acidchloride phthalocyanine covalently attached onto a preformed mercaptoethanol SAM: A novel method. *Electrochim Acta*. 2006;51(17):3489-3494. doi:10.1016/J.ELECTACTA.2005.10.004

27. Navarro LA, Enciso AE, Matyjaszewski K, Zauscher S. Enzymatically Degassed Surface-Initiated Atom Transfer Radical Polymerization with Real-Time Monitoring. *J Am Chem Soc*. 2019;141:3100-3109. doi:10.1021/jacs.8b12072
28. Mecwan MM, Taylor MJ, Graham DJ, Ratner BD. Highly-reactive haloester surface initiators for ARGET ATRP readily prepared by radio frequency glow discharge plasma. *Biointerphases*. 2019;14:41006. doi:10.1116/1.5110163
29. Horbett TA. Protein adsorption on biomaterials. In: *Biomaterials: Interfacial Phenomena and Applications*. Vol 199. ; 1982:233-244. doi:10.1021/ba-1982-0199.ch017
30. Bayston R, Grove N, Siegel J, Lawellin D, Barsham S. Prevention of hydrocephalus shunt catheter colonisation in vitro by impregnation with antimicrobials. *J Neurol Neurosurg Psychiatry*. 1989;52:605-609. doi:10.1136/jnnp.52.5.605
31. Fisher LE, Hook AL, Ashraf W, et al. Biomaterial modification of urinary catheters with antimicrobials to give long-term broadspectrum antibio fi lm activity. *J Control Release*. 2015;202:57-64. doi:10.1016/j.jconrel.2015.01.037
32. Desai NP, Hubbell JA. Solution technique to incorporate polyethylene oxide and other water-soluble polymers into surfaces of polymeric biomaterials. *Biomaterials*. 1991;12(2):144-153. doi:10.1016/0142-9612(91)90193-E
33. Dai H, Wu J, Wang Y, et al. Diffusion of Levofloxacin Mesylate in Agarose Hydrogels Monitored by a Refractive-Index Method. *J Appl Polym Sci*. 2010;21:3000-3006. doi:10.1002/app
34. Pelton AD, Etsell TH. Analytical Solution of Fick's Second Law When the Diffusion Coefficient Varies Directly as Concentration. *Acta Metall*. 1972;20:1269-1274.
35. Nance EA, Woodworth GF, Sailor KA, et al. A Dense Poly(Ethylene Glycol) Coating Improves Penetration of Large Polymeric Nanoparticles Within Brain Tissue. *Sci Transl Med*. 2012;4(149):149ra119-149ra119. doi:10.1126/scitranslmed.3003594
36. Vrany JD, Stewart PS, Suci PA. Comparison of recalcitrance to ciprofloxacin and levofloxacin exhibited by Pseudomonas aeruginosa biofilms displaying rapid-transport characteristics. *Antimicrob Agents Chemother*. 1997;41(6):1352-1358.

37. Tan S, Dai H, Wu J, Zhao N, Zhang X, Xu J. Optical investigation of diffusion of levofloxacin mesylate in agarose hydrogel. *J Biomed Opt*. 2009;14(5):050503. doi:10.1117/1.3227034
38. Horbett TA. Adsorption of proteins from plasma to a series of hydrophilic-hydrophobic copolymers. II. Compositional Analysis With the Prelabeled Protein Technique. *J Biomed Mater Res*. 1981;15(5):673-695. doi:10.1002/jbm.820150506
39. Speight RE, Cooper MA. A Survey of the 2010 Quartz Crystal Microbalance Literature. *J Mol Recognit*. 2012;25:451-473. doi:10.1002/jmr.2209
40. Phan HTM, Bartelt-Hunt S, Rodenhausen KB, Schubert M, Bartz JC. Investigation of bovine serum albumin (BSA) attachment onto self-assembled monolayers (SAMs) using combinatorial quartz crystal microbalance with dissipation (QCM-D) and spectroscopic ellipsometry (SE). *PLoS One*. 2015;10(10). doi:10.1371/JOURNAL.PONE.0141282
41. Dolatshahi-Pirouz A, Rechendorff K, Hovgaard MB, Foss M, Chevallier J, Besenbacher F. Bovine serum albumin adsorption on nano-rough platinum surfaces studied by QCM-D. *Colloids Surfaces B Biointerfaces*. 2008;66:53-59. doi:10.1016/j.colsurfb.2008.05.010
42. Dixon MC. Quartz Crystal Microbalance with Dissipation Monitoring: Enabling Real-Time Characterization of Biological Materials and Their Interactions. *J Biomol Tech*. 2008;19:151-158.
43. Costa D, Garrain P-A, Baaden M. Understanding small biomolecule-biomaterial interactions: A review of fundamental theoretical and experimental approaches for biomolecule interactions with inorganic surfaces. *J Biomed Mater*. 2012:1210-1222. doi:10.1002/jbm.a.34416
44. Harrison ET. Combining Surface Analytical and Computational Techniques to Investigate Orientation Effects of Immobilized Proteins. 2017.
45. Zaera F. Probing liquid/solid interfaces at the molecular level. *Chem Rev*. 2012;112(5):2920-2986. doi:10.1021/cr2002068
46. Ogi H. Wireless-electrodeless quartz-crystal-microbalance biosensors for studying interactions among biomolecules: A review. *Proc Japan Acad Ser B*. 2013;89(9):401-417.
47. Mashaghi A, Mashaghi S, Reviakine I, Heeren RMA, Sandoghdar V, Bonn M. Label-free characterization of biomembranes: From structure to dynamics. *Chem Soc Rev*. 2014;43(3):887-900. doi:10.1039/c3cs60243e

48. Yuan Z, Tai H, Bao X, Liu C, Ye Z, Jiang Y. Enhanced humidity-sensing properties of novel graphene oxide/zinc oxide nanoparticles layered thin film QCM sensor. *Mater Lett*. 2016;174:28-31. doi:10.1016/j.matlet.2016.01.122
49. Iruthayaraj J, Olanya G, Claesson PM. Viscoelastic Properties of Adsorbed Bottle-brush Polymer Layers Studied by Quartz Crystal Microbalance s Dissipation Measurements. *J Phys Chem C*. 2008;112:15028-15036. doi:10.1021/jp804395f
50. Constantinides G, Ilke Kalcioglu Z, Mcfarland M, Smith JF, Van Vliet KJ. Probing mechanical properties of fully hydrated gels and biological tissues. *J Biomech*. 2008;41:3285-3289. doi:10.1016/j.jbiomech.2008.08.015
51. Wang H, Chen S, Li L, Jiang S. Improved method for the preparation of carboxylic acid and amine terminated self-assembled monolayers of alkanethiolates. *Langmuir*. 2005;21(7):2633-2636. doi:10.1021/la046810w
52. Ratner BD, Hoffman AS. Non-Fouling Surfaces. In: *Biomaterials Science - An Introduction to Materials in Medicine*. 3rd ed. Elsevier; 2013:241-247.
53. d'Avanzo N, Celia C, Barone A, et al. Immunogenicity of Polyethylene Glycol Based Nanomedicines: Mechanisms, Clinical Implications and Systematic Approach. *Adv Ther*. 2020;3(3). doi:10.1002/ADTP.201900170
54. Thi TTH, Pilkington EH, Nguyen DH, Lee JS, Park KD, Truong NP. The Importance of Poly(ethylene glycol) Alternatives for Overcoming PEG Immunogenicity in Drug Delivery and Bioconjugation. *Polymers (Basel)*. 2020;12(2):298. doi:10.3390
55. Ishihara K. *Bioinspired Phospholipid Polymer Biomaterials for Making High Performance Artifcial Organs*. Vol 1.; 2000. http://www.iop.org/journals/STAM. Accessed May 14, 2020.
56. Zhang L, Cao Z, Bai T, et al. Zwitterionic hydrogels implanted in mice resist the foreign-body reaction. *Nat Biotechnol*. 2013;31(6):553-556. doi:10.1038/nbt.2580
57. Zheng J, Xiao J, Wu J, et al. Zwitterionic poly(sulfobetaine methacrylate) hydrogels with optimal mechanical properties for improving wound healing in vivo Materials Chemistry B Materials for biology and medicine Zwitterionic poly(sulfobetaine methacrylate) hydrogels with optimal mech. *J Mater Chem B*. 2019;7(10):1697-1707. doi:10.1039/c8tb02590h
58. Cheng G, Zhang Z, Chen S, Bryers JD, Jiang S. Inhibition of bacterial adhesion and

biofilm formation on zwitterionic surfaces. *Biomaterials*. 2007;28:4192-4199. doi:10.1016/j.biomaterials.2007.05.041

59. Zhang Z, Chao T, Chen S, Jiang S. Superlow Fouling Sulfobetaine and Carboxybetaine Polymers on Glass Slides. *Langmuir*. 2006;22:10072-10077. doi:10.1021/la062175d
60. Jiang S, Cao Z. Ultralow-fouling, functionalizable, and hydrolyzable zwitterionic materials and their derivatives for biological applications. *Adv Mater*. 2010;22(9):920-932. doi:10.1002/adma.200901407
61. Wu J, Xiao Z, Chen A, et al. Sulfated zwitterionic poly(sulfobetaine methacrylate) hydrogels promote complete skin regeneration. *Acta Biomater*. 2018;71:293-305. doi:10.1016/j.actbio.2018.02.034
62. Sarbu T, Matyjaszewski K. ATRP of Methyl Methacrylate in the Presence of Ionic Liquids with Ferrous and Cuprous Anions. *Macromol Chem Phys*. 2001;202(17):3379-3391.
63. Simakova A, Averick SE, Konkolewicz D, Matyjaszewski K. Aqueous ARGET ATRP. *Macromolecules*. 2012;45:6371-6379. doi:10.1021/ma301303b
64. Mecwan MM, Dong X, Shi GH, Ratner BD. Plasma Polymerized HMDSO Coatings For Syringes To Minimize Protein Adsorption. *J Pharm Sci*. 2021;110(4):1710-1717.
65. Inoue Y, Ishihara K. Reduction of protein adsorption on well-characterized polymer brush layers with varying chemical structures. *Colloids Surfaces B Biointerfaces*. 2010;81:350-357. doi:10.1016/j.colsurfb.2010.07.030
66. Ladd J, Zhang Z, Chen S, Hower JC, Jiang S. Zwitterionic Polymers Exhibiting High Resistance to Nonspecific Protein Adsorption from Human Serum and Plasma. *Biomacromolecules*. 2008;9(5):1357-1361. doi:10.1021/bm701301s
67. Matyjaszewski K, Dong H, Jakubowski W, Pietrasik J, Kusumo A. Grafting from Surfaces for Everyone: ARGET ATRP in the Presence of Air. *Langmuir*. 2007;23:4528-4531. doi:10.1021/la063402e
68. Montheard J-P, Chatzopoulos M, Chappard D. 2-Hydroxyethyl Methacrylate (HEMA): Chemical Properties and Applications in Biomedical Fields. *J Macromol Sci Part C Polym Rev*. 1992;32(1):1-34. doi:10.1080/15321799208018377
69. Kett W. A Brief History of Contact Lenses. Contact Lens Manufacturers Association. https://www.contactlenses.org/timeline.htm. Published 2015. Accessed May 22, 2020.

70. Carr LR, Zhou Y, Krause JE, Xue H, Jiang S. Uniform zwitterionic polymer hydrogels with a nonfouling and functionalizable crosslinker using photopolymerization. *Biomaterials*. 2011;32(29):6893-6899. doi:10.1016/j.biomaterials.2011.06.006
71. Li A, Benetti EM, Tranchida D, Clasohm JN, Schonherr H, Spencer ND. Surface-Grafted, Covalently Cross-Linked Hydrogel Brushes with Tunable Interfacial and Bulk Properties. *Macromolecules*. 2011;44:5344-5351. doi:10.1021/ma2006443
72. Ratner BD. The Biocompatibility Manifesto: Biocompatibility for the Twenty-first Century. *J Cardiovasc Transl Res*. 2011;4(5):523-527. doi:10.1007/s12265-011-9287-x
73. Jeon SI, Lee JH, Andrade JD, De Gennes PG. Protein-surface interactions in the presence of polyethylene oxide. I. Simplified theory. *J Colloid Interface Sci*. 1991;142(1):149-158. doi:10.1016/0021-9797(91)90043-8
74. Jeon SI, Andrade JD. Protein-surface interactions in the presence of polyethylene oxide. II. Effect of protein size. *J Colloid Interface Sci*. 1991;142(1):159-166. doi:10.1016/0021-9797(91)90044-9
75. Prime KL, Whitesides GM. Self-Assembled Organic Monolayers: Model Systems for Studying Adsorption of Proteins. *Science (80-)*. 1991;252:1164-1167. http://www.jstor.org/stable/2876292. Accessed February 5, 2018.
76. Vaisocherová H, Yang W, Zhang Z, et al. Ultralow Fouling and Functionalizable Surface Chemistry Based on a Zwitterionic Polymer Enabling Sensitive and Specific Protein Detection in Undiluted Blood Plasma. *Anal Chem*. 2008;80(20):7894-7901. doi:10.1021/ac8015888
77. Leng C, Hung H-C, Sun S, et al. Probing the Surface Hydration of Nonfouling Zwitterionic and PEG Materials in Contact with Proteins. *Appl Mater Interfaces*. 2015;7:16881-16888. doi:10.1021/acsami.5b05627
78. Huang H, Zhang C, Crisci R, et al. Strong Surface Hydration and Salt Resistant Mechanism of a New Nonfouling Zwitterionic Polymer Based on Protein Stabilizer TMAO. *J Am Chem Soc*. 2021;143(40):16786-16795. doi:10.1021/jacs.1c08280
79. He M, Gao K, Zhou L, et al. Zwitterionic materials for antifouling membrane surface construction. *Acta Biomater*. 2016;40:142-152. doi:10.1016/j.actbio.2016.03.038
80. Li D, Wei Q, Wu C, et al. Superhydrophilicity and strong salt-affinity: Zwitterionic polymer grafted surfaces with significant potentials particularly in biological systems. *Adv*

Colloid Interface Sci. 2020;278(53):1-18. doi:10.1016/j.cis.2020.102141

81. Chen S, Li L, Zhao C, Zheng J. Surface hydration: Principles and applications toward low-fouling/nonfouling biomaterials. *Polymer (Guildf)*. 2010;51:5283-5293. doi:10.1016/j.polymer.2010.08.022
82. Yang W, Chen S, Cheng G, et al. Film Thickness Dependence of Protein Adsorption from Blood Serum and Plasma onto Poly(sulfobetaine)-Grafted Surfaces. *Langmuir*. 2008;24:9211-9214. doi:10.1021/la801487f
83. Li A, Benetti EM, Tranchida D, Clasohm JN, Schonherr H, Spencer ND. Surface-Grafted, Covalently Cross-Linked Hydrogel Brushes with Tunable Interfacial and Bulk Properties. *Macromolecules*. 2011;44:5344-5351. doi:10.1021/ma2006443
84. Nagasawa D, Azuma T, Noguchi H, Uosaki K, Takai M. Role of Interfacial Water in Protein Adsorption onto Polymer Brushes as Studied by SFG Spectroscopy and QCM. *J Phys Chem C*. 2015;119(30):17193-17201. doi:10.1021/acs.jpcc.5b04186
85. Sundaram HS, Han X, Nowinski AK, et al. Achieving One-Step Surface Coating of Highly Hydrophilic Poly(Carboxybetaine Methacrylate) Polymers on Hydrophobic and Hydrophilic Surfaces. *Adv Mater Interfaces*. 2014;1(6):1-8. doi:10.1002/admi.201400071
86. Zhang Z, Vaisocherová H, Cheng G, Yang W, Xue H, Jiang S. Nonfouling Behavior of Polycarboxybetaine-Grafted Surfaces: Structural and Environmental Effects. *Biomacromolecules*. 2008;9:2686-2692. doi:10.1021/bm800407r
87. Leng C, Huang H, Zhang K, et al. Effect of Surface Hydration on Antifouling Properties of Mixed Charged Polymers. *Langmuir*. 2018;34(22):6538-6545. doi:10.1021/acs.langmuir.8b00768
88. Zhang C, Parada GA, Zhao X, Chen Z. Probing Surface Hydration and Molecular Structure of Zwitterionic and Polyacrylamide Hydrogels. *Langmuir*. 2019;35:13292-13300. doi:10.1021/acs.langmuir.9b02544
89. Leng C, Han X, Shao Q, et al. In Situ Probing of the Surface Hydration of Zwitterionic Polymer Brushes: Structural and Environmental Effects. *J Phys Chem C*. 2014;118:15840-15845. doi:10.1021/jp504293r
90. Jeanette Steine M, Weidner T, McCrea K, Castner DG, Ratner BD. Hydration of sulphobetaine and tetra(ethylene glycol)-terminated self-assembled monolayers studied by sum frequency generation vibrational spectroscopy. *J Phys Chem B*. 2009;113(33):11550-

11556. doi:10.1021/jp9015867

91. Okur HI, Hladílkova J, Rembert KB, et al. Beyond the Hofmeister Series: Ion-Specific Effects on Proteins and Their Biological Functions. *J Phys Chem B*. 2017;121:1997-2014. doi:10.1021/acs.jpcb.6b10797
92. Hildebrand V, Laschewsky A, Päch M, Müller-Buschbaum P, Papadakis CM. Effect of the zwitterion structure on the thermo-responsive behaviour of poly(sulfobetaine methacrylates). *Polym Chem*. 2016;8:310-322. doi:10.1039/c6py01220e
93. Lin C-H, Luo S-C. Combination of AFM and Electrochemical QCM-D for Probing Zwitterionic Polymer Brushes in Water: Visualization of Ionic Strength and Surface Potential Effects. *Langmuir*. 2021;37:12476-12486. doi:10.1021/acs.langmuir.1c02230
94. Guthrie LA, McPhail LC, Henson PM, Johnston RBJ. Priming of neutrophils for enhanced release of oxygen metabolites by bacterial lipopolysaccharide. *J Exp Med*. 1984;160:1656-16971. doi:10.1017/CBO9781107415324.004
95. Doerfler ME, Danner RL, Shelhamer JH, Parillo JE. Bacterial lipopolysaccharides prime human neutrophils for enhanced production of leukotriene B4. *J Clin Invest*. 1989;83(3):970-977. doi:10.1172/JCI113983
96. Aida Y, Pabst MJ. Neutrophil responses to lipopolysaccharide. Effect of adherence on triggering and priming of the respiratory burst. *J Immunol*. 1991;146(4):1271-1276. http://www.ncbi.nlm.nih.gov/pubmed/1846896.
97. Kirby AC, Yrlid U, Wick MJ. The Innate Immune Response Differs in Primary and Secondary Salmonella Infection . *J Immunol*. 2002;169(8):4450-4459. doi:10.4049/jimmunol.169.8.4450
98. Yin J, Ferguson TA. Identification of an IFN-γ-Producing Neutrophil Early in the Response to Listeria monocytogenes . *J Immunol*. 2009;182(11):7069-7073. doi:10.4049/jimmunol.0802410
99. Odegaard JI, Ricardo-Gonzalez RR, Goforth MH, et al. Macrophage-specific PPARγ controls alternative activation and improves insulin resistance. *Nature*. 2007;447(7148):1116-1120. doi:10.1038/nature05894
100. Hesketh M, Sahin KB, West ZE, Murray RZ. Macrophage phenotypes regulate scar formation and chronic wound healing. *Int J Mol Sci*. 2017;18(7):1-10. doi:10.3390/ijms18071545

101. Silva D-A, Yu S, Ulge UY, et al. De novo design of potent and selective mimics of IL-2 and IL-15. *Nature*. 2019;565:186-191. doi:10.1038/s41586-018-0830-7
102. Jewett JC, Sletten EM, Bertozzi CR. Rapid Cu-Free Click Chemistry with Readily Synthesized Biarylazacyclooctynones. *J Am Chem Soc*. 2010;132:3688-3690. doi:10.1021/ja100014q
103. Embaby AM, Schoffelen S, Kofoed C, Meldal M, Diness F. Rational Tuning of Fluorobenzene Probes for Cysteine-Selective Protein Modification. *Angew Chemie*. 2018;130(27):8154-8158. doi:10.1002/ANGE.201712589
104. Kolb HC, Finn MG, Sharpless KB. Click Chemistry: Diverse Chemical Function from a Few Good Reactions. *Angew Chemie*. 2001:2004-2021. https://onlinelibrary.wiley.com/doi/pdfdirect/10.1002/1521-3773%2820010601%2940%3A11%3C2004%3A%3AAID-ANIE2004%3E3.0.CO%3B2-5. Accessed November 27, 2022.
105. Cowdrey WA, Hughes ED, Ingold CK, Masterman S, Scott AD. Reaction Kinetics and the Walden Inversion. Part VI. Relation of Steric Orientation to Mechanism in Substitutions involving Halogen Atoms and Simple or Substituted Hydroxyl Groups. *J Chem Soc*. 1937:1252-1271.
106. Bento AP, Bickelhaupt FM. Nucleophilicity and Leaving-Group Ability in Frontside and Backside SN2 Reactions. *J Org Chem*. 2008;73:7290-7299. doi:10.1021/jo801215z
107. Bonato L, Taleb N, Gingras V, et al. Duration of Catheter Use in Patients with Diabetes Using Continuous Subcutaneous Insulin Infusion: A Review. *Diabetes Technol Ther*. 2018;20(7):506-515. doi:10.1089/dia.2018.0110
108. Anderson VR, Perry CM. Levofloxacin: A review of its use as a high-dose, short-course treatment for bacterial infection. *Drugs*. 2008;68(4):535-565. doi:10.2165/00003495-200868040-00011
109. Dajcs JJ, Thibodeaux BA, Marquart ME, Girgis DO, Traidej M, O'Callaghan RJ. Effectiveness of ciprofloxacin, levofloxacin, or moxifloxacin for treatment of experimental Staphylococcus aureus keratitis. *Antimicrob Agents Chemother*. 2004;48(6):1948-1952. doi:10.1128/AAC.48.6.1948-1952.2004
110. *Levaquin (Levofloxacin) Labeling*.; 2013. https://www.accessdata.fda.gov/drugsatfda_docs/label/2013/020634s065,020635s071,021

721s032lbl.pdf. Accessed October 18, 2017.

111. Stewart PS, Costerton JW. Antibiotic Resistance of Bacteria in Biofilms. *Lancet*. 2001;358:135-138.

112. Grice EA, Segre JA. The skin microbiome. *Nat Rev Microbiol*. 2011;9(4):244-253. doi:10.1038/nrmicro2537

113. Lister PD. Pharmacodynamics of moxifloxacin and levofloxacin against Staphylococcus aureus and Staphylococcus epidermidis in an in vitro pharmacodynamic model. *Clin Infect Dis*. 2001;32 Suppl 1(Suppl 1):S33-8. doi:10.1086/319374

114. Almuzara M, Limansky A, Ballerini V, Galanternik L, Famiglietti A, Vay C. In vitro susceptibility of Achromobacter spp. isolates: comparison of disk diffusion, Etest and agar dilution methods. *Int J Antimicrob Agents*. 2010;35:68-71. doi:10.1016/j.ijantimicag.2009.08.015

115. Kawazu K, Midori Y, Shiono H, Ota a. Characterization of the carrier-mediated transport of levofloxacin, a fluoroquinolone antimicrobial agent, in rabbit cornea. *J Pharm Pharmacol*. 1999;51(7):797-801. doi:10.1211/0022357991773168

116. Lam MW, Mabury SA. Photodegradation of the pharmaceuticals atorvastatin, carbamazepine, levofloxacin, and sulfamethoxazole in natural waters. *Aquat Sci*. 2005;67:177-188. doi:10.1007/s00027-004-0768-8

117. Higuchi T. Mechanism of sustained-action medication. Theoretical analysis of rate of release of solid drugs dispersed in solid matrices. *J Pharm Sci*. 1963;52(12):1145-1149. doi:10.1002/jps.2600521210

118. Siepmann J, Peppas NA. Higuchi equation: Derivation, applications, use and misuse. *Int J Pharm*. 2011;418:6-12. https://ac.els-cdn.com/S0378517311002687/1-s2.0-S0378517311002687-main.pdf?_tid=0f789f49-224b-4517-8449-86256b4860fd&acdnat=1523312998_d8afd505249cf0b32e768759c97257cc. Accessed April 9, 2018.

119. Thakkar VT, Shah PA, Soni TG, Parmar MY, Gohel MC, Gandhi TR. Goodness-of-Fit Model-Dependent Approach for Release Kinetics of Levofloxacin Hemihydrates Floating Tablet. *Dissolution Technol*. 2009;16(1):35-39. doi:10.14227/DT160109P35

120. Korsmeyer RW, Gurny R, Doelker E, Buri P, Peppas NA. Mechanisms of solute release from porous hydrophilic polymers. *Int J Pharm*. 1983;15:25-35. https://ac.els-

cdn.com/0378517383900649/1-s2.0-0378517383900649-main.pdf?_tid=f731a538-5162-419f-bc73-d1dd8ca1c242&acdnat=1534361366_f03d922b9150b4ef497020f300bdc078. Accessed August 15, 2018.

121. Law HT, Fleming RH, Gilmore MF., McCarthy ID, Hughes SPF. In vitro measurement and computer modelling of the diffusion of antibiotic in bone cement. *J Biomed Eng*. 1986;8:149-155. https://www.medengphys.com/article/0141-5425(86)90050-6/pdf. Accessed July 20, 2018.
122. Meulemans A, Paycha F, Hannoun P, Vulpillat M. Measurement and Clinical and Pharmacokinetic Implications of Diffusion-Coefficients of Antibiotics in Tissues. *Antimicrob Agents Chemother*. 1989;33(8):1286-1290. doi:10.1128/AAC.33.8.1286
123. Bauer AW, Kirby WMM, Sherris JC, Turck M. Antibiotic Susceptibility Testing By A Standardized Single Disk Method. *Am J Clin Pathol*. 1966;45(4):493-496. https://www.asm.org/ccLibraryFiles/FILENAME/0000000295/105bauer.pdf. Accessed October 18, 2017.
124. Bonaventura G Di, D'antonio D, Catamo G, Ballone E, Piccolomini R. Comparison of Etest, agar dilution, broth microdilution and disk diffusion methods for testing in vitro activity of levofloxacin against Staphylococcus spp. isolated from neutropenic cancer patients. *Int J Antimicrob Agents*. 2002;19:147-154. www.ischemo.org. Accessed August 14, 2018.
125. Yu C, Li L, Chen W, et al. Levofloxacin Susceptibility Testing for Helicobacter pylori in China: Comparison of E-Test and Disk Diffusion Method. *Helicobacter*. 2011;16(2):119-123. doi:10.1111/j.1523-5378.2011.00820.x

VITA

Education

UNIVERSITY OF WASHINGTON Sept. 2016 – Dec. 2022
Doctor of Philosophy (PhD) (Chemical Engineering: Data Science)
Department of Chemical Engineering
Dissertation: Approaches and preparation for extending insulin catheter longevity
Committee chair: Prof. Buddy D. Ratner
Committee members: Prof. David G. Castner; Prof. Elizabeth A. Nance, Prof. David M. Shechner

UNIVERSITY OF WASHINGTON Sept. 2016 – June 2020
Masters of Science in Chemical Engineering (M.S.)
Department of Chemical Engineering

ARIZONA STATE UNIVERSITY Aug. 2012-May 2016
Bachelors of Science in Engineering (B.S.E.)
School for Engineering of Matter, Transport, and Energy
Major: Chemical Engineering
Minor: Materials Science & Engineering
Honors: Magna Cum Laude
Barrett, the Honors College
NAE Grand Challenges Scholars Program
2016 Outstanding Honors Thesis Award

PRESCOTT HIGH SCHOOL Aug. 2009-May 2012
Honors: National Honor Society

Research Experience

BUDDY D. RATNER RESEARCH GROUP Jan. 2017-Dec. 2022
POLYMERIC BIOMATERIALS AND BIOCOMPATIBILITY
Graduate Research Assistant, PhD Student

- Project: Improving longevity for insulin catheters by reducing the foreign body response
    - Designed polymeric zwitterionic coating to reduce protein attachment, utilizing ARGET-ATR polymerization and plasma-deposited initiator, characterization using XPS, profilometry, ellipsometry, QCM-D, SFG, and radiolabeled protein adsorption
        - Paper submitted: **J King**, P Kaur, and B Ratner. pSBMA coatings grafted using radio frequency glow discharge plasma-deposited halogen initiator reduces non-specific protein adsorption.
        - Paper in preparation: **J King**, S Liu, K Wu, P Kaur, and B Ratner. Effect of grafting density and chain length of pSBMA brushes as measured by QCM-D

- Designed method for immobilizing ultra-stable synthetic IL-4 on the surface of the catheter to encourage macrophages to an alternative (M2) phenotype, utilizing an S_N2 reaction and plasma-deposited or SAM anchor, characterization using XPS and fibroblast adhesion for immobilized RGD-containing peptides
    - Paper in preparation: **J King**, S Creason, M Wyatt, and B Ratner. Surface-stable, cysteine-containing biomolecules immobilized with S_N2 retain bioactivity.
- Designed method of antibiotic integration and controlled release from the catheter polymer matrix to inhibit biofilm formation as well as a method for calculating the antibiotic concentration around the catheter
    - Paper submitted: **J King** and B Ratner. Levofloxacin impregnation and extended release: concentration model for insulin catheters.

- Side Project: With Center for Dialysis and Innovation (CDI), predict urea concentration from optical absorption spectra using various Scikit-Learn algorithms in Python

MARY LAURA LIND RESEARCH GROUP Aug. 2013-May 2016
ADVANCED MEMBRANE LAB
Undergraduate Researcher, Fulton Undergraduate Research Stipend Recipient

- Assisted PhD student, Afsaneh Khosravi, PhD, with dissertation project
- Project: Mixed matrix osmosis membranes to recover potable water from urinary waste for the International Space Station
- Synthesized water-selective LTA zeolites, assembled membranes, performed water flux testing on the prepared membranes, monitored chemical resistance of impermeable polymer matrix for over 2 years
- Khosravi, A., **King, J. A.,** Maltagliati, A., Dopilka, A., Kline, K., Nguyen, T., ... & Lind, M. L. (2016). Coarsening and spinodal decomposition of zeolite linde type a precursor gels aged at low temperatures. Crystal Growth & Design, 16(6), 3224-3230.
- Khosravi, A., **King, J. A.,** Jamieson, H. L., & Lind, M. L. (2014). Latex barrier thin film formation on porous substrates. Langmuir, 30(46), 13994-14003.
- Poster presenter at ICES 2014, Tucson, AZ
- Poster presenter at AIChE 2014, Atlanta, GA
- Poster presenter at ACS Polymeric Membranes 2015, Asilomar, CA
- Poster presenter at AIChE 2015, Salt Lake City, UT

TRANSLATIONAL GENOMICS RESEARCH INSTITUTE Summer 2014
Research Intern

- Directed by Frederic Zenhausern, PhD, MBA and Jian Gu, PhD
- Project: Microfluidic device fabrication to monitor cancerous cells using AI screening
- Designed and fabricated a microfluidic device using PDMS soft lithography for cell swelling to use for *in-situ* microscopy for metaphase cytogenetic assays

Computational Experience

DIRECT Capstone Mar. 2021 – June 2021
Surrodash

- Sponsored by Just-Evotec Biologics
- Generated data from mechanistic model predicting therapeutic yield and purity during purification
- Trained surrogate models with Scikit-Learn to make the predictions in $1/6^{th}$ the time as the mechanistic model
- Built dashboard app in Plotly dash to visualize predictions for real-time use by scientists
- https://github.com/Just-DIRECT-Capstone/Protein-Purification-Model-Public

DIRECT Term Project Jan. 2021 – Mar. 2021
Interstellar iN-Situ Predictive Algorithm for Cellular Engineering (InSpace)

- Predicted relative viability of bacterial-of-interest in spaceflight conditions
- Our project:
    - Retrieved protein sequence from the NCBI (GI number) using Biopython
    - Obtained properties of protein sequence
        - Molecular weight, polarity, isoelectricity, aromaticity
    - Predicted microbial log2FC (viability metric) for survivability in space environment
        - Utilized non-linear regression (bagging regressor)
- https://github.com/UWInSpace/InSpace

Publications and Presentations

King, J. A., Ratner, B. D. (2021). Effects of Zwitterionic Polymer Brush Density and Chain Length on Resisting Protein Adsorption. In 2021 *Society for Biomaterials Annual Meeting and Exposition*. SFB. Presentation.

- **Award:** STAR Award for graduate student presentation

King, J. A., Ratner, B. D. (2019). Antibiotic Extended Release Concentration Quantification By Semi-empirical Model For Insulin Delivery Catheters. In *2019 Society for Biomaterials Annual Meeting and Exposition*. SFB. Poster.

King, J. A., (2022). Surface conjugation of cysteine-containing peptides. *Biomaterials Seminar, UW*. Presentation.

King, J. A., (2021). Surface-grafted zwitterionic coatings reduce protein adsorption for insulin catheters. *Biomaterials Seminar, UW*. Presentation.

King, J. A., P. Kaur, B. D. Ratner, (2021). Effects of Zwitterionic Polymer Brush Density and Chain Length on Resisting Protein Adsorption. *Graduate Student Syposium, UW Chemical Engineering*. Presentation.

King, J. A., (2020). Zwitterionic polymer coating to reduce protein attachment at low surface density. *Biomaterials Seminar, UW*. Presentation.

King, J. A., (2019). Resisting protein adsorption using zwitterionic coatings on polymeric substrates. *Biomaterials Seminar, UW*. Presentation.

King, J. A., (2018). Integration of zwitterionic nonfouling coating with antibiotic extended release for implantable biomaterials. *Biomaterials Seminar, UW*. Presentation.

Khosravi, A., **King, J. A.**, Maltagliati, A., Nguyen, T., & Thomas, M. (2015). Effect of low temperature gel aging on zeolite LTA particle size and morphology in template-free hydrogel process. In *Particle Technology Forum 2015-Core Programming Area at the 2015 AIChE Annual Meeting* (pp. 52-53). AIChE.

Khosravi, A., **King, J. A.**, Maltagliati, A., Dopilka, A., Kline, K., Nguyen, T., ... & Lind, M. L. (2016). Coarsening and Spinodal Decomposition of Zeolite Linde Type A Precursor Gels Aged at Low Temperatures. *Crystal Growth & Design*, *16*(6), 3224-3230.

Khosravi, A., **King, J. A.**, Jamieson, H. L., & Lind, M. L. (2014). Latex barrier thin film formation on porous substrates. *Langmuir*, *30*(46), 13994-14003.

Completed PhD Coursework

CHEM E 512: Methods of Engineering Analysis — Autumn 2016
Credits: 3.0, Grade: 3.4

CHEM E 525: Chemical Engineering Thermodynamics — Autumn 2016
Credits: 4.0, Grade: 3.1

CHEM E 530: Momentum, Heat, and Mass Transfer I — Autumn 2016
Credits: 4.0, Grade: 3.0

CHEM E 560: Reactions at Surfaces — Winter 2017
Credits: 3.0, Grade: 3.0

CHEM E 558: Surface Analysis — Spring 2017
Credits: 3.0, Grade: 3.4

BIOEN 599: Special Topics in Bioengineering: Microscopy and Optics — Spring 2017
Credits: 3.0, Grade: 3.8

CHEM E 545: Data Science Methods for Clean Energy Research — Winter 2021
Credits: 3.0, Grade: 3.9

CHEM E 546: Software Engineering for Molecular Data Scientists — Winter 2021
Credits: 3.0, Grade: 3.9

CHEM E 547: Data Science Capstone Project — Spring 2021
Credits: 3.0, Grade: 4.0

Employment History

UNIVERSITY OF WASHINGTON, Seattle, WA — Sept. 2016 – Dec. 2022
Graduate Research Assistant and Graduate Teaching Assistant

RECREATION ENGINEERING, INC. Summer 2013 & Summer 2015
Prescott, AZ
Engineering Intern

- Project lead (2015): researched and developed an ASTM test method and apparatus for measuring acceleration on water slides, defended the method at the ASTM F24 committee meeting in San Diego in October 2015.
    - Prepared ASTM Standard 3493
- Engineering Assistant (2013): Assist lead engineer in tasks such as taking biodynamic measurements and inspecting amusement rides, completed an evacuation study for a new ride and drafted the evacuation protocol of which is being used in Orlando, FL and Singapore, prepared reports for clients with the collected and analyzed data from acceleration measurements and inspections

Leadership Activities and Community Participation

C-HACK
University of Washington
Volunteer Jan. 2022

- Lead breakout rooms during the chemical engineering department's hackathon for undergraduate students
- Teach Python and coding fundamentals

SOCIETY FOR BIOMATERIALS May 2019-Sept. 2022
University of Washington Chapter
President

- Chair of organizing committee for UW Biomaterials Day 2019, a one-day symposium focused on biomaterials research by faculty and students to build our community and encourage collaboration regionally (Pacific Northwest), including a visiting keynote speaker from Johns Hopkins and a panel of biomaterials start-up representatives
- Organize continuing events for the biomaterials research community at UW to encourage networking and collaboration

Biomaterials Research Outreach

- Volunteered to teach middle school science classes for a day with hands-on activities to encourage biomaterials research ideas, science, and enthusiasm

ASSOCIATION FOR CHEMICAL ENGINEERING GRADUATE STUDENTS Jan. 2018-Dec. 2018
University of Washington
Professional Development Chair

- Hosted a variety of thought-provoking speakers for informal talks over morning coffee with the chemical engineering department's current graduate students, encouraged networking and preparation for a career after graduate school

WOMEN IN CHEMICAL ENGINEERING June 2017-Present
University of Washington
Community Director June 2017-June 2018

- Organized events and activities to engage undergraduate and graduate chemical engineering students in the department to promote a stronger sense of community and inclusivity
- Organized a 5k fun run in spring of 2017 and 2018 as a fundraiser for the student organization and to promote healthy living and community engagement
- Participated in numerous STEM outreach events with the student organization, promoting science and engineering in a fun and accessible manner for K-12 students

Discovery Days May '17, '18, '19

- Volunteered at an annual multi-day K-12 outreach event at UW teaching science and engineering through hands-on demonstrations

ENGINEERING PROJECTS IN COMMUNITY SERVICE (EPICS) Aug. 2013-Dec. 2015
Arizona State University
Team Lead

- Responsible for encouraging the team's goals and keeping progress on-track, served as the main contact with the community partner and industry professionals
- Collaborated with a team of 5 students to design a device to peel, slice, dry, and package mangos in Kenya to promote food security

AMERICAN INSTITUTE OF CHEMICAL ENGINEERS Aug. 2012-Present
Arizona State University

- President (2015-16) —promote AIChE mission statement, provide professional development events for members, served as the main contact for connection between undergraduate chemical engineering students and industry professionals
- Secretary (2014-15) – kept meeting records, communicated as liaison between members and officers, organized guest speakers
- Chem-E Car Team Member (2013-2015)–Designed an 'eco-friendly' car fueled by ethanol for competition
- Attended and competed in the research poster competition at the 2014 AIChE Annual Student Conference in Atlanta, GA and at the 2015 meeting in Salt Lake City, UT

BARRETT MENTORING PROGRAM Aug. 2013-May 2016
MENTOR
Arizona State University

- Volunteer mentor for incoming freshman providing role-model characteristics and advice
- Held one-on-one meetings and group events with students to make the transiting into college easier for freshman, provided necessary first-year resources to mentees
- Continue professional mentorship with multiple students that I mentored at ASU

E2 CAMP COUNCELOR Summer ’13, ’14, ‘15
Arizona State University

- Volunteer at the freshman engineering orientation camp put on by the College of Engineering at ASU and create positive atmosphere
- Lead a group of freshman throughout the camp through various activities while displaying role-model characteristics

INTRA-MURAL FLAG FOOTBALL, BASKETBALL, AND ULTIMATE FRISBEE
Arizona State University Aug. 2012-Dec. 2010

- Played on multiple flag football and basketball teams with other engineering students and occasionally a faculty member
- Flag football team captain (2013-2014) – attended captains’ meetings, maintained the roster, safety officer

University of Washington Mar. 2019-Aug. 2019

- Played on graduate student ultimate Frisbee team in the chemical engineering department

Teaching Assistantships

TRANSPORT PROCESSES I – FLUID MECHANICS Fall 2022
University of Washington
SURFACE ANALYSIS METHODS Spring 2021
University of Washington
TRANSPORT PROCESSES II – HEAT TRANSFER Winter 2021
University of Washington
TRANSPORT PROCESSES I – FLUID MECHANICS Fall 2020
University of Washington
SURFACE ANALYSIS METHODS Spring 2020
University of Washington
TRANSPORT PROCESSES II – HEAT TRANSFER Winter 2020
University of Washington
SURFACE ANALYSIS METHODS Spring 2019
University of Washington

PROCESS DESIGN II – CHEMICAL ENGINEERING SENIOR DESIGN Spring 2017
University of Washington
PERSPECTIVES ON GRAND CHALLENGES OF ENGINEERING Spring 2015
Arizona State University
INTRODUCTION TO ENGINEERING Spring 2014
Arizona State University

Personal Interests

- Hiking, camping/backpacking, skiing, staring at mountains, being outdoors, yoga
- Track NYT Daily Mini crossword puzzle times and other features
- Paddle boarding – In August 2021 I started the Seattle Stand Up Paddle boarding group. We met every week during the summer/early fall and have over 250 members!
- Healthy recipes – design and publish easy-to-make nutritious and wholesome recipes for friends and family to promote wellness
- Distance running – completed a marathon (3:45) in Sept. 2019 and I'm very proud, but I cannot run anymore due to foot injury
- Making a really good cup of coffee